TECOM Project No. 8-ES-685-CPB-003

DPG Document No. DPG-FR-98-001

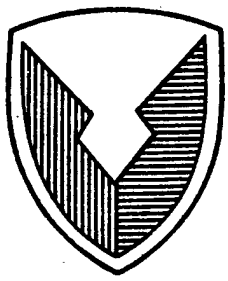

US ARMY
MATERIEL COMMAND

CUSTOMER REPORT

DIPOLE PRIDE 26: PHASE II OF DEFENSE SPECIAL WEAPONS AGENCY TRANSPORT AND DISPERSION MODEL VALIDATION

CHRISTOPHER A. BILTOFT

Meteorology & Obscurants Division
West Desert Test Center

U.S. Army Dugway Proving Ground
Dugway, Utah 84022-5000

JANUARY 1998

Prepared for:
Defense Special Weapons Agency
6801 Telegraph Road
Alexandria, VA 22310

U.S. Army Test and Evaluation Command
Aberdeen Proving Ground, MD 21005-5055

Distribution unlimited.

Disposition Instructions

Destroy this report when no longer needed. Do not return it to the originator.

Disclaimer Statement

The views, opinions, and findings in this report are those of the author and should not be construed as an official Department of the Army position unless so designated by other official documentation.

Trade Name Statement

The use of trade names in this report does not constitute an official endorsement of the use of such commercial hardware or software. This report may not be cited for purposes of advertisement.

REPORT DOCUMENTATION PAGE

Form Approved
OMB No. 0704-0188

1. AGENCY USE ONLY *(Leave blank)*	2. REPORT DATE	3. REPORT TYPE AND DATES COVERED Final Report
	21 January 1998	Final, 04 Nov 96 - 21 Jan 98

4. TITLE AND SUBTITLE
DIPOLE PRIDE 26: PHASE II OF DEFENSE SPECIAL WEAPONS AGENCY TRANSPORT AND DISPERSION MODEL VALIDATION

5. FUNDING NUMBERS
8-ES-685-CPB-003/K4

6. AUTHOR(S)
Christopher A. Biltoft

7. PERFORMING ORGANIZATION NAME(S) AND ADDRESS(ES)
Meteorology & Obscurants Division
West Desert Test Center
U.S. Army Dugway Proving Ground
Dugway, UT 84022-5000

8. PERFORMING ORGANIZATION REPORT NUMBER
DPG-FR-98-001

9. SPONSORING/MONITORING AGENCY NAME(S) AND ADDRESS(ES)
Defense Special Weapons Agency
6801 Telegraph Road
Alexandria, VA 22310

10. SPONSORING/MONITORING AGENCY REPORT NUMBER

11. SUPPLEMENTARY NOTES

12a. DISTRIBUTION/AVAILABILITY STATEMENT
Distribution Unlimited

12b. DISTRIBUTION CODE

13. ABSTRACT *(Maximum 200 words)*

The Dipole Pride 26 test program conducted 04-21 November at the Nevada Test Site Yucca Flat constituted Phase II of the Defense Special Weapons Agency (DSWA) Transport and Dispersion Model Validation Program. Dipole Pride 26 was conducted to acquire a puff dispersion database over mesoscale (5-25 km) distances for validation of integrated mesoscale wind field and dispersion models, in particular the Hazard Prediction and Assessment Capability (HPAC) model suite. The test program consisted of 23 sulfur hexafluoride puff releases into the atmosphere with crosswind sampling lines at distances of 5 to 25 km downrange, providing information on puff crosswind and alongwind dimensions, and peak concentration. Of the 23 puff releases, 17 provided useful puff dimension information at one or more sampling lines. This report summarizes Dipole Pride 26 puff and micrometeorological data. The entire data set is available on compact disk.

14. SUBJECT TERMS
atmospheric dispersion, dispersion model validation, atmospheric tracer, puff dispersion, sulfur hexafluoride, SCIPUFF, DSWA, tracer gas experiments

15. NUMBER OF PAGES

16. PRICE CODE

17. SECURITY CLASSIFICATION OF REPORT	18. SECURITY CLASSIFICATION OF THIS PAGE	19. SECURITY CLASSIFICATION OF ABSTRACT	20. LIMITATION OF ABSTRACT
UNCLASSIFIED	UNCLASSIFIED	UNCLASSIFIED	UL

FOREWORD

Dipole Pride 26 test program participants included support elements from the Department of Energy (DOE), the National Oceanographic and Atmospheric Administration Air Resources Laboratory (NOAA ARL), the Department of the Army (DA), and several contractors. Test program oversight and logistical support were provided by the DOE Nevada Operations Office. The NOAA ARL Special Operations and Research Division (ARL/SORD) provided meteorological support, while the NOAA ARL Field Research Division (ARL/FRD) performed the tracer gas measurements using sulfur hexafluoride detectors. The U.S. Army Dugway Proving Ground West Desert Test Center (DPG/WDTC) designed and managed the test program, operated the puff dissemination system, and provided micrometeorological measurements. Test program contractors included Logicon RDA, The Aerospace Corporation, and Bechtel Nevada. Logicon contributed technical expertise to various aspects of test design, The Aerospace Corporation operated remote sensing equipment to track the puffs, and Bechtel Nevada provided onsite logistical support.

Blank Page

ACKNOWLEDGMENTS

The Phase II Dipole Pride 26 (DP26) Defense Special Weapons Agency (DSWA) model validation program included support elements from the Department of Energy (DOE) Nevada Test Site staff managed by MAJ Paul Loomis. Test program participants included the National Oceanographic and Atmospheric Administra-tion Air Resources Laboratory (NOAA ARL), the Department of the Army (DA), DSWA, and several contractors. Dr. Darryl Randerson, Director of the NOAA ARL Special Operations and Research Division (SORD) provided operating space at the Yucca Flat Weather Station and laboratory space for the gas laboratory in Mercury, Nevada. Mr. Ray Dennis, Senior SORD Meteorological technician, and his crew provided invaluable day-to-day meteorological support. Drs. David George and Thomas Watson of the NOAA ARL Field Research Division (FRD) managed the field crews and gas laboratory personnel that collected the sulfur hexafluoride sampler data. LTC A.J. Kuehn represented DSWA at the test site, with Drs. Gary Ganong and William Espander from Logicon RDA providing valuable technical assistance. Puff imagery and FTIR spectronomy were provided by The Aerospace Corporation under the direction of Dr. Kenneth Herr. Charles Birdsong, Christopher Woldruff, and David Petrie of the DPG West Desert Test Center (WDTC) Test Operations Division operated the dissemination system, provided puff source dimensions, and collected micrometeorological data. Drs. Tom Watson, Steve Hanna, and Darryl Randerson provided external review of this report. Mrs. Susan Gross of the WDTC Meteorology & Obscurants Division provided word processing support.

Blank Page

EXECUTIVE SUMMARY

Phase II of the Defense Special Weapons Agency (DSWA) Transport and Dispersion Model Validation Program (Dipole Pride 26) was conducted at Yucca Flat on the Nevada Test Site in November 1996. The Phase II test objective was to acquire a data base for the validation of integrated mesoscale wind field and dispersion models, in particular the Hazard Prediction and Assessment Capability (HPAC) model suite. This objective was achieved by releasing tracer gas (sulfur hexafluoride) puffs, with downwind tracer sampling at distances ranging to 20 km along with extensive measurements to document meteorological conditions. DSWA sponsored the Phase II model validation test series as part of its counterproliferation model development and validation effort.

A total of 23 puff releases were completed during the trials series, including 5 into nocturnal drainage flows. Significant terrain effects observed during puff travel through Yucca Flat included pooling at Yucca Lake during drainage flows, and upslope (katabatic) flows as the mountains on either side of Yucca Flat received solar heating. Crosswind puff dispersion was sampled at three sampling lines located along roads 2 to 20 km downrange of the source. Alongwind puff growth was also measured along the middle sampling line, but interpretation of these measurements is complicated by disseminator system leaks.

This report presents lateral (σ_y) and alongwind (σ_t) puff dispersion summaries obtained from tracer concentration measurements, plus detailed explanations of puff dissemination and sigma calculation procedures. Remote imagery was used to obtain information on vertical dispersion and the puff centroid position. Results from the fixed sampling lines, which include whole air sampler data and continuous analyzer data, are available on a compact disk along with the supporting meteorological and micrometeorological data. Report documentation includes the puff dissemination conditions, downwind dispersion, atmospheric stability, site roughness, and micrometeorological summaries needed for dispersion model validation.

Blank Page

TABLE OF CONTENTS

LIST OF FIGURES

LIST OF TABLES

SECTION 1. INTRODUCTION

Responding to a shortfall in downwind hazard effects modeling identified during Operation Desert Storm, the Defense Special Weapons Agency (DSWA) has developed and is evaluating the performance of the Hazard Prediction and Assessment Capability (HPAC) model suite. HPAC includes a diagnostic wind field model coupled with an atmospheric transport and dispersion model to provide decision makers with a tool for predicting windborne hazards that arise as a consequence of toxic materials released into the atmosphere. The HPAC development effort began with the recognition that the ensemble mean predictions available from the current generation of atmospheric dispersion models used for chemical and biological (CB) hazard assessments are of limited operational utility. Ensemble mean predictions provide an estimate of the concentrations or dosages that would be obtained by averaging the results for a large number of replications of the same release, but include no information about the distribution of single event concentrations or dosages. Current hazard assessment models also cannot estimate the probability of exceeding critical hazard thresholds. These deficiencies complicate the interpretation of CB hazard model predictions and limit their usefulness in operational military situations.

Given the limited operational usefulness of ensemble mean predictions, DSWA identified the need for a probabilistic atmospheric dispersion model. In addition to providing a prediction of ensemble mean concentrations or dosages, a probabilistic dispersion model uses higher order statistical terms to define the probability that dosages or peak concentrations at points of interest exceed some critical value specified by the user. This probabilistic output requires that the model be able to predict the concentration or dosage cumulative distribution function (CDF), which in turn requires that the model be able to predict both the concentration (or dosage) means and variances. The Second Order Closure Integrated Puff (SCIPUFF®) model (Titan Corporation, 1996), which predicts the required means and variances through a second-order closure solution of the advection-diffusion equation, is the HPAC dispersion model component.

SCIPUFF uses a generalized Gaussian tensor to describe puff concentrations. The model's derivation begins by integrating the conservation equations to obtain differential equations for the concentration moments that explicitly include wind-shear effects. Second-order closure is used to relate these higher-order terms to turbulence parameters such as velocity cross-correlations and turbulence length scales. In contrast to current generation Gaussian puff models, SCIPUFF's second-order closure methodology yields theoretically consistent predictions of dosage and concentration variances in addition to their ensemble means. These means and variances are applied in a clipped-normal probability distribution to predict concentration and dosage CDFs.

In the fall of 1995, DSWA contacted the Dugway Proving Ground (DPG) West Desert Test Center (WDTC) Meteorology & Obscurants Division (WD-M) for assistance in the development and implementation of a transport and dispersion model validation program. WD-M convened a meeting of atmospheric transport and dispersion modeling experts in February 1996 to recommend a model validation program. Attendees included representatives from the Joint Services, the National Oceanic and Atmospheric Administration (NOAA), and the trinational (U.S., UK, and Canada) Technical Panel 9 of The Technical Cooperation Program (TTCP) Subgroup E on CB Defense. Recognizing the limitations of the data from CB weapons tests and previous field dispersion experiments, the attendees agreed that new data sets and model validation procedures were needed to validate SCIPUFF's probabilistic output. Consequently, the attendees suggested conceptual designs for a series of field tests to create high resolution puff data sets accompanied by detailed meteorological documentation.

The DSWA Model Validation Program has had two phases to date. Phase I, conducted 9-26 September 1996 at DPG, consisted of observations of short-range (200 to 1200 m) puff releases for CDF evaluations. Phase II considered transport and diffusion to mesoscale distances (10 to 20 km). The Phase II subtest, known as Dipole Pride 26 (DP26), consisted of a series of puff releases conducted at the Nevada Test Site on 4-21 November 1996. This report documents the Phase II (DP26) test program and its results. Detailed sampler data and supporting meteorological and micrometeorological measurements are also available on magnetic and/or optical media.

SECTION 2. TEST DESCRIPTION

2.1 TEST SITE

Yucca Flat (37° N, 116° W) is a north-south oriented basin 30 km in length and 12 km in width surrounded on all sides by higher terrain. Yucca Lake, at a height of 1195 m above mean sea level (MSL), is a seasonally dry lake bed at the south end of the basin that forms the lowest part of the Yucca Flat. The basin is surrounded by mountains extending to 1800 m MSL or higher on the west through north and to 1500 m MSL or higher on the east. The basin slopes upward toward the north at an average angle of 0.3°. Wind flow through Yucca Flat is strongly influenced by the surrounding terrain. Passes to the northeast and south form the main ventilation channels through Yucca Flat. Early morning drainage flows from the north cause pools of cold air to accumulate over Yucca Lake. Solar heating of higher terrain at the north end of Yucca Flat generally draws a southerly flow through the basin during daylight hours.

The principal test-related facilities within Yucca Flat included the Yucca Flat Weather Station (designated UCC for meteorological reports) on the western edge of Yucca Lake; the Buster-Jangle Yankee intersection (designated BJY), a position near the intersection of Rainer Mesa Road and Mercury Highway; and a network of meteorological data (MEDA) stations within and around Yucca Flat. These locations are shown on Figure 1, and their latitude and longitude positions are given in Table 1. The ARL/SORD meteorological building at UCC served as both the test program command post and a release point for radiosonde and pilot balloon (pibal) flights. A pibal station and wind profiling radar were also stationed at BJY. Tower-mounted sonic anemometer/thermometers (sonics) were operated near BJY and at a site, designated YFW in this report, that is 100 m east of UCC.

Table 1. Dipole Pride 26 Test Site and MEDA Station Locations.

Position	Latitude (°N)	Longitude (°W)
Area 1 (MEDA 1, elevation 1265 m)	37.0275	116.0917
Area 2 (MEDA 2, elevation 1341 m)	37.1392	116.1058
Area 3 (MEDA 3, elevation 1207 m)	37.0042	116.0317
Area 9 (MEDA 9, elevation 1290 m)	37.1358	116.0400
BJY (MEDA 17, elevation 1244 m)	37.0625	116.0525
DAF (MEDA 28, elevation 1107 m)	36.8925	116.0375
YFW (MEDA 6, elevation 1195 m)	36.9583	116.0467
MON (MEDA 10, elevation 1570 m)	36.9400	116.0792
CSE (Cane Springs Road East)	36.8512	115.9985
N2 (North Dissemination Site 2)	37.1586	116.0967
N3 (North Dissemination Site 3)	37.1500	116.0625
S2 (South Dissemination Site 2)	36.9570	116.0498
S3 (South Dissemination Site 3)	36.9512	116.0100
Sampler Site 101 (West End North Line)	37.1383	116.1230
Sampler Site 130 (East End North Line)	37.1227	116.0410
Sampler Site 201 (West End Middle Line)	37.0557	116.0920
Sampler Site 230 (East End Middle Line)	37.0493	116.0090
Sampler Site 301 (West End South Line)	36.9906	116.0930
Sampler site 330 (East End South Line)	36.9954	116.0160

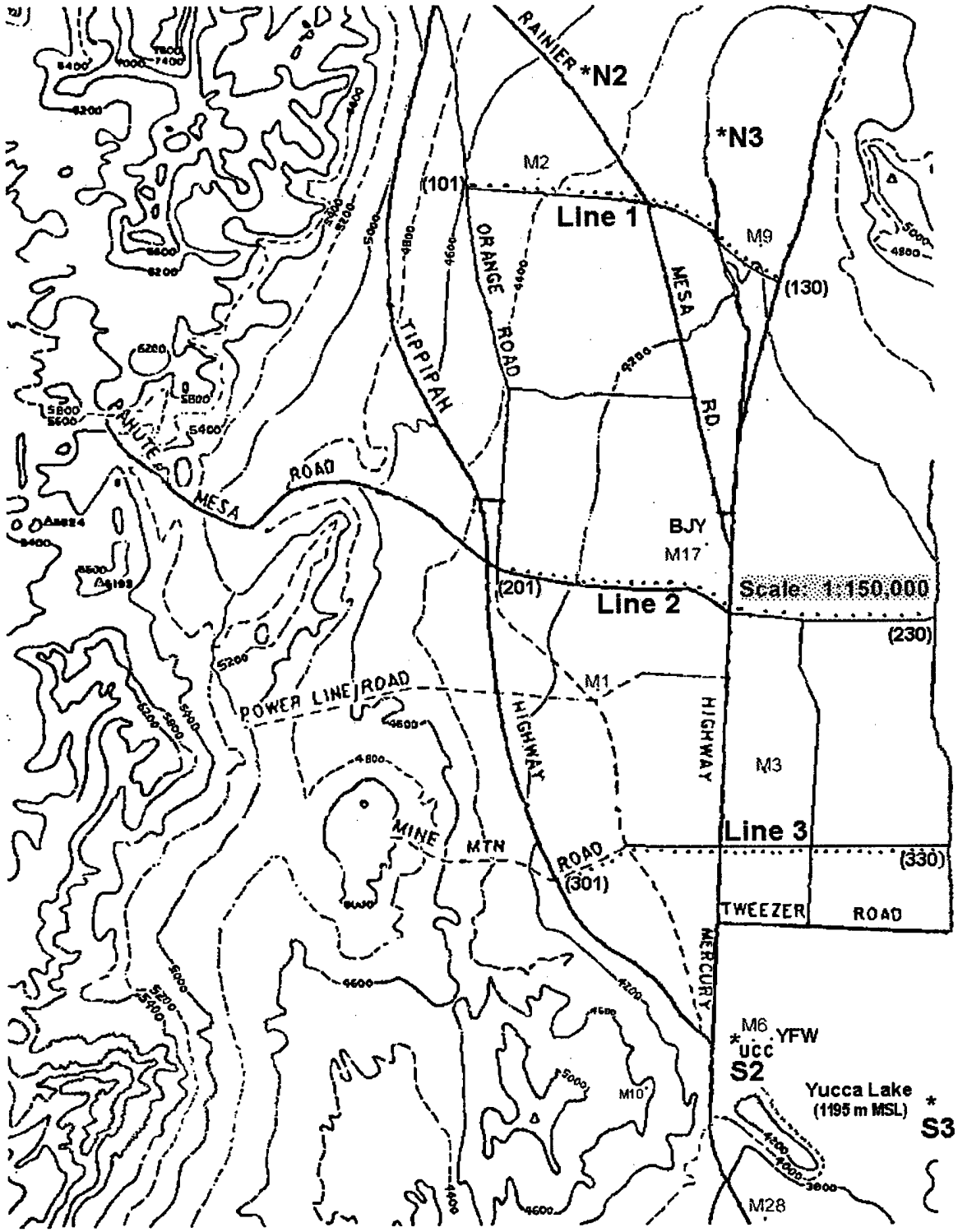

Figure 1. Dipole Pride 26 test site at Yucca Flat, with the locations of puff release sites (S2, S3, N2, and N3), three concentration sampling lines, MEDA Stations (M1, M2, M3, M6, M9, M10, and M28), and primary instrumentation positions (BJY, UCC, and YFW) indicated.

2.2 FIELD TEST DESIGN

The Dipole Pride 26 (DP26) field test was designed to use fixed sampling lines and a mobile dissemination system to document puff dispersion utilizing the predominant north-south flow through Yucca Flat. Six dissemination positions, three on the north side and three on the south side of Yucca Flat, were selected for the truck-mounted disseminator to accommodate wind direction variations. Only sites S2, S3, N2, and N3 were actually used for dissemination.

The dissemination system was built by Consumers Pipe in Las Vegas, NV. It consisted of gas cylinders, the tracer gas sulfur hexafluoride (SF_6), a compressor, actuators, fill hoses, and plumbing mounted on the bed of a government-furnished 5-ton truck. Gas was released through two cylinders with fast-acting solenoid-actuated butterfly valves. Each release was completed within 2 seconds of valve opening. The cylinders were designed to be operated either singly or together. Each cylinder had a volume of 0.15 m^3 and held approximately 10 kg of SF_6 when filled to the design pressure of 150 lbs per square inch (105,465 kg/m^2). Table 2 gives the calculated quantities of SF_6 released for each trial, and Appendix B describes the methodology used to calculate release quantities.

The released SF_6 puffs were sampled using six TGA-4000 Tracer Gas Analyzers and ninety whole air samplers dispersed along three sampling lines. Technicians operated the TGA-4000s, which were installed within half-ton cargo vans. These technicians also serviced whole air samplers mounted on posts 1.5 m above ground level (AGL) along sampling line roads. The fast-response TGA-4000s provided real time information on the arrival and departure of each puff and measured the high-frequency (4-Hz) variations of the gas concentration field within the passing puffs. The whole air samplers provided only coarse (15-min) time resolution, but the time-averaged gas concentration measurements from the 30 whole air samplers stationed along east-west roads crossing Yucca Flat provided the spatial resolution required for puff lateral dimension calculations. Additional whole air samplers were positioned away from the planned puff trajectory as background SF_6 references, and dual samplers were mounted at some sampling stations for quality control.

DP26 sampling lines were established along the following roads: Road 2-04 between Orange Road and Mercury Highway (Line 1, sampler positions 101 through 130); Pahute Mesa Road between Orange Road and Orange Blossom Road (Line 2, sampler positions 201 through 230); Mine Mountain Road between Tippipah Highway and Orange Blossom Road (Line 3, sampler positions 301 through 330). The TGA-4000s were stationed at 1500-m intervals along Sampling Line 2 (Pahute Mesa Road) to maximize the possibility of intercepting portions of the cloud crossing this line. Mean whole air sampler spacing along Lines 1, 2, and 3 were 259, 256, and 237 m, respectively. Sampler spacing, line length, and number was chosen as a compromise between four constraints: (1) containing the entire puff width within a sampling line; (2) intercepting the puff with at least six samplers; (3) remaining within the confines of existing roads; and (4) not exceeding technician servicing capabilities. This compromise optimized sampling along Line 2, which was roughly 10 km from the north and south dissemination positions. Pre-trial modeling suggested a sampler spacing of 250-300 m as the best compromise between the first and second constraints. The third and fourth constraints limited sampler line length and the number of positions within a sampling line.

Puff infrared (IR) imagery was obtained by WDTC personnel at the time of release, and the dispersing puff was tracked downrange using an array of mobile imagers operated by The Aerospace Corporation. The principal purposes of this imagery were to document initial puff dimensions and to resolve in time and three-dimensional space the puff centroid positions as these centroids crossed the sampling lines. Operators of the Aerospace

imagers selected their positions prior to puff release based on release location and wind conditions.

The Dipole Pride 26 test series was designed to complement puff dispersion measurements with extensive meteorological documentation. This documentation included surface-based and upper air measurements and weather analysis and forecasting support from the ARL/SORD facility in Las Vegas, NV. Surface measurements included wind, temperature, humidity, and pressure data obtained over 15-min averaging periods from an array of MEDA stations located in and around Yucca Flat. These measurements were supplemented with temperature and momentum flux and turbulence information obtained using sonic anemometer/thermometers mounted on towers at BJY and YFW. Pibal and radiosonde flights provided wind and thermodynamic profiles through the lower troposphere. ARL/SORD reactivated its radiosonde site UUC at the Yucca Flat Weather Station during DP26 to launch radiosonde flights every 3 hours while trials were in process. Pibals were also launched every hour from BJY and UUC (except during radiosonde flights), and occasionally from Cane Springs Road. A 924-MHz wind profiling radar positioned near BJY provided intermittent wind profiles during testing. MEDA station, pibal, radiosonde, and profiler data are available on floppy disks or CD ROM. The sonic anemometer/thermometer measurements require extensive processing to produce useful statistical results. These statistical results are presented in this report, while the basic data are available from DPG by special request.

2.3 TEST INSTRUMENTATION

2.3.1 TGA-4000 Continuous SF_6 Analyzer

The TGA-4000 is designed to provide real-time fast response (better than 1 Hz) SF_6 concentration measurements. It consists of a catalytic reactor, a dryer, and an electron capture detector (ECD) to measure halogenated compounds such as SF_6. Because the detector responds to oxygen, the TGA-4000 uses the catalytic reactor to convert molecular oxygen to water and a dryer subsequently removes the water from the airstream. Any SF_6 above a picogram threshold remaining in the airstream after these operations produces a voltage proportional to its concentration as the airstream passes through the ECD. The TGA-4000, its associated plumbing, and a data acquisition and display system fit into a ½-ton cargo van, which can be driven into sampling position. The van also serves as a power source for the TGA-4000. Scientech, Inc. of Pullman, WA, who built the TGA-4000, report a bench-top noise level of 5 part per trillion by volume (pptv) and a response time of 0.86 s (Benner and Lamb, 1985). A 4-Hz data acquisition rate was used with the TGA-4000 instruments during DP26. Further details on the TGA-4000 can be found in Watson et al. (1998) or Bowers et al. (1994).

2.3.2 Whole Air Samplers

Whole air samplers, also known as sequential bag samplers (Bowers et al, 1994), consist of a cartridge containing a programmable microprocessor and twelve 1-l Tedlar™ bags, with each bag connected to a small air pump. A "D" cell battery provides power for the whole air sampler unit. The cartridge is mounted within a waxed cardboard box that fits onto a mounting bracket. During DP26 each sampler was mounted on a post at a height of 1.5 m above ground level (AGL). The sampler can be programmed to sequentially fill each of the bags over time periods ranging from 10 min to several hours, thereby providing a concentration measurement integrated over the selected sampling period. A 15-min sampling period was used during DP26 as the best compromise between the desire for maximum time resolution and the need to sample during the 3-hour duration of a typical test. The bag 1 fill sequence was programmed to begin at puff dissemination time on the two sampling lines closest to the disseminator, and was delayed for 30 min on the furthest

sampling line. Once the fill sequence on bag 12 was completed, the cartridges containing sealed bags were dismounted and taken to a field gas laboratory set up in Mercury, NV for separation by species. Chemical species separation was performed using a gas chromatograph and an electron capture detector. Further details on whole air sampler operation during DP26 are given by Watson et al (1998).

2.3.3 Sonic Anemometer/Thermometers

A sonic anemometer/thermometer (sonic) consists of a transducer array containing paired sets of ultrasonic transmitters and receivers, a system clock, and circuitry designed to measure intervals of time from the transmission to the reception of sound pulses traveling between transducer pairs. The sonics used during Dipole Pride 26 were the Applied Technologies, Inc. 3-axis ATI Model RSWS-201/3A, which provides three dimensional (u, v, and w) wind components and speed of sound. These sonics were mounted at 10 and 14 m AGL on towers near the Buster-Jangle Yankee (BJY) intersection and at a tower designated YFW located 100 m east of the Yucca Flat Weather Station (UCC). Sonic locations were confined to these sites by the need for a suitable mounting tower and 110 VAC power. The 3-axis sonics resolve all components of the three-dimensional wind vector. The speed of sound measurements were converted to sonic temperature, which is essentially equivalent to the virtual temperature. With a data rate of 10 Hz and an acoustic pathlength between transducers of 15 cm, the sonics provide sufficient temporal and spatial resolution to measure mean wind plus the fluctuating components needed to define turbulence intensities and the fluxes of heat and momentum. Procedures described in the American Society for Testing of Materials (ASTM) standard practice for obtaining wind and temperature measurements from sonics (ASTM 1997A) were used to obtain wind component and speed of sound measurements to within ± 3 cm/s.

2.3.4 MEDA Stations

ARL/SORD operates a continuously monitoring network of remote meteorological stations (MEDA stations) across the Nevada Test Site. Each station in the MEDA network reports a measurement of temperature, pressure, humidity, wind speed, and wind direction every 15 min. There is a time tag at the end of each MEDA data block. For example, data collected during the period 0230 - 0245 Pacific Standard Time (PST) are reported at 0245 PST. With the exception of wind sensors mounted at 10 m, MEDA station instruments are mounted at 2 m AGL. MEDA station data are transmitted via radio to a centralized data collection point. The reported temperature, pressure, and humidity are the last available readings during each 15-min reporting interval. Wind speed and direction are obtained over a 5-min averaging period immediately prior to the reporting time, with maximum and minimum speeds taken from 1-s readings during the entire 15-min period. The MEDA station data displays in the Yucca Flat Weather Station served as the primary source of wind information for DP26 test conduct.

2.3.5 Radiosonde

A radiosonde system consists of a balloon-borne instrument package that rises through the atmosphere, providing profiles of wind, temperature, humidity, and height at 10-s intervals throughout the flight. Data packets from this instrument are transmitted via radio link to a base station where they are logged and subjected to quality control. Each profile is reduced to measurements at standard pressure levels (the mandatory levels) and significant inflection points (significant levels). The radiosonde system used at NTS is the automatic radio-theodolite (ART), which tracks the balloons with a ground-based radio theodolite. The ART tracks the ascending balloon, providing elevation and azimuth angle readings which, after time-synchronization with pressure readings, are converted to profiles of wind speed and direction. The ART system used during DP26 was located at the Yucca

Flat Weather Station (UCC). It provided wind and thermodynamic profiles every 3 hours during the test program. The ART measurement uncertainties are ±0.6 °C for temperature, ±10% for relative humidity, and ±1 m/s for winds (RCC-MG, 1992).

2.3.6 Pibal

The pilot balloon (pibal) is an optically-tracked free balloon used to obtain profiles of wind speed and direction. Hundred gram (100-g) pibals provided boundary layer wind profiles during this test program. When filled to its design lift weight, a 100-g pibal has an ascent rate that is large in comparison with typical atmospheric vertical motions. Standard tables are used to relate a pibal's flight time to its height AGL. Optical tracking with a theodolite provides azimuth and elevation readings taken at 30-s intervals. These readings, combined with tabulated height versus time data, provide sufficient information to calculate layer-averaged wind speeds and directions. Pibal wind profiles are typically accurate to within ± 2 m/s (RCC-MG, 1992). The Digital Pibal (DIGIPI) Systems used at NTS feature shaft encoders to digitally record theodolite angles every 30 s. The angular data are stored in a microcomputer linked to a communications device that transmits these data to the central computer during a polling sequence. DIGIPI units were stationed at BJY and UCC, and occasionally at Cane Springs Road (CSE) in Frenchman Flat, providing hourly wind profiles during the test program.

2.3.7 Infrared Imaging Radiometers

Infrared imaging radiometers (imagers) are passive optical devices sensitive to IR energy in the 8- to 12-mm portion of the IR spectrum. Because SF_6 has a distinct absorption band in this portion of the spectrum, the passage of a SF_6 puff across the imager's field of view registers as a temperature change when compared with the background image. IR imagers were used to determine initial puff dimensions (source size) and to track the puffs as they traversed the sampling lines. Source size characterization was done using an Inframetrics Model 600L Imaging Radiometer, which has a typical thermal sensitivity of 0.05 °C, a scan rate of 50 Hz, and a 7-bit (128 levels) image resolution. Three Sterling-cooled Agema Thermovision 900 digital IR imagers, each equipped with a narrowband filter centered around the main SF_6 absorption band, were used to monitor SF_6 puff travel across the sampling lines. These imagers are characterized by a 15-Hz scan rate (non-interlaced) and a thermal sensitivity of 0.08 °C. The spectral resolution and field of view varied with the filters and lenses used. These images captured information on puff concentration column density and centroid height.

2.3.8 Fourier Transform Infrared Spectrometer

The Fourier transform infrared spectrometer (FTIR) is a remote imaging device designed to measure the scene spectrum within the 8- to 12-mm band. Because all materials that absorb IR energy have unique absorption band signatures, an FTIR is able to resolve the contents of a dispersing cloud if a sufficient signature is present. These instruments are most useful when the background within their fields of view is constant and the target tracer cloud is easily distinguishable from the background thermal signature. Consequently, the FTIRs were oriented toward the (relatively cold) clear sky to detect the arrival and passage across the field of view of the (relatively warm) SF_6 puffs. Sulfur hexafluoride is an ideal tracer because it exhibits a sharp peak at an inverse wavelength of 950 cm^{-1}. When processed through a "special ratio" algorithm (Polak et al., 1995) designed to remove background and noise, the SF_6 transmission or absorption peak emerges and can be used for quantitative estimation of puff column density.

The FTIR supporting DP26 was an Intillitec M21 chemical agent detector. This instrument features a spectral resolution of 1.5 cm^{-1}, a 5.25-Hz scan rate, a 25-milliradian field of view, and a sensitivity of 1.5 x 10^{-8} W cm^{-2} sr^{-1}/cm^{-1}. Spectrometers were mounted in the Aerospace Corporation Ram Van which was positioned to intercept the passing SF_6 puff centroid, and in the Aerospace Tonka Van, which followed the puff and made traverses through it as it dispersed downrange. Reports from these two vans provided real-time information on puff location and dispersion, and follow-on analysis of these data could provide valuable puff position information.

2.3.9 Dissemination System

The SF_6 gas release system consisted of two vertically-mounted cylinders, solenoid-operated actuators, and a control panel with remote enable and function buttons. The cylinders had a volumetric capacity of 0.15 m^3 and vented through a top-mounted 25-cm (10-in) butterfly valve. Trial preparation began with the filling of one or both cylinders with SF_6 gas to a pressure of approximately 150 psig. A cylinder pressure of 150 psig was high enough to quickly expel the contained gas, but low enough to prevent the SF_6 from liquifying, thereby producing a puff while minimizing unwanted momentum and dense gas effects on initial puff dimensions. Remote control buttons were used to enable and operate the valves either together or separately. Each cylinder was instrumented with a surface-mounted thermometer and internal cylinder gage pressure transducer to provide the measurements required for calculation of the released mass. The release system was mounted on the bed of a 5-ton flatbed truck. This truck was driven to one of the designated release locations prior to the beginning of each trial fill procedure. The release mass calculation procedure is described in Section 3.1.3, with further details provided in Appendix E. Table 2 in Section 3 lists the mass of SF_6 calculated for each release.

Blank Page

SECTION 3. TRIAL DATA SUMMARIES

3.1 DISSEMINATION SUMMARIES

3.1.1 Trial Name And Time Convention

Dipole Pride 26 trials are named DSWAXX, where XX is a sequential numbering of trials (01 through 17). All SF_6 gas concentration data are identified by trial name. Several of the trials included two sets of disseminations, the second release being staggered 90 min behind the first. Consequently, trial names are supplemented with a release time convention of JJJhhmm. The release time convention for DP26 consists of the three-digit Julian date (JJJ) followed by the hour and minute of the dissemination in Pacific Standard Time (PST). Dissemination dates, times, and locations are presented in Table 2.

Two time conventions are used with DP26 meteorological data. The MEDA station data collected during the test program and archived on CD are presented in PST, with the time stamp taken from the end of the averaging period. The radiosonde and pibal launch times are also presented in PST. In contrast, the 15-min averaged sonic anemometer data documented in this report and on CD take their time stamp from the beginning of the averaging period and are presented in Universal Coordinated Time (UTC), which is 8 hours ahead of PST. For example, MEDA station data for the period 1500-1515 PST are labeled 1515, while sonic data from the same period are labeled 2300 UTC.

3.1.2 Dissemination Procedures

Trial preparation began with a decision to disseminate from one of the north (N2, N3) or south (S2, S3) positions. The truck-mounted disseminator system was then driven to that position. The SF_6 dissemination cylinder fill procedure began upon receipt of range safety clearance from the DOE Nevada Operations Office representative. The cylinder(s) to be used on a trial were filled to a nominal gage pressure of 150 psi. Cylinder pressures and temperatures were reported when the fill procedure was completed. Small SF_6 leaks caused by temperature-induced flexing of the packing material between the cylinders and valve flanges often occurred during the fill procedure. Leaks were minimized by tightening the bolts securing the valve and actuator components to the cylinder, but elevated SF_6 background concentrations due to disseminator leaks are apparent in the sampler data for some trials. Table 2 includes comments concerning trials where leaks were most noticeable.

3.1.3 Dissemination Mass Calculations

Given a known cylinder volume, the cylinder temperature, and internal pressure, it is possible to calculate the mass of material released. Dr. William Espander performed a series of mass calculations based on the Law of Corresponding States, a Virial equation, and a Martin-Hou equation (Mears et al, 1969). While the results from these three methods were similar, Dr. Espander recommends the Martin-Hou method because it is based on actual SF_6 experimental data. Table 2 includes disseminated mass calculated using the Martin-Hou method. Details of Dr. Espander's DP26 calculation procedures are presented in Appendix C.

Table 2. Dipole Pride 26 Dissemination Times, Masses, And Comments.

Release date/time (JJJhhmm)	Date	Dissemination		Number of Cylinders	Mass Released (Kg)	Comments
		Time (PST)	Location			
3091441	4 Nov	1441	S2	2	8.0	Bulk of puff missed samplers
3110800	6 Nov	0845	N3	1	11.5	SF_6 leak in actuator arm; puff missed grid
3130400	8 Nov	0400	N3	1	12.3	Puff near ground; 2 segments; pooling at Yucca Lake
3140400	9 Nov	0400	N3	1	11.5	Puff near ground; pooling at Yucca lake
3140538	9 Nov	0538	N3	1	11.5	Pooling at Yucca Lake
3160440	11 Nov	0440	N2	1	11.5	Puff lifting off surface
3170400	12 Nov	0400	N2	1	11.6	Puff stalled on Pahute Mesa Rd, pooling
3171300	12 Nov	1300	S3	2	19.3	1.5 s between releases
3171447	12 Nov	1447	S3	1	10.0	Cylinder failed to function at 1445; OK at 1447
3181400	13 Nov	1400	S2	1	10.4	Continuous analyzers detecting possible freon source leak from somewhere on NTS
3190900	14 Nov	0900	N2	1	11.3	Winds light & variable
3191430	14 Nov	1430	N2	1	10.6	Puff above sampler lines
3191551	14 Nov	1551	N2	1	10.8	Puff in contact with surface
3200900	15 Nov	0900	N2	1	11.5	Possible leak; tightened gasket
3201030	15 Nov	1030	N2	1	11.3	
3201430	15 Nov	1430	N2	2	21.6	0.5 s between releases, puff lofting
3211300	16 Nov	1300	S2	2	21.1	0.7 s between releases
3231130	18 Nov	1130	S2	1	10.8	Disseminator leaks
3231300	18 Nov	1300	S2	2	20.2	
3241200	19 Nov	1200	S3	2	20.3	Puff passing east of samplers
3241330	19 Nov	1330	S2	2	20.3	Puff passing west of samplers
3251200	20 Nov	1200	S3	2	20.4	Puff lofting
3251330	20 Nov	1330	S2	2	20.1	Puff west of line, rising over hills NW

3.1.4 Release Dimensions

An IR imager positioned 100 m east or west (crosswind) of the disseminator provided puff alongwind and vertical dimension information. Release duration (usually 1-2 s) is the time between the opening of the first valve to the evacuation of the last cylinder. The release durations were subjectively determined from visual inspection of the puff release imagery. Useable puff images were not obtained for each release, and those that were available are subject to uncertainties in interpretation. Consequently, this report provides no trial-by-trial source dimension information. However, there was enough useful data to define general source dimension characteristics. Momentum of the exiting gas typically carried the puff centroid to a height of 6 ± 2 m, creating SF_6 puff with a vertical dimension of 4 ± 0.5 m. The initial alongwind puff diameter averaged 7.5 ± 2m. Because the two cylinders were separated by less than 2 m, the number of cylinders used during a release had a negligible effect on source dimensions.

3.2 TRIAL CONCENTRATION SUMMARIES

3.2.1 Detector Placement And Sampling

A. Whole Air Samplers. Thirty whole air samplers were mounted on posts 1.5 m AGL at nominal 300-m intervals along each sampling line. The operators of the six van-mounted continuous analyzers also performed the whole air sampler programming, two being responsible for each sampling line. Upon notification of a trial start time by the test director, operators downloaded to each whole air sampler a start time and a 15-min sampling interval. The two sampling lines closest to the release point were programmed to begin sampling at the projected release time (actual release times were occasionally delayed), while the furthest line of samplers was programmed with a 30-min delay. Once the sampling began, the program stepped through a procedure that sequentially filled Bags 1 through 12. Sampling for each trial was complete upon the sealing of Bag 12 on the sampling line furthest from the source. The sealed bags were taken to the gas laboratory for analysis at the end of each trial.

B. Continuous Analyzers. Upon completion of sampling line programming, the TGA-4000 operators drove their vans to their sampling stations. On the first trial (DSWA01), each pair of vans was stationed on its respective sampling lines (Vans 3 and 4 on Line 1, Vans 1 and 6 on Line 2, and Vans 2 and 5 on Line 3). However, for the remainder of the trials, a decision was made to maximize coverage on the sampling line along Pahute Mesa Road by stationing the vans as indicated in Table 3. This arrangement provided real-time gas concentration readings at 1500-m intervals across Line 2 (see Figure 1).

Table 3. Continuous Analyzer Van Locations by Sampler Station Number.

Van 1	Van 2	Van 3	Van 4	Van 5	Van 6
230	224	212	218	206	201

3.2.2 Sampler Summaries

Concentration measurements obtained by the samplers are archived on a CD produced by ARLFRD. The CD contains three directories: (1) visualization images (Directory: IMAGES) that include Yucca Flat terrain overlaid with MEDA station winds and bargraph depictions of the time variations of SF_6 concentrations; (2) a directory of the time-resolved

TGA-4000 data; (3) a directory of the whole air sampler data in time-position arrays. The IMAGES directory presents an animated depiction of the puff concentration field moving in stages through the sampling lines. The other directories present SF_6 concentration data by position and bag number (whole air sampler data) or by van number and time (TGA-4000 data).

Whole air sampler results were analyzed to obtain normalized concentration maxima and cloud widths (σ_y) for each trial where most of the puff crossed the sampling lines. Normalization was accomplished by dividing the 15-min averaged concentration maxima by source strength as described below. The results are presented in Table 4. The 15-min time resolution available from the whole air samplers is insufficient to resolve alongwind cloud growth (σ_t) dimensions or centroid passage time. Continuous analyzer data and remote imagery were included in the Dipole Pride 26 test to provide better temporal resolution of puff centroid locations. However, because the continuous analyzers were stationed only along Line 2 and the puff imagery has not been analyzed, alongwind cloud dimensions are only available from Line 2. The available σ_t results are summarized in Table 5.

3.2.3 Sampler Quality Control

Watson et al. (1998) use limit of detection (LOD) and limit of quantitation (LOQ) to evaluate TGA-4000 system performance. LOD is the lowest concentration at which SF_6 can be detected, defined as three times the standard deviation of measurements at zero concentration, as determined by analysis of signal noise. The LOQ is defined as the minimum concentration measured with a relative error within ± 30 percent at the 95 percent confidence level (Taylor, 1987). Watson et al. (1998) report LODs ranging from 15 to 42 pptv and LOQs ranging from 50 to 140 pptv for the six TGA-4000 units deployed during Dipole Pride 26.

Whole air sampler quality control included a well-defined series of procedural steps designed to minimize loss, contamination, and mislabeling of samples as well as the use of duplicate samples, blanks, and spikes to define accuracy and precision. Sampler quality control and performance are described in detail by Watson et al. (1998). A total of 19,688 samples were collected. Of these, 1,386 were rendered unusable, yielding a data recovery rate of 93 percent. In addition, the released puff apparently missed the sampling lines during Trials 1, 2, 8, and 10. Consequently, sampler data from these trials were not processed and are not included in the trials tabular data. This reduces the available sampler data to 77 percent.

LOD baseline, accuracy, precision, and threshold are figures of merit for whole air sampler measurements. Whole air sampler baseline and accuracy were determined using blanks and spikes. A blank is a sample collected using the standard sampling protocol, but with the bags within the sampler cartridge containing only ultra high purity air. A spike is a set of sampler cartridges containing a known concentration of SF_6 that is subject to the same processing as test data. Analysis of 455 blank samples yielded a mean of 4 pptv with a standard deviation of 7 pptv. This result produces an LOD baseline of 21 pptv. Spike analysis produced a mean spike-to-standard difference of 6 pptv with a standard deviation of 15 pptv. Watson et al. (1998) define system accuracy at ± 15 pptv. Whole air sampler precision was determined by comparing the results from sets of duplicate samplers positioned on sampling Stations 115, 215, and 315. These duplicate samples were divided into three ranges for analysis: 0 to 100, 100 to 500, and greater than 500 pptv. Watson et al. (1998) estimate precision at the 95% confidence level as ±42% for the 0 to 100 range, ±32% for the 100 to 500 range, and ±12% for concentrations greater than 500 pptv. Threshold considerations include the effects of analytical uncertainties and

any atmospheric background accumulation of SF_6. Accordingly, samples of measurements taken from bags exposed to ambient air not in the vicinity of the puffs were selected for statistical analysis. These samples produced a mean concentration of 4.5 pptv with a standard deviation of 1.73. There was also no noticeable increase in the SF_6 background levels from the beginning to the end of the trials program. The background threshold, the lowest likely non-zero reading to be obtained from whole air samplers operating in background air, is taken as three standard deviations beyond the sample mean, or 9.7 pptv. The range between threshold and LOD baseline concentration levels (~10 to 21 pptv) is a "grey area" in which measurement results are greater than those expected from the SF_6 background, but less than the baseline concentration expected at the edge of a well-defined SF_6 puff. Concentration measurements in this range are associated either with fugitive emissions from a leaking disseminator, or with the periphery of a very diffuse puff.

3.2.4 Puff Width Estimates

The whole air sampler data available for each trial consist of samples from 30 crosswind sampler positions along each of the three lines. Whole air samplers mounted at the sampling positions provided 12 (Bags 1 through 12) time-sequenced concentration measurements, generating a 30 x 12 array of concentration measurements at each sampling line. Figure 2 depicts this array for the middle sampling line of Trial DSWA12. The 15-min sampling intervals set for each bag provided insufficient temporal resolution to estimate centroid passage time or σ_t. However, the 300-m sampler line spacing usually provided a sufficient number of above-threshold concentration measurements along each sampling line (a minimum of six is desirable) to generate histograms of the lateral puff concentration distribution. Gaussian fits to these histograms were used to determine puff width sigmas (σ_y). "Best estimates" of σ_y were obtained using the following procedure:

1. Define a coordinate system. The DP26 field test domain was bounded in latitude by the north and south puff release positions (N2, N3, S2, and S3), and in longitude by sampling positions that define the east and west ends of each sampling line. Watson et al. (1998) provide latitude and longitude measurements for each sampler station and puff release position. The position of a puff crossing a sampling line was determined by the location of its centroid relative to the sampler positions, where the centroid was defined as the center of mass of the concentration distribution. To determine the centroid location, a coordinate system was established along each line with a local origin at each line's eastern-most sampling position (130 for Line 1, 230 for Line 2, 330 for Line 3). All other samplers along each line were assigned locations at nominal 300-m increments west of these origins. This arrangement defined a lateral distance in meters from the local origin for every sampler position along each line, and these distances were used with the sampler concentration measurements to create the distance-concentration histograms shown in Appendix B. The histogram centroid distances, determined using procedures described below, were then translated back to latitude/ longitude positions. This centroid position information was used with release position information to determine straight-line distances from the puff's source location to its position as it crossed each sampling line. These distances are listed under "Distance from Source" in Table 4.

2. Determine the puff histogram concentration maximum (C_m). For each 30 X 12 whole air sampler concentration array, the near-surface puff concentration maximum C_m was identified as the sampler position and bag number near the array concentration centroid reporting the maximum concentration. Occasionally, two adjacent bags provided high concentrations (within 10 percent of each other). In this case, the true C_m likely passed between or over both array positions. In these cases, the σ_y computation procedure was performed using each set of bag concentration data. Table 4 lists the 15-min averaged puff C_m presented in pptv and as normalized (divided) by the quantity of SF_6

released (see Table 3) using a conversion procedure described by ASTM Standard Practice D1914-95 (ASTM, 1997B). The normalized C_m are given in units of $m^{-3} \times 10^{-15}$.

3. Define a puff width histogram. The bag number associated with the puff concentration maximum identifies a row of 30 measurements obtained along a particular sampling line taken during the same 15-min period as the measured concentration maximum. Concentration measurements and position information from the selected row were used to construct the puff width histogram. All sampler position measurements reporting above-baseline concentrations (in excess of 21 pptv) within this time period were used in the histogram. Figure 2 illustrates a whole air sampler concentration array obtained during Trial DSWA12, Line 2 with the concentrations used to define puff width during centroid passage highlighted in bold type. A total of 40 useful histograms, identified in Table 4 by trial name, release time, sampling line number, and bag number, were obtained from the Dipole Pride 26 data set. Appendix B contains additional puff width histogram information, including conversions from bag numbers to sampling times.

For some trials, above-baseline concentrations were measured at the extreme east and/or west sampler positions, indicating that the puff lateral dimensions likely extended beyond the sampler line. If the missing data were well within the tail of the distribution (greater than one standard deviation from the centroid), the missing part of the histogram was filled in using estimates of centroid shape and area to permit statistical analysis of the histogram. Histogram statistics affected by this procedure are enclosed by parentheses in Table 4.

4. Plot the histogram and fit a Gaussian curve. The crosswind spread of diffusing material is traditionally described in terms of a Gaussian σ_y. Although material released into the atmosphere initially has strong concentration gradients at the boundaries, entrainment of clean air into the puff and diffusive mixing quickly destroys these gradients and often creates a crosswind concentration field that resembles a Gaussian distribution. How well a sampled concentration field, as represented by its concentration histogram, fits a Gaussian distribution was described using a goodness-of-fit parameter and the histogram's skewness and kurtosis.

The apparent shape of a puff's crosswind concentration distribution, as represented by its concentration histogram, is influenced by sampler spacing resolution, and the nature of the flow into which it is released. When a small puff passes over only a few crosswind samplers, it typically produces a leptokurtic (exaggerated peakedness) crosswind concentration histogram as a consequence of poor spatial resolution. This effect is evident in some of the concentration histograms obtained from puffs crossing the nearest sampling line. As the puff continues to expand while moving downwind, it progressively crosses more sampling stations on a crosswind line and the sampler spacing-induced leptokurtic effect diminishes. With progressively greater mixing, the histogram eventually assumes a platykurtic (exaggerated flatness) profile. Wind shear and divergence can also skew the concentration distribution and/or create secondary peaks, causing the concentration field to resemble a skewed and/or bimodal distribution. Therefore, the concentration-distance histograms are characterized in Table 4 using a "best-fit" σ_y supplemented by the coefficients of skewness and kurtosis and a measure of the mean square departure from the idealized Gaussian distribution.

The histogram analysis procedure began with keying position and concentration data into the Jandel Scientific SigmaPlot® graphing program. A transform "GAUSq.XFM" was written to operate on these data. GAUSq.XFM calculates the histogram area (A), puff centroid (center of mass) position along the sampling line, "best-fit" σ_y, and the mean square error of the Gaussian curve fit to the histogram data. The best-fit σ_y is the one that simultaneously matches histogram area (retaining mass continuity) and minimizes the least-squares error in the Gaussian fit to the histogram data.

Location	Bag 1	Bag 2	Bag 3	Bag 4	Bag 5	Bag 6	Bag 7	Bag 8	Bag 9	Bag 10	Bag 11	Bag 12
201	3	4	5	4	4	5	3	5	5	3	4	6
202	3	3	18	3	3	5	3	3	3	3	2	3
203	3	3	**36**	3	3	3	3	3	3	3	3	2
204	3	6	**44**	8	3	3	4	3	3	3	4	3
205	5	3	**37**	9	3	6	3	5	6	4	6	5
206	3	5	**56**	5	3	2	4	3	3	6	4	5
207	3	3	**52**	3	3	3	3	3	3	2	3	2
208	2	5	**44**	3	2	2	3	3	3	3	3	3
209	3	5	**52**	7	6	3	7	3	4	4	3	4
210	3	7	**89**	11	9	3	3	4	3	8	3	3
211	3	3	**98**	11	3	3	3	3	3	2	3	3
212	3	8	**96**	15	0	3	7	6	5	4	3	5
213	4	5	**78**	18	5	5	4	**43**	5	5	5	5
214	3	8	**82**	31	4	5	7	**56**	6	5	5	3
215	3	3	**80**	34	3	3	3	**93**	36	2	3	3
216	4	4	**78**	34	3	4	5	**69**	30	3	4	4
217	3	4	**100**	35	3	4	5	**53**	26	4	3	3
218	3	3	**119**	39	4	4	6	**62**	23	3	3	3
219	2	7	**133**	56	9	6	7	**45**	24	6	5	5
220	2	3	**99**	72	3	4	8	**14**	24	3	4	6
221	3	7	**114**	75	5	7	3	**28**	23	5	3	8
222	3	6	**119**	62	5	5	6	**22**	29	4	4	6
223	2	2	**121**	54	3	3	3	12	18	3	2	3
224	2	3	**107**	53	3	2	3	3	20	3	2	3
225	3	6	**84**	39	5	7	3	7	20	9	7	6
226	4	4	**61**	29	5	4	5	5	12	5	4	4
227	2	2	**38**	4	6	4	3	5	14	3	7	5
228	2	2	**39**	3	3	3	3	2	3	3	3	2
229	2	4	6	3	5	3	3	2	3	2	3	3
230	3	3	13	4	3	7	3	3	6	3	3	6

Figure 2. Sulfur hexafluoride concentrations in pptv arrayed by bag number and whole air sampler location along Line 2 during Trial DSWA12 following puff releases at 0900 and 1030 PST on 15 November 1996. Puff concentration data included in puff width histograms (described in 3.2.4) are indicated in bold type. Bag 1 provides the time-mean concentration during the first 15-min time period after dissemination, followed successively by Bags 2 through 12.

Table 4. Dipole Pride 26 Lateral Dispersion Summary (time in PST).

Trial Name	Release date/time (JJJhhmm)	Line Number	Bag Number	Distance from Source (m)	Observed Maximum Concentration (pptv)	Observed Maximum Concentration ($m^{-3} \times 10^{-15}$)	Best Fit σ_y (m)	Coefficient of Skewness (ND)	Coefficient of Kurtosis (ND)	Normal Departure (%)	Crossing Angle (degrees)
DSWA03	3130400	1	1	1731	14244	6.577	139	0.091	0.745	6.7	83
DSWA03	3130400	2	3	10726	1725	0.795	(999)	(0.169)	(1.511)	(27.0)	83
DSWA03	3130400	3	8	17187	97	0.046	1163	0.589	2.082	41.7	71
DSWA03	3130400	3	9	17273	90	0.043	962	0.267	2.498	19.1	69
DSWA04	3140400	1	1	1989	13966	6.762	431	-0.601	2.608	22.4	70
DSWA04	3140400	2	3	11456	1304	0.633	1323	0.405	2.281	33.1	70
DSWA04	3140400	2	4	12023	1633	0.794	(580)	(0.352)	(3.315)	(15.4)	66
DSWA04	3140538	1	8	2564	7823	3.779	509	0.165	2.170	37.9	70
DSWA04	3140538	3	11	17542	158	0.075	(1661)	(0.208)	(0.937)	(28.9)	85
DSWA05	3160440	1	3	3945	7093	3.455	239	0.675	4.305	21.7	78
DSWA05	3160440	2	6	11752	2148	1.044	(999)	(-0.016)	(0.429)	(40.4)	73
DSWA05	3160440	3	10	18505	672	0.327	(994)	(0.187)	(0.744)	(56.3)	74
DSWA06	3170400	1	2	2284	9889	4.792	374	0.257	1.532	77.9	76
DSWA06	3170400	2	7	12806	3240	1.569	453	0.729	3.058	34.6	48
DSWA06	3170400	3	10	18888	819	0.400	1379	2.394	7.774	111.7	74
DSWA07	3171300	1	4	19858	385	0.104	(2335)	(0.853)	(2.752)	(57.5)	46
DSWA07	3171300	2	3	10893	634	0.172	924	0.127	1.932	32.1	78
DSWA07	3171300	3	2	4991	4625	1.262	(422)	(-0.025)	(0.276)	(59.2)	82
DSWA09	3181400	1	4	18975	174	0.090	(1250)	(0.136)	(2.302)	(13.7)	72
DSWA09	3181400	2	4	10743	661	0.341	831	-0.164	2.152	18.9	70
DSWA11	3191551	1	7	2336	27582	13.770	159	-0.028	12.765	3.9	80
DSWA11	3191551	2	10	12334	4890	2.441	597	-0.141	1.288	15.1	60
DSWA11	3191551	3	11	18788	924	0.468	1087	0.564	2.365	24.7	73
DSWA12	3200900	2	3	13013	133	0.062	2028	0.275	1.849	22.7	73
DSWA12	3200900	3	3	18987	125	0.060	(1604)	(0.356)	(2.367)	(20.1)	73
DSWA12	3201030	1	7	2917	5173	2.421	207	0.006	2.324	7.5	55
DSWA12	3201030	2	8	13033	93	0.044	768	-0.263	0.933	27.1	74
DSWA13	3201430	1	1	2438	8190	2.002	106	-3.150	98.607	7.6	78
DSWA13	3201430	2	2	13325	303	0.074	513	0.223	4.510	16.2	67
DSWA13	3201430	3	1	19222	89	0.022	(570)	(-0.026)	(2.568)	(18.1)	68
DSWA14	3211300	1	3	20865	273	0.070	(1239)	(-0.268)	(2.323)	(14.0)	79
DSWA14	3211300	3	2	4426	2502	0.647	267	0.4856	4.768	24.0	70
DSWA15	3231130	2	4	10115	199	0.099	1126	0.220	2.231	23.7	84
DSWA15	3231130	3	2	4215	824	0.410	457	-0.149	0.530	32.9	87
DSWA15	3231300	3	7	4296	1154	0.305	220	0.564	3.316	16.8	80
DSWA16	3241330	1	8	20385	102	0.027	1508	-0.250	2.332	19.8	80
DSWA16	3241330	2	8	10806	894	0.233	434	0.622	4.700	13.5	65
DSWA16	3241330	3	7	4197	3555	0.927	218	0.808	3.783	36.7	80
DSWA17	3251200	2	3	10763	753	0.193	(693)	(0.489)	(2.210)	(25.3)	87
DSWA17	3251330	1	9	20359	170	0.045	(2917)	(-0.148)	(1.956)	(27.2)	85

For each Gaussian curve of area A and dimension σ_y, there is a unique concentration maximum C_g defined by

$$\sigma_y C_g = A/(2p)^{0.5} \quad . \qquad (3\text{-}1)$$

Thus, the $\sigma_y C_g$ product defines a family of curves where either s_y or C_g can serve as an independent variable. If the histogram C_m is specified as C_g, Equation (3-1) defines a σ_y for the Gaussian profile that matches the histogram concentration maximum. However, this s_y may not provide the best least-squares fit to the entire histogram. As noted above, the best least-squares fit was obtained by iterative convergence. Because the SigmaPlot® transform programming does not provide a capability to converge on the best Gaussian fit to histogram data, the best-fit σ_y was obtained by running several consecutive solutions for GAUSq.XFM. GAUSq.XFM includes one σ_y solution with the histogram C_m input as C_g (Solution 1), a second solution which calculates a s_y using the standard second-moment statistical methodology (see Kendall and Stuart, 1963), and a third "intermediate" solution based on a mean C_g derived from the concentration maxima for Solutions 1 and 2. The original C_m-based solution usually produced a relatively small σ_y for the Gaussian curve fitted to the histogram maximum concentration, which may be the σ_y of greatest interest if predicting the maximum concentration is the primary modeling objective. The second (Kendall and Stewart) solution typically produced a larger σ_y (and smaller C_g) than the first solution, with the third solution producing σ_y and C_g intermediate between the first two. Figure 3 illustrates a sample histogram with the three fitted Gaussian curves. GAUSq.XFM calculated the mean square error of each fit to the histogram and normalized it by the total histogram concentration ΣC_i. Convergence was achieved by repetitively solving the transform using C_g estimates that produced progressively smaller mean square errors. Sufficient convergence was achieved when the difference in normalized error between any two successive GAUSq.XFM solutions produced error differences that were less than 10 percent of the minimum normalized error. For each puff, Table 4 gives the best-fit Gaussian σ_y and its error (listed as "normal departure, %"). An additional transform (Gausfit.XFM) provided histogram coefficients of skewness and kurtosis using the method described in Kendall and Stuart (1963). These statistics are also presented in Table 4. Appendix B contains printouts of the Gausfit and GAUSq transforms, plots of each histogram, and the best-fit Gaussian curve.

Final considerations for lateral dimension determination include detachment of the puff centroid from the surface and blending of the puff into the background. When the bulk of the puff is detached from the surface, the lateral dimension σ_y indicated by the concentration measurements along the sampling lines may not represent the actual puff σ_y. For example, centroid liftoff was observed on Line 3 during release 3181400. This puff lofted the first sampling line, producing a small C_m and an uncertain σ_y. No histograms or σ_y estimates are presented for this event because they may not be representative of values at the elevation of the plume centroid.

As a puff proceeds downrange, it becomes progressively more dilute and eventually blends into the background. Accurate determination of σ_y becomes difficult when puff concentrations diminish to magnitudes between threshold and baseline concentration levels. The point at which σ_y can no longer be determined using the present methodology is subjective, as the dilution process is gradual and "grey area" puff concentrations affect most puff dimension estimates to some degree. Because puff or plume borders are often defined at 10 percent of the maximum concentration, the puff σ_y estimates in this report are based on only those histograms that contained a maximum concentration in excess of 10 times the threshold (>97 pptv). Other puff histogram data were considered too dilute for accurate σ_y determination.

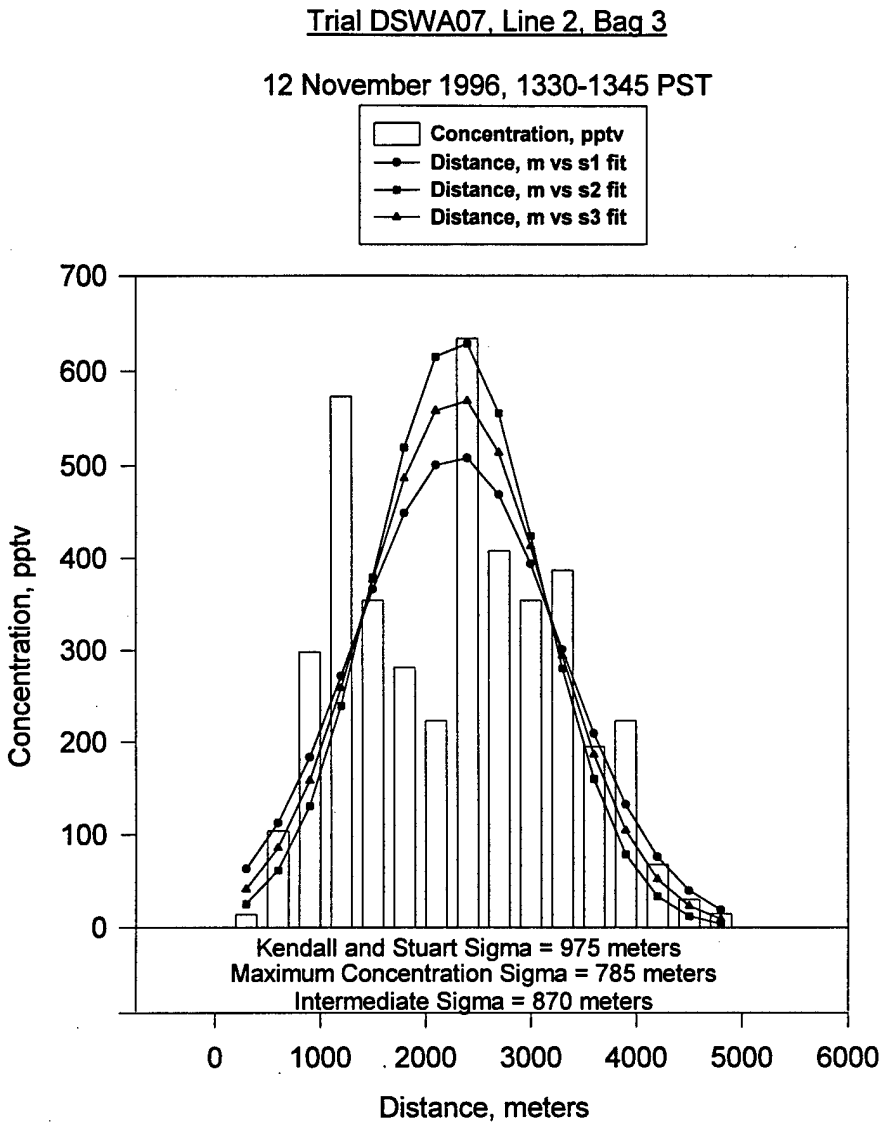

Figure 3. Test DSWA07, Line 2, Bag 3 (30-45 minutes after puff release) histogram and Gaussian curves obtained using three fit methods used in GAUSq.XFM.

5. Compute puff crosswind σ_y using 16-84 percentiles from the histogram CDF. The sampler position and concentration information used to calculate the best-fit s_y (Step 4 above) was also used to obtain independent histogram σ_y estimates based on the 16th and 84th percentiles of the concentration cumulative distribution function (CDF). Because 68 percent of the area under a normal curve falls with ±1 standard deviation of the mean, the distance between the locations of the 16th and 84th percentiles spans 2 sigmas. Dr. Steven Hanna (personal communication) considers this sigma estimation method, which requires interpolation to locate the 16th and 84th percentile positions within the histogram, to be more robust than the moment method. Sigma estimates obtained using the "Best-Fit" and "16-84" methods were nearly identical (within ±10%) for most cases, and differed markedly for only two cases (DSWA06, Line 3; DSWA14, Line 1) where the concentration distributions were strongly skewed and had a poor fit to the Gaussian distribution.

6. Calculate puff travel distances and crossing angles at each sampler line. The latitude and longitude of each puff centroid crossing position was calculated using the puff centroid line crossing position determined in Step 2 above. These, along with the latitude and longitude of the appropriate release position, were used to compute the distances in meters between each puff's origin and its positions as it crossed the sampling lines. The source-to-sampler line crossing distances are shown under the column labeled "distance from source" in Table 4. The distances were originally calculated using the assumption of a spherical earth. Recalculation with corrections for the oblate spheroid shape of the earth produced distances diminished by a factor of 0.2 percent. The distances presented in Table 4 and Table 5 include this correction.

The sampling line segments at the point of puff crossing were often not straight, nor were they normal to the wind direction. This suggests a need to consider the apparent increase in a puff's σ_y as it crosses a sampling line at an angle of less than 90 degrees. The puff crossing angle was determined by the approach angle of the puff centroid to the line that it crossed. Puff crossing angle estimates were obtained by plotting puff centroid tracks from the puff origin to each successive sampling line crossing position. Crossing angle results presented in Table 4 only estimate the puff centroid crossing angle. Most of the crossing angles were found to be large (>45 degrees), indicating that crossing angle effects on the magnitude of σ_y are small. The σ_y information provided in Table 4 are not adjusted for crossing angle.

3.2.5 Puff Alongwind Dispersion Estimates

The 15-min whole air sampler time resolution was insufficient to determine puff arrival and passage times with the desired accuracy. However, the 4-Hz resolution of the TGA-4000 measurements provided detailed alongwind histogram data that permitted a precise determination of puff centroid times of arrival and transport speeds. The difference between the time of a puff's release and the arrival of its centroid at a sampling line defines puff travel time, and the straight-line distance traveled by the puff centroid from its source to a sampling line divided by puff travel time yielded a transport speed. Puff release time, centroid arrival time, and transport speed are included in Table 5. Puff statistical summary data are missing for Trial DSWA11 because the gas concentration dilution system had not been turned on, causing overranging at concentrations in excess of 6934 pptv.

Two continuous analyzers were initially stationed on each sampling line, but after Trial DSWA01 all six continuous analyzers were stationed at positions along Line 2 to maximize the probability of the puff centroid passing near at least one of these instruments. Thus, alongwind puff dimension estimates are available only for puffs crossing Line 2.

Table 5. Dipole Pride 26 Alongwind Dispersion Summary.

Trial Name	Release date/time (JJJhhmm)	Position Number	Distance from Source (m)	Peak Concentration (pptv)	Peak Concentration ($m^{-3}X10^{-15}$)	Best Fit Sigma t (s)	Coefficient of Skewness (ND)	Coefficient of Kurtosis (ND)	Normal Departure (%)	Centroid Transport Arrival (hhmmss)	Centroid Transport Speed (m/s)
DSWA03	3130400	206	10726	2891	1.332	215	0.656	2.896	25.0	043519	5.06
DSWA04	3140400	224	11817	5088	2.474	134	0.686	3.218	21.6	044331	4.52
DSWA05	3160440	201	11437	2475	1.203	918	0.010	2.023	14.0	055545	2.51
DSWA06	3170400	212	12304	2875	1.392	969	0.615	2.648	34.0	051209	2.84
DSWA07	3171300	224	10813	1803	0.489	104	-0.001	0.104	32.2	134513	3.98
DSWA07	3171300	230	10902	1895	0.514	177	0.834	2.802	37.9	134806	3.78
DSWA07	3171447	230	10902	4157	1.128	103	0.502	2.361	26.3	153622	3.68
DSWA11	3191551	212	12304	*M	M	M	M	M	M	165522	3.18
DSWA12	3200900	218	13151	352	0.164	214	0.173	2.398	22.0	094148	5.24
DSWA12	3201030	218	13151	835	0.389	101	0.437	2.013	35.4	105827	3.75
DSWA14	3211300	201	11589	818	0.210	175	-0.195	1.058	36.9	133730	5.15
DSWA16	3241200	224	10813	443	0.115	190	-0.316	1.003	36.4	123720	4.83
DSWA16	3241330	206	11090	3084	0.804	99	0.009	0.016	30.7	135817	6.53
DSWA17	3251200	224	10813	1677	0.430	74	-0.383	1.696	28.5	123639	4.92
DSWA17	3251330	201	11589	897	0.230	165	0.428	2.373	20.7	141028	4.77

*M = missing. Concentration measurements in excess of 6934 pptv are truncated.

The transforms described in Section 3.2.4 and a methodology similar to that used for puff width estimates were also applied to alongwind concentration histograms. The coordinate system used to define puff release and sampler positions was also used to define the distance from the source to centroid arrival at Line 2. The best-fit σ_t defined the puff alongwind dimension. Table 5 presents alongwind puff characteristics, including departure of the puff time histogram data from the best-fit Gaussian curve and histogram skewness and kurtosis.

3.3 MICROMETEOROLOGICAL SUMMARIES

3.3.1 Statistical Summaries

Sonic anemometer/thermometer wind and temperature component measurements at the BJY and YFW sites were reduced to 15-min averaged statistical summaries for the duration of each trial. This averaging produced micrometeorological statistics for periods that correspond to the MEDA data and whole air sampler averages. The statistical summaries presented in Appendix A of this report include the most relevant mean and second moment quantities: the mean wind speed and direction, horizontal wind angle standard deviation, alongwind and crosswind velocity variances, and fluxes of temperature and momentum. These 15-min averaged quantities were also used to define the trial-averaged stabilities in Table 6.

3.3.2 Roughness Length Estimates

The principal application of surface roughness length z_o is as a constant in the logarithmic wind profile equation. It is a parameterization of the degree of obstruction to free flow presented by a surface to air moving over a surface. Both the size and spacing of flow obstructions contribute to the magnitude of z_o. When flow is reasonably steady and fully turbulent, the wind speed at z is related to friction velocity u_* and z/z_o by

$$u_z = (u_* / k)\,[\ln(z / z_o) + \psi_m], \tag{3-1}$$

where k is the von Karman constant (0.4 ± 0.02) and ψ_m is a stability-dependent diabatic influence function. The diabatic influence function approaches zero as heat flux approaches zero. Thus, the logarithmic wind profile equation provides a means of solving for z_o in quasi-steady near-neutral conditions when rearranged as follows:

$$z_O = z\ e^{(-ku_z / u_*)}. \tag{3-2}$$

The 15-min micrometeorological summaries obtained from the sonics at BJY and YFW were examined for cases of steady, fully developed turbulent flow. Equation (3-2) was used in these cases to solve for z_o. This procedure yielded a z_o of 0.032 m with a standard deviation of 0.012 m at BJY, and an average z_o of 0.045 m with a standard deviation of 0.026 m at YFW. Because YFW is on the edge of the Yucca Lake salt flat, southerly flow over the relatively open lake bed encounters less roughness than northerly flow over the more densely vegetated lake bed rim. Northerly flow over YFW produced a z_o of 0.061 m with a standard deviation of 0.029 m, while southerly flow at YFW yielded a z_o of 0.032 m and a standard deviation of 0.016 m.

3.3.3 Boundary Layer Stability

The stability of the atmospheric layer into which a puff is released can be used to parameterize the turbulence available to disperse the puff material. Stability can be parameterized in various ways ranging from a simple Pasquill-Gifford methodology (usually

based on wind speed, cloud cover, and sun angle) to the Obukhov length L, which is inversely proportional to the ratio of buoyancy and shear terms in the turbulent kinetic energy equation. Surface weather observations and MEDA station data are sufficient for the Pasquill-Gifford methodology, while the sonic data from BJY and YFW provide the fluxes of heat and momentum that can be used to calculate L. Table 6 lists the wind speed and cloud cover information required for the Pasquill-Gifford methodology along with friction velocities, temperature fluxes, and estimates of L derived from sonic data.

The trial-averaged friction velocity, temperature flux, and Obukhov length estimates presented in Table 6 were calculated using the 15-min averaged sonic statistical summaries provided in Appendix A. Although the 15-min average is somewhat arbitrary and truncates some of the low frequency motions acting on the puff, this averaging period is expected to capture most of the energy involved in the internal mixing of puff material. The scales of motion eliminated by this "high pass" filtering are more likely involved with gross puff movement or displacement.

A major advantage of using a sonic anemometer/thermometer is that the higher order statistics needed to characterize the state of the atmospheric boundary layer can be obtained directly from the measurements using eddy correlation techniques. However, it is often difficult to obtain statistically stable and representative momentum and temperature fluxes, particularly during light winds. Busch and Panofsky (1968) recognize this problem and consider direct momentum flux measurements to be unreliable when the friction velocity is less than 0.32 m/s. Fortunately, momentum flux is strongly correlated with the standard deviation of vertical velocity σ_w. Biltoft (1997) finds that a σ_w/u_* ratio of 1.3 can provide reasonable u_* estimates under low wind conditions. This ratio was used to estimate u_* in the low wind speed cases where reliable eddy correlation measurements of friction velocity were not available.

Temperature flux measurements during light winds are also problematic. A quiescent nocturnal boundary layer is characterized by small vertical motions that are poorly correlated with small temperature fluctuations punctuated by intermittent turbulence bursts. A majority of the vertical heat transfer occurs during these intermittent bursts. Although the long term net area temperature flux must be downward, individual turbulence bursts observed using measurements at a single site may produce results of either sign. Consequent-ly, there can be considerable uncertainty in the representativeness of tempera-ture flux measurements obtained from a single measurement location in a quiescent nocturnal boundary layer. These conditions were observed at YFW during the early morning releases. The resultant temperature flux and Obukhov length calculations are suspect, especially for Trials DSWA03 and DSWA06.

3.4 MEDA STATION AND UPPER AIR DATA

MEDA station data available during Dipole Pride 26 include 15-min measurements of wind speed, wind direction, temperature, and pressure. The most relevant MEDA stations (those located in or near Yucca Flat) are indicated on Figure 1 and in Table 1. Upper air summaries include hourly pibal flights interspersed with radiosonde flights taken every 3 hours. The pibal flights were launched from DIGIPID stations at BJY, UCC, and CSE and radiosonde flights were launched from the UCC site. MEDA station, pibal, and radiosonde flight data are available on disk and on CD.

3.5 PUFF IMAGERY

Aerospace Corporation used infrared imagers and FTIRs to document the position of each puff as it progressed downwind from the release point. In some cases, the puff was tracked well beyond the most distant sampling line. Of particular relevance to this data set is the position information obtained as the puff centroids crossed the sampling lines. This

information is needed to define transport wind speeds and to determine whether the centroid was in contact with the surface-based sampler arrays or passed over them. Unfortunately, puff imagery was not available before the completion of this report.

Blank Page

SECTION 4. CONCLUSIONS AND RECOMMENDATIONS

The Dipole Pride 26 test program produced a comprehensive set of long range puff dispersion data accompanied by extensive meteorological measurements. Some puffs were tracked to distances in excess of 20 km, providing an opportunity to validate both the transport and diffusion components of integrated wind field and dispersion model systems. This report presents puff σ_y and σ_t summaries obtained from tracer concentration measurements along with trial micrometeorological statistics. Data sets on CD ROM supplement the summaries presented in this report. With the exception of unanalyzed puff imagery, this report and the associated CD ROM constitute a fairly complete documentation of the Dipole Pride 26 test program. Analysis of the Aerospace Corporation puff imagery could provide valuable information on puff vertical dimensions and would provide independent estimates of puff arrival times and transport speeds.

The 15-min averaged micrometeorological statistics from BJY and YFW exhibit interesting features that deserve further study. The fluxes and variances sometimes change by more than an order of magnitude from one 15-min period to the next and vary greatly between sites, indicating the presence of terrain-induced non-stationarity and inhomogeneity representative of dispersion conditions in mountain-valley desert terrain. Detailed analysis of micrometeorological conditions and related puff behavior are beyond the scope of this report, but terrain-induced differential heating and cooling appeared to exert major influences on puff behavior. Differential heating of mountain slopes created local flows that sometimes drew puff material up the slopes rather than along the major axis of the valley. Also, cold air draining from the north often pools in the Yucca Lake basin during the early morning hours. These pools of confined cold air stagnate over Yucca Lake until post-sunrise surface heating destroys them. Puffs released into this early morning drainage often did not clear Yucca Lake until several hours after sunrise.

Table 6. Dipole Pride 26 Atmospheric Stability Summary.

Trial Name	Release date/time (JJJhhmm)	10 m Wind Speed (m/s)		Cloud Cover (tenths)	Cloud Height (m)	Friction Velocity (m/s)		Temperature Flux (m °K/s)		Obukhov Length (m)	
		BJY	YFW			BJY	YFW	BJY	YFW	BJY	YFW
DSWA01	3091441	2.7	3.7	9	7600	.2467	.2766	.0113	-.0022	-98	707
DSWA03	3130400	3.8	2.0	0	--	.1747	.0466	-.0194	.0007	19	-10
DSWA04	3140400	4.9	3.2	3	7600	.2331	.0794	-.0342	-.0039	26	9
DSWA04	3140538	5.1	2.4	1	7600	.2538	.0942	-.0188	-.0080	634	8
DSWA05	3160440	2.4	0.8	10	6100	.0516	.0535	-.0008	-.0032	12	3
DSWA06	3170400	2.6	0.7	10	7600	.0563	.0524	-.0004	.0011	32	-9
DSWA07	3171300	4.1	3.5	10	7600	.2942	.2183	.0795	.0340	-24	-23
DSWA07	3171447	4.4	3.1	10	7600	.2671	.1529	.0352	-.0031	-41	88
DSWA09	3181400	3.0	1.5	5	4300	.1955	.1734	.0122	.0020	-46	-192
DSWA11	3191430	3.1	2.7	5	9150	.1915	.1837	.0170	.0036	-30	-127
DSWA11	3191551	3.2	2.4	8	7600	.1199	.1115	-.0159	-.0116	8	9
DSWA12	3200900	5.1	4.0	10	6100	.3974	.3064	.0634	.0466	-72	-44
DSWA12	3201030	7.1	3.3	5	2130	.4997	.2637	.1292	.0532	-71	-25
DSWA13	3201430	7.7	6.8	8	1830	.5658	.5357	.0078	.0175	-1709	-645
DSWA14	3211300	4.7	4.2	1	7600	.3430	.2865	.1034	.0789	-28	-22
DSWA15	3231130	2.4	3.5	3	1220	.3042	.3450	.0988	.1200	-21	-25
DSWA15	3231300	5.0	4.4	2	1220	.3900	.3230	.1025	.0716	-43	-35
DSWA16	3241200	4.9	4.2	1	7600	.3403	.3679	.1180	.1126	-25	-33
DSWA16	3241330	5.3	7.0	8	6100	.3616	.4783	.0526	.0264	-67	-308
DSWA17	3251200	5.0	3.8	1	7600	.3418	.2560	.1387	.0809	-22	-15
DSWA17	3251330	4.9	4.5	2	7600	.2937	.2531	.0591	.0386	-32	-31

SECTION 5. APPENDICES

APPENDIX A. MICROMETEOROLOGICAL SUMMARIES

The micrometeorological summaries include 15-min averages of sonic anemometer/thermometer measurements made at BJY and YFW. The measurement height was 10 m AGL. The summaries include average wind speed and direction, horizontal wind angle standard deviation (σ_θ), alongwind velocity variance ($\overline{u'u'}$), vertical velocity variance ($\overline{w'w'}$), vertical sonic temperature flux ($\overline{w'T'}$), and momentum flux ($\overline{u'w'}$).

Dipole Pride 26 Micrometeorological Data Summary

Trial: DSWA01 Release Julian Date/Time: 3091445 Date/Time (PST): 04 November 1445-1730 Source Location: S2

Start Time (UTC)	BJY WS (m/s)	YFW WS (m/s)	BJY HD (Deg)	YFW HD (Deg)	BJY σθ (Deg)	YFW σθ (Deg)	BJY u'u' (m^2/s^2)	YFW u'u' (m^2/s^2)	BJY w'w' (m^2/s^2)	YFW w'w' (m^2/s^2)	BJY w'T' (mT/s)	YFW w'T' (mT/s)	BJY u'w' (m^2/s^2)	YFW u'w' (m^2/s^2)
2245	3.6	4.1	183	195	17.9	16.7	0.690	1.041	0.202	0.206	.0497	.0287	-.0849	-.1568
2300	3.9	4.1	193	195	29.3	13.7	1.763	1.107	0.206	0.157	.0472	.0184	-.0787	-.0997
2315	3.4	4.7	227	200	16.5	12.4	0.756	1.150	0.129	0.179	.0307	.0129	-.0728	-.1194
2330	2.6	4.2	237	199	13.8	10.9	0.850	0.746	0.103	0.158	.0101	-.0064	-.0433	-.0686
2345	2.8	3.8	226	203	10.6	9.6	0.414	0.390	0.100	0.107	-.0078	-.0051	-.0715	-.0623
0000	2.3	4.0	231	212	12.3	10.0	0.387	0.866	0.065	0.155	-.0043	-.0209	-.0168	-.1296
0015	1.9	3.3	239	210	14.5	8.5	0.202	0.413	0.063	0.079	-.0164	-.0208	-.0375	-.0324
0030	2.0	3.1	268	206	16.1	9.0	0.083	0.477	0.032	0.085	-.0083	-.0196	-.0038	-.0283
0045	1.8	2.3	291	219	12.5	10.6	0.191	0.168	0.026	0.038	.0006	-.0066	.0074	-.0119
0100	1.2	M*	270	M	21.9	M	0.133	M	0.029	M	-.0108	M	-.0090	M
0115	1.2	M	344	M	21.5	M	0.091	M	0.017	M	.0047	M	.0012	M

* Missing

Dipole Pride 26 Micrometeorological Data Summary

Trial: DSWA03 Release Julian Date/Time: 3130400 Date/Time (PST): 08 November 0400-0700 Source Location: N3

Start Time (UTC)	BJY WS (m/s)	YFW WS (m/s)	BJY HD (Deg)	YFW HD (Deg)	BJY σθ (Deg)	YFW σθ (Deg)	BJY u'u' (m^2/s^2)	YFW u'u' (m^2/s^2)	BJY w'w' (m^2/s^2)	YFW w'w' (m^2/s^2)	BJY w'T' (mT/s)	YFW w'T' (mT/s)	BJY u'w' (m^2/s^2)	YFW u'w' (m^2/s^2)
1200	3.4	1.6	337	348	10.6	8.4	0.619	0.184	0.062	0.003	-.0212	.0002	-.0216	-.0042
1215	4.3	2.4	335	348	5.3	4.5	0.307	0.049	0.039	0.001	-.0241	.0014	-.0424	-.0009
1230	3.7	2.9	340	354	6.7	3.1	0.363	0.086	0.024	0.002	-.0113	.0028	-.0123	.0037
1245	3.9	2.8	336	350	4.2	4.6	0.204	0.081	0.023	0.003	.0004	.0024	-.0008	.0012
1300	3.5	2.6	336	350	6.1	5.4	0.333	0.070	0.028	0.003	-.0112	-.0083	-.0169	-.0015
1315	4.1	3.1	331	349	6.4	6.0	0.462	0.063	0.077	0.002	-.0362	.0013	-.0683	.0015
1330	4.9	1.8	325	350	4.9	14.1	0.284	0.902	0.083	0.013	-.0350	-.0029	-.0579	.0028
1345	4.8	1.6	321	353	5.0	16.9	0.225	0.110	0.063	0.006	-.0290	-.0009	-.0407	.0020
1400	4.5	0.4	321	357	5.2	36.0	0.322	0.121	0.151	0.002	-.0320	-.0006	-.0441	.0022
1415	3.5	0.8	333	360	7.1	13.6	0.321	0.127	0.038	0.002	-.0193	.0012	-.0304	-.0017
1430	3.0	1.3	349	321	12.9	16.3	0.560	0.100	0.024	0.003	-.0137	.0117	-.0230	.0025
1445	2.5	3.0	338	339	5.4	8.8	0.059	0.242	0.007	0.004	-.0070	.0002	-.0041	.0039

Dipole Pride 26 Micrometeorological Data Summary

Trial: DSWA04 Release Julian Date/Time: 3140400 Date/Time (PST): 09 November 0400-0530 Source Location: N3

Start Time (UTC)	BJY WS (m/s)	YFW WS (m/s)	BJY HD (Deg)	YFW HD (Deg)	BJY σθ (Deg)	YFW σθ (Deg)	BJY u'u' (m^2/s^2)	YFW u'u' (m^2/s^2)	BJY w'w' (m^2/s^2)	YFW w'w' (m^2/s^2)	BJY w'T' (mT/s)	YFW w'T' (mT/s)	BJY u'w' (m^2/s^2)	YFW u'w' (m^2/s^2)
1200	4.9	3.2	320	339	4.6	7.4	0.324	0.035	0.087	0.001	-.0340	-.0019	-.0509	.0001
1215	5.5	3.3	321	351	6.4	3.6	0.481	0.033	0.087	0.002	-.0431	-.0001	-.0649	-.0001
1230	4.1	3.5	313	326	7.0	11.6	0.395	0.060	0.093	0.011	-.0284	-.0153	-.0566	.0005
1245	4.4	3.0	314	319	6.0	7.0	0.227	0.114	0.086	0.012	-.0256	.0052	-.0537	-.0003
1300	5.0	3.1	321	329	4.8	10.1	0.301	0.153	0.092	0.026	-.0355	.0079	-.0594	-.0024
1315	5.4	3.0	321	339	5.0	10.7	0.371	0.101	0.106	0.012	-.0385	-.0191	-.0784	-.0032

Dipole Pride 26 Micrometeorological Data Summary

Trial: DSWA04 Release Julian Date/Time: 3140538 Date/Time (PST): 09 November 0530-0800 Source Location: N3

Start Time (UTC)	BJY WS (m/s)	YFW WS (m/s)	BJY HD (Deg)	YFW HD (Deg)	BJY σθ (Deg)	YFW σθ (Deg)	BJY u'u' (m^2/s^2)	YFW u'u' (m^2/s^2)	BJY w'w' (m^2/s^2)	YFW w'w' (m^2/s^2)	BJY w'T' (mT/s)	YFW w'T' (mT/s)	BJY u'w' (m^2/s^2)	YFW u'w' (m^2/s^2)
1330	5.1	2.7	314	324	5.2	15.9	0.247	0.166	0.094	0.006	-.0305	-.0023	-.0614	-.0013
1345	4.9	2.9	310	317	4.3	11.5	0.209	0.107	0.069	0.017	-.0323	.0253	-.0463	-.0002
1400	5.0	2.9	311	351	5.5	11.1	0.253	0.087	0.071	0.013	-.0280	-.0332	-.0482	.0001
1415	5.4	3.7	322	359	5.0	3.2	0.338	0.078	0.111	0.005	-.0335	-.0052	-.0805	.0012
1430	5.7	2.7	322	002	5.2	5.8	0.416	0.202	0.151	0.006	-.0321	-.0115	-.0935	-.0097
1445	5.8	2.2	323	353	5.4	6.6	0.398	0.053	0.148	0.008	-.0236	-.0099	-.0953	.0000
1500	5.4	2.1	327	355	5.1	12.8	0.396	0.163	0.132	0.019	-.0173	-.0162	-.0867	-.0096
1515	4.7	1.1	331	352	7.1	13.4	0.653	0.051	0.088	0.010	-.0010	.0009	-.0649	-.0036
1530	4.8	1.5	341	004	5.1	11.2	0.402	0.181	0.102	0.017	.0056	-.0127	-.0754	-.0135
1545	4.2	2.6	348	007	7.5	12.2	0.586	0.149	0.123	0.049	.0045	-.0152	-.0764	-.0028

Dipole Pride 26 Micrometeorological Data Summary

Trial: DSWA05 Release Julian Date/Time: 3160440 Date/Time (PST): 11 November 0440-0740 Source Location: N2

Start Time (UTC)	BJY WS (m/s)	YFW WS (m/s)	BJY HD (Deg)	YFW HD (Deg)	BJY $\sigma\theta$ (Deg)	YFW $\sigma\theta$ (Deg)	BJY u'u' (m^2/s^2)	YFW u'u' (m^2/s^2)	BJY w'w' (m^2/s^2)	YFW w'w' (m^2/s^2)	BJY w'T' (mT/s)	YFW w'T' (mT/s)	BJY u'w' (m^2/s^2)	YFW u'w' (m^2/s^2)
1240	2.8	0.6	335	048	6.2	17.7	0.083	0.008	0.002	0.001	.0030	-.0003	-.0034	.0003
1255	3.0	1.0	336	024	9.1	9.1	0.020	0.018	0.002	0.001	-.0031	.0001	-.0008	-.0017
1310	3.1	0.5	346	300	3.9	40.8	0.030	0.014	0.002	0.003	-.0004	.0022	.0006	-.0001
1325	3.0	1.1	343	276	7.1	9.5	0.041	0.071	0.002	0.003	.0000	-.0022	-.0001	-.0012
1340	2.9	1.4	346	314	7.6	22.3	0.204	0.138	0.002	0.005	-.0041	-.0051	.0007	-.0001
1355	2.5	1.3	343	028	9.9	14.2	0.135	0.101	0.005	0.004	.0037	-.0305	.0036	-.0019
1410	3.0	0.5	350	288	3.3	38.5	0.056	0.054	0.001	0.002	.0006	-.0041	-.0013	-.0024
1425	2.6	0.7	346	302	4.6	14.5	0.016	0.052	0.001	0.008	-.0020	-.0029	.0003	-.0033
1440	2.1	0.8	346	037	4.2	32.0	0.036	0.069	0.002	0.003	-.0002	.0015	-.0019	.0008
1455	1.7	0.5	001	008	10.2	25.8	0.112	0.068	0.005	0.009	.0000	.0091	.0022	-.0010
1510	1.0	0.9	018	003	14.0	20.4	0.065	0.146	0.013	0.009	-.0043	-.0078	-.0056	-.0091
1525	1.4	0.7	014	061	7.9	28.1	0.067	0.133	0.017	0.010	-.0030	.0021	-.0116	-.0048

Dipole Pride 26 Micrometeorological Data Summary

Trial: DSWA06 Release Julian Date/Time: 3170400 Date/Time (PST): 12 November 0400-0730 Source Location: N2

Start Time (UTC)	BJY WS (m/s)	YFW WS (m/s)	BJY HD (Deg)	YFW HD (Deg)	BJY σθ (Deg)	YFW σθ (Deg)	BJY u'u' (m^2/s^2)	YFW u'u' (m^2/s^2)	BJY w'w' (m^2/s^2)	YFW w'w' (m^2/s^2)	BJY w'T' (mT/s)	YFW w'T' (mT/s)	BJY u'w' (m^2/s^2)	YFW u'w' (m^2/s^2)
1200	2.7	1.7	352	328	9.0	6.6	0.047	0.013	0.002	0.001	-.0019	-.0068	-.0003	-.0013
1215	3.1	1.6	335	335	4.4	6.2	0.040	0.008	0.003	0.001	-.0019	.0024	.0005	.0009
1230	3.6	1.2	337	324	3.6	11.1	0.146	0.082	0.003	0.002	-.0005	-.0029	-.0007	-.0034
1245	3.1	1.2	333	045	2.6	26.2	0.137	0.302	0.001	0.003	-.0011	.0006	-.0037	-.0057
1300	2.7	0.6	326	096	1.8	32.4	0.063	0.038	0.002	0.004	.0006	-.0007	.0001	-.0019
1315	1.9	0.2	351	062	11.7	47.1	0.063	0.023	0.002	0.003	-.0015	-.0010	-.0024	-.0013
1330	2.3	0.3	351	315	7.1	36.9	0.120	0.019	0.004	0.001	.0025	-.0005	-.0031	.0004
1345	2.0	0.3	349	069	6.6	33.7	0.050	0.028	0.005	0.001	-.0019	-.0002	-.0025	-.0012
1400	1.8	0.3	344	040	6.8	44.3	0.025	0.032	0.004	0.001	-.0005	-.0009	.0014	-.0008
1415	1.9	0.3	339	331	6.5	25.8	0.038	0.035	0.001	0.003	-.0015	.0012	-.0009	-.0002
1430	3.0	0.6	356	303	4.5	18.0	0.161	0.013	0.003	0.001	.0106	-.0005	-.0068	-.0001
1445	3.0	0.4	354	330	7.3	22.0	0.029	0.039	0.002	0.003	-.0030	.0000	.0000	.0003
1500	2.9	0.7	344	016	4.4	39.9	0.203	0.069	0.016	0.003	-.0041	.0027	-.0099	-.0041
1515	2.0	1.0	333	060	7.2	10.1	0.122	0.058	0.027	0.011	-.0016	.0224	-.0230	-.0075

Dipole Pride 26 Micrometeorological Data Summary

Trial: DSWA07 Julian Date/Time: 3171300 Date/Time (PST): 12 November 1300-1445 Source Location: S3

Start Time (UTC)	BJY WS (m/s)	YFW WS (m/s)	BJY HD (Deg)	YFW HD (Deg)	BJY $\sigma\theta$ (Deg)	YFW $\sigma\theta$ (Deg)	BJY u'u' (m^2/s^2)	YFW u'u' (m^2/s^2)	BJY w'w' (m^2/s^2)	YFW w'w' (m^2/s^2)	BJY w'T' (mT/s)	YFW w'T' (mT/s)	BJY u'w' (m^2/s^2)	YFW u'w' (m^2/s^2)
2100	4.2	3.9	157	140	12.5	12.7	0.582	0.302	0.128	0.053	.0672	.0237	-.0494	-.0399
2115	4.2	3.7	159	136	11.2	11.7	0.577	0.547	0.148	0.073	.0945	.0521	-.1107	-.0737
2130	4.2	3.0	163	156	11.0	14.4	0.800	0.527	0.175	0.109	.0900	.0671	-.1189	-.0681
2145	4.2	3.2	153	155	13.8	12.5	0.494	0.758	0.177	0.138	.0962	.0569	-.0906	-.0492
2200	4.0	3.4	164	143	10.4	11.2	0.414	0.583	0.158	0.094	.0922	.0198	-.0408	-.0248
2215	4.2	3.1	160	142	9.7	19.4	0.462	0.302	0.119	0.065	.0513	.0164	-.0653	-.0214
2230	3.9	3.9	157	129	10.2	14.5	0.464	0.362	0.119	0.032	.0652	.0020	-.0914	-.0222

Dipole Pride 26 Micrometeorological Data Summary

Trial: DSWA07 Release Julian Date/Time: 3171447 Date/Time (PST): 12 November 1445-1600 Source Location: S3

Start Time (UTC)	BJY WS (m/s)	YFW WS (m/s)	BJY HD (Deg)	YFW HD (Deg)	BJY σθ (Deg)	YFW σθ (Deg)	BJY u'u' (m^2/s^2)	YFW u'u' (m^2/s^2)	BJY w'w' (m^2/s^2)	YFW w'w' (m^2/s^2)	BJY w'T' (mT/s)	YFW w'T' (mT/s)	BJY u'w' (m^2/s^2)	YFW u'w' (m^2/s^2)
2245	4.3	3.1	153	135	9.8	8.0	0.473	0.253	0.102	0.047	.0454	-.0054	-.0726	-.0096
2300	4.5	3.1	153	135	7.4	8.6	0.339	0.282	0.109	0.032	.0251	-.0008	-.0701	-.0217
2315	M*	M	M	M	M	M	M	M	M	M	M	M	M	M

* Missing

Dipole Pride 26 Micrometeorological Data Summary

Trial: DSWA09 Release Julian Date/Time: 3181400 Date/Time (PST): 13 November 1400-1700 Source Location: S2

Start Time (UTC)	BJY WS (m/s)	YFW WS (m/s)	BJY HD (Deg)	YFW HD (Deg)	BJY σθ (Deg)	YFW σθ (Deg)	BJY u'u' (m^2/s^2)	YFW u'u' (m^2/s^2)	BJY w'w' (m^2/s^2)	YFW w'w' (m^2/s^2)	BJY w'T' (mT/s)	YFW w'T' (mT/s)	BJY u'w' (m^2/s^2)	YFW u'w' (m^2/s^2)
2200	3.9	2.5	155	137	10.9	10.0	0.556	0.256	0.105	0.044	.0286	-.0019	-.0500	-.0136
2300	3.6	2.3	152	139	11.0	14.8	0.552	0.382	0.087	0.066	.0161	.0026	-.0709	-.0474
2230	2.4	1.8	175	150	23.9	25.6	0.839	0.311	0.071	0.073	.0129	.0041	-.0342	-.0263
2245	2.8	1.7	176	140	14.6	33.1	0.738	0.704	0.071	0.079	.0095	.0046	-.0566	-.0667
2300	3.0	1.4	173	182	10.8	28.7	0.457	0.474	0.118	0.062	.0539	.0153	-.1215	-.0076
2315	3.7	1.2	168	185	8.3	41.0	0.416	0.291	0.082	0.086	.0097	.0090	-.0420	-.0197
2330	2.7	1.3	168	156	10.2	28.0	0.343	0.161	0.060	0.043	.0020	-.0019	-.0491	.0041
2345	1.9	0.9	189	154	7.7	59.0	0.177	0.750	0.022	0.026	-.0014	-.0061	-.0159	.0119
0000	2.8	0.5	185	233	6.1	70.4	0.111	0.109	0.022	0.015	-.0060	-.0007	-.0127	.0010
0015	3.5	1.7	179	174	5.1	10.9	0.439	0.132	0.008	0.014	-.0030	-.0046	-.0041	-.0072

Dipole Pride 26 Micrometeorological Data Summary

Trial: DSWA11 Release Julian Date/Time: 3191430 Date/Time (PST): 14 November 1430-1545 Source Location: N2

Start Time (UTC)	BJY WS (m/s)	YFW WS (m/s)	BJY HD (Deg)	YFW HD (Deg)	BJY σθ (Deg)	YFW σθ (Deg)	BJY u'u' (m^2/s^2)	YFW u'u' (m^2/s^2)	BJY w'w' (m^2/s^2)	YFW w'w' (m^2/s^2)	BJY w'T' (mT/s)	YFW w'T' (mT/s)	BJY u'w' (m^2/s^2)	YFW u'w' (m^2/s^2)
2230	4.7	4.1	348	341	8.1	10.1	0.778	0.506	0.156	0.141	.0832	.0263	-.1253	-.1017
2245	3.9	3.4	345	343	12.7	11.9	1.087	0.470	0.100	0.084	.0081	-.0022	-.0698	-.0468
2300	2.8	2.7	350	343	8.0	6.1	0.307	0.286	0.041	0.044	-.0022	-.0105	-.0353	-.0362
2315	2.2	1.9	359	345	3.9	5.8	0.068	0.070	0.010	0.012	-.0020	.0046	-.0050	-.0055
2330	1.8	1.3	000	303	4.5	18.1	0.079	0.021	0.003	0.004	-.0020	-.0003	-.0027	.0006

Dipole Pride 26 Micrometeorological Data Summary

Trial: DSWA11 Release Julian Date/Time: 3191551 Date/Time (PST): 14 November 1545-1800 Source Location: N2

Start Time (UTC)	BJY WS (m/s)	YFW WS (m/s)	BJY HD (Deg)	YFW HD (Deg)	BJY σθ (Deg)	YFW σθ (Deg)	BJY u'u' (m^2/s^2)	YFW u'u' (m^2/s^2)	BJY w'w' (m^2/s^2)	YFW w'w' (m^2/s^2)	BJY w'T' (mT/s)	YFW w'T' (mT/s)	BJY u'w' (m^2/s^2)	YFW u'w' (m^2/s^2)
2345	2.0	2.1	001	268	6.2	5.8	0.248	0.080	0.004	0.029	-.0011	-.0130	-.0062	-.0097
0000	3.0	2.2	350	264	4.7	5.9	0.194	0.104	0.011	0.040	-.0010	-.0219	-.0100	-.0201
0015	3.8	2.3	354	254	7.7	5.3	0.198	0.038	0.035	0.010	-.0171	-.0039	-.0266	.0007
0030	2.6	2.0	343	242	14.1	41.1	0.234	1.090	0.011	0.025	-.0050	-.0348	-.0050	-.0021
0045	3.6	1.5	327	012	5.0	51.7	0.979	1.087	0.029	0.038	-.0278	.0027	-.0382	-.0124
0100	3.5	1.7	350	340	19.1	11.9	0.467	0.042	0.023	0.005	-.0235	-.0086	-.0202	.0014
0115	4.1	2.9	009	310	5.5	12.4	0.197	0.433	0.057	0.015	-.0360	-.0114	-.0279	-.0025
0130	M*	3.7	M	325	M	9.2	M	0.104	M	0.011	M	-.0021	M	-.0084
0145	M	3.3	M	299	M	6.3	M	0.093	M	0.016	M	-.0112	M	.0012

* Missing

Dipole Pride 26 Micrometeorological Data Summary

Trial: DSWA12 Release Julian Date/Time: 3200900 Date/Time (PST): 15 November 0900-1030 Source Location: N2

Start Time (UTC)	BJY WS (m/s)	YFW WS (m/s)	BJY HD (Deg)	YFW HD (Deg)	BJY σθ (Deg)	YFW σθ (Deg)	BJY u'u' (m^2/s^2)	YFW u'u' (m^2/s^2)	BJY w'w' (m^2/s^2)	YFW w'w' (m^2/s^2)	BJY w'T' (mT/s)	YFW w'T' (mT/s)	BJY u'w' (m^2/s^2)	YFW u'w' (m^2/s^2)
1700	2.5	2.9	353	330	18.6	11.5	0.564	0.197	0.134	0.091	.0764	.0329	-.0659	-.0313
1715	4.0	2.6	005	338	10.9	18.8	0.925	1.215	0.163	0.160	.0627	.0746	-.1189	-.0782
1730	4.2	4.5	006	353	10.2	10.4	0.738	0.583	0.131	0.153	.0414	.0608	-.1238	-.0947
1745	5.7	4.3	003	350	11.0	8.0	1.701	0.492	0.213	0.151	.0440	.0397	-.2452	-.1249
1800	7.2	4.9	352	348	5.4	9.1	0.928	0.540	0.250	0.170	.0425	.0362	-.1875	-.1113
1815	7.2	4.6	343	358	7.2	7.7	1.101	0.672	0.233	0.157	.1131	.0353	-.2064	-.1230

Dipole Pride 26 Micrometeorological Data Summary

Trial: DSWA12 Release Julian Date/Time: 3201030 Date/Time (PST): 15 November 1030-1230 Source Location: N2

Start Time (UTC)	BJY WS (m/s)	YFW WS (m/s)	BJY HD (Deg)	YFW HD (Deg)	BJY σθ (Deg)	YFW σθ (Deg)	BJY u'u' (m^2/s^2)	YFW u'u' (m^2/s^2)	BJY w'w' (m^2/s^2)	YFW w'w' (m^2/s^2)	BJY w'T' (mT/s)	YFW w'T' (mT/s)	BJY u'w' (m^2/s^2)	YFW u'w' (m^2/s^2)
1830	6.1	3.8	350	004	10.7	18.8	1.208	1.334	0.244	0.186	.1408	.0632	-.1780	-.1355
1845	6.3	1.9	002	007	11.0	53.8	1.547	0.844	0.237	0.194	.1275	.1064	-.1799	-.0347
1900	6.9	4.5	340	013	8.6	23.7	1.141	3.129	0.271	0.209	.0882	.0571	-.1767	-.1308
1915	7.7	3.1	342	010	11.6	16.2	2.046	0.624	0.376	0.114	.1919	.0367	-.3482	-.0533
1930	8.0	3.0	332	036	8.9	25.9	1.447	1.266	0.417	0.095	.1179	.0188	-.3495	-.0483
1945	7.9	3.4	340	315	11.8	20.9	1.546	0.771	0.368	0.142	.1240	.0290	-.2905	-.0812
2000	7.3	3.0	342	307	11.9	30.1	1.333	0.939	0.259	0.167	.1066	.0780	-.2121	.0098
2015	6.9	3.6	338	302	10.3	21.8	1.270	1.956	0.319	0.132	.1369	.0361	-.2626	-.0625

Dipole Pride 26 Micrometeorological Data Summary

Trial: DSWA13 Release Julian Date/Time: 3201430 Date/Time (PST): 15 November 1430-1610 Source Location: N2

Start Time (UTC)	BJY WS (m/s)	YFW WS (m/s)	BJY HD (Deg)	YFW HD (Deg)	BJY σθ (Deg)	YFW σθ (Deg)	BJY u'u' (m^2/s^2)	YFW u'u' (m^2/s^2)	BJY w'w' (m^2/s^2)	YFW w'w' (m^2/s^2)	BJY w'T' (mT/s)	YFW w'T' (mT/s)	BJY u'w' (m^2/s^2)	YFW u'w' (m^2/s^2)
2230	5.6	5.3	329	324	13.3	14.6	1.091	2.477	0.227	0.202	.0112	.0212	-.1756	-.0852
2245	5.7	5.3	335	334	14.8	12.1	4.068	1.833	0.235	0.187	.0179	.0225	-.2141	-.1997
2300	9.0	5.5	344	325	7.9	13.6	2.612	1.166	0.447	0.212	.0290	.0389	-.4210	-.1636
2315	9.2	6.8	344	343	9.2	14.1	2.596	3.963	0.427	0.345	-.0056	.0071	-.3864	-.3430
2330	8.9	8.4	342	347	6.0	8.1	2.420	3.545	0.455	0.467	.0011	.0212	-.4000	-.4612
2345	7.2	8.0	329	344	10.0	6.7	1.418	2.127	0.335	0.405	-.0021	-.0027	-.2378	-.3219
0000	8.6	8.3	343	345	6.1	7.9	2.440	3.336	0.446	0.456	.0033	.0141	-.4062	-.4343

Dipole Pride 26 Micrometeorological Data Summary

Trial: DSWA14 Release Julian Date/Time: 3211300 Date/Time (PST): 16 November 1300-1500 Source Location: S2

Start Time (UTC)	BJY WS (m/s)	YFW WS (m/s)	BJY HD (Deg)	YFW HD (Deg)	BJY σθ (Deg)	YFW σθ (Deg)	BJY u'u' (m^2/s^2)	YFW u'u' (m^2/s^2)	BJY w'w' (m^2/s^2)	YFW w'w' (m^2/s^2)	BJY w'T' (mT/s)	YFW w'T' (mT/s)	BJY u'w' (m^2/s^2)	YFW u'w' (m^2/s^2)
2100	3.3	3.7	160	139	23.1	12.0	0.889	0.696	0.202	0.123	.1471	.0942	-.0736	-.1069
2115	4.5	4.3	163	132	14.9	15.5	1.510	0.519	0.159	0.105	.0777	.0672	-.1315	-.0475
2130	4.4	3.5	165	154	11.5	14.8	1.061	0.563	0.185	0.205	.1137	.1444	-.0771	-.1299
2145	4.5	4.5	156	133	17.5	12.3	1.455	0.986	0.216	0.152	.1175	.0775	-.1160	-.0348
2200	4.9	4.5	149	155	13.5	20.8	0.844	1.644	0.197	0.229	.1216	.0597	-.1296	-.0921
2215	4.7	3.9	155	161	14.7	14.2	0.718	2.040	0.195	0.187	.0951	.0939	-.1162	-.1111
2230	5.3	4.6	155	157	10.5	14.1	1.164	1.048	0.182	0.172	.0861	.0579	-.1510	-.0769
2245	5.7	4.5	163	154	8.1	14.6	1.073	0.865	0.180	0.124	.0682	.0365	-.1462	-.0574

Dipole Pride 26 Micrometeorological Data Summary

Trial: DSWA15 Release Julian Date/Time: 3231130 Date/Time (PST): 18 November 1130-1300 Source Location: S2

Start Time (UTC)	BJY WS (m/s)	YFW WS (m/s)	BJY HD (Deg)	YFW HD (Deg)	BJY σθ (Deg)	YFW σθ (Deg)	BJY u'u' (m^2/s^2)	YFW u'u' (m^2/s^2)	BJY w'w' (m^2/s^2)	YFW w'w' (m^2/s^2)	BJY w'T' (mT/s)	YFW w'T' (mT/s)	BJY u'w' (m^2/s^2)	YFW u'w' (m^2/s^2)
1930	2.2	2.7	170	179	23.9	27.3	0.869	1.464	0.145	0.256	.0852	.1462	.0206	-.0352
1945	2.8	2.5	174	130	23.0	17.5	0.967	1.471	0.152	0.109	.0562	.0509	-.0759	-.0217
2000	2.8	3.9	194	160	17.2	22.5	0.450	0.927	0.170	0.210	.1155	.1231	-.0275	-.0815
2015	2.0	3.3	147	140	19.4	22.1	0.276	1.993	0.107	0.144	.0596	.0663	.0006	-.0299
2030	2.7	3.5	154	154	21.3	31.8	1.593	3.540	0.201	0.241	.1943	.1020	-.0009	-.1699
2045	1.6	5.1	191	159	56.0	21.0	0.853	1.311	0.163	0.247	.0821	.1235	.0052	-.0948

Dipole Pride 26 Micrometeorological Data Summary

Trial: DSWA15 Release Julian Date/Time: 3231300 Date/Time (PST): 18 November 1300-1500 Source Location: S2

Start Time (UTC)	BJY WS (m/s)	YFW WS (m/s)	BJY HD (Deg)	YFW HD (Deg)	BJY σθ (Deg)	YFW σθ (Deg)	BJY u'u' (m^2/s^2)	YFW u'u' (m^2/s^2)	BJY w'w' (m^2/s^2)	YFW w'w' (m^2/s^2)	BJY w'T' (mT/s)	YFW w'T' (mT/s)	BJY u'w' (m^2/s^2)	YFW u'w' (m^2/s^2)
2100	4.3	3.7	152	161	40.2	17.1	5.850	0.988	0.189	0.237	.0898	.1194	-.4003	-.0874
2115	4.6	3.5	152	150	17.2	13.3	1.250	1.201	0.225	0.149	.1282	.0654	-.0458	-.0787
2130	4.0	2.9	189	187	25.0	18.3	0.746	1.658	0.218	0.184	.0973	.1130	-.0818	-.1122
2145	4.9	4.1	207	190	14.6	15.5	1.828	1.162	0.269	0.177	.1127	.0854	-.1072	-.0274
2200	5.2	4.4	205	174	12.2	17.7	1.227	0.923	0.223	0.187	.1084	.0629	-.0776	-.0925
2215	5.9	5.2	205	176	14.5	11.7	1.828	0.978	0.251	0.214	.1009	.0622	-.2070	-.1326
2230	6.0	6.4	207	186	10.9	13.1	1.587	1.366	0.265	0.258	.0865	.0370	-.1700	-.1926
2245	4.9	5.2	215	173	14.8	18.5	1.028	1.527	0.219	0.162	.0960	.0279	-.1265	-.1112

Dipole Pride 26 Micrometeorological Data Summary

Trial: DSWA16 Release Julian Date/Time: 3241200 Date/Time (PST): 19 November 1200-1330 Source Location: S3

Start Time (UTC)	WS (m/s) BJY	WS (m/s) YFW	HD (Deg) BJY	HD (Deg) YFW	$\sigma\theta$ (Deg) BJY	$\sigma\theta$ (Deg) YFW	u'u' (m^2/s^2) BJY	u'u' (m^2/s^2) YFW	w'w' (m^2/s^2) BJY	w'w' (m^2/s^2) YFW	w'T' (mT/s) BJY	w'T' (mT/s) YFW	u'w' (m^2/s^2) BJY	u'w' (m^2/s^2) YFW
2000	4.8	3.6	162	165	10.8	20.1	0.950	1.086	0.221	0.206	.1714	.1289	-.0762	-.0310
2015	4.4	3.6	145	147	15.2	13.2	1.301	0.644	0.217	0.181	.1353	.1152	-.1380	-.0972
2030	5.3	4.2	144	155	10.8	17.2	1.399	1.935	0.213	0.222	.1514	.1208	-.1163	-.1871
2045	5.0	4.7	132	152	8.5	16.7	0.808	2.129	0.177	0.229	.1139	.1420	-.0833	-.2274
2100	4.4	4.0	137	165	10.4	14.5	0.589	0.937	0.138	0.245	.0646	.1118	-.1006	-.1336
2115	5.4	5.4	140	160	7.9	10.4	0.964	1.100	0.142	0.239	.0713	.0571	-.1806	-.1360

Dipole Pride 26 Micrometeorological Data Summary

Trial: DSWA16 Release Julian Date/Time: 3241330 Date/Time (PST): 19 November 1330-1530 Source Location: S2

Start Time (UTC)	BJY WS (m/s)	YFW WS (m/s)	BJY HD (Deg)	YFW HD (Deg)	BJY σθ (Deg)	YFW σθ (Deg)	BJY u'u' (m^2/s^2)	YFW u'u' (m^2/s^2)	BJY w'w' (m^2/s^2)	YFW w'w' (m^2/s^2)	BJY w'T' (mT/s)	YFW w'T' (mT/s)	BJY u'w' (m^2/s^2)	YFW u'w' (m^2/s^2)
2130	6.7	5.9	142	157	5.9	11.2	0.920	2.055	0.186	0.313	.0562	.0920	-.1379	-.2302
2145	5.9	8.8	145	142	9.2	7.1	1.296	1.676	0.259	0.101	.1373	.0691	-.2073	-.2228
2200	6.3	7.4	149	147	9.5	9.1	1.606	1.405	0.284	0.285	.1126	.0379	-.2571	-.1961
2215	7.1	6.8	154	159	8.5	8.7	1.289	2.082	0.276	0.294	.0904	.0424	-.1261	-.2360
2230	6.4	7.5	149	167	7.3	8.4	1.217	1.969	0.212	0.348	.0250	.0148	-.1819	-.2477
2245	5.1	6.3	151	163	7.5	10.0	0.800	1.658	0.155	0.341	.0020	-.0133	-.0951	-.2291
2300	2.9	5.7	152	166	18.6	9.2	0.838	1.836	0.073	0.205	.0006	-.0109	-.0398	-.0845
2315	1.7	7.4	075	165	16.8	7.2	0.211	3.334	0.032	0.369	-.0031	-.0207	-.0006	-.3836

Dipole Pride 26 Micrometeorological Data Summary

Trial: DSWA17 Release Julian Date/Time: 3251200 Date/Time (PST): 20 November 1200-1330 Source Location: S3

Start Time (UTC)	WS (m/s) BJY	WS (m/s) YFW	HD (Deg) BJY	HD (Deg) YFW	$\sigma\theta$ (Deg) BJY	$\sigma\theta$ (Deg) YFW	u'u' (m^2/s^2) BJY	u'u' (m^2/s^2) YFW	w'w' (m^2/s^2) BJY	w'w' (m^2/s^2) YFW	w'T' (mT/s) BJY	w'T' (mT/s) YFW	u'w' (m^2/s^2) BJY	u'w' (m^2/s^2) YFW
2000	4.7	3.7	165	146	13.0	13.3	1.067	1.522	0.238	0.154	.1728	.0815	-.1410	-.0640
2015	5.3	4.3	154	150	10.7	12.0	1.002	0.636	0.203	0.166	.1324	.0883	-.1240	-.0830
2030	5.3	3.6	157	141	13.1	20.3	0.666	1.549	0.266	0.131	.1385	.0794	-.1136	-.0292
2045	5.2	3.6	155	157	12.2	20.9	0.771	1.153	0.241	0.175	.1730	.0877	-.1674	-.0329
2100	4.7	3.7	144	151	12.7	19.4	0.592	1.237	0.170	0.159	.1057	.0939	-.0582	-.1129
2115	4.7	4.2	136	138	10.8	15.2	0.789	1.350	0.173	0.104	.1097	.0545	-.0968	-.0713

Dipole Pride 26 Micrometeorological Data Summary

Trial: DSWA17 Release Julian Date/Time: 3251330 Date/Time (PST): 20 November 1330-1530 Source Location: S2

Start Time (UTC)	BJY WS (m/s)	YFW WS (m/s)	BJY HD (Deg)	YFW HD (Deg)	BJY σθ (Deg)	YFW σθ (Deg)	BJY u'u' (m^2/s^2)	YFW u'u' (m^2/s^2)	BJY w'w' (m^2/s^2)	YFW w'w' (m^2/s^2)	BJY w'T' (mT/s)	YFW w'T' (mT/s)	BJY u'w' (m^2/s^2)	YFW u'w' (m^2/s^2)
2130	4.6	4.2	141	128	9.2	14.7	0.587	0.921	0.122	0.112	.0587	.0431	-.0440	-.0766
2145	5.2	4.7	148	131	9.6	10.7	0.792	1.352	0.151	0.113	.0770	.0274	-.0850	-.0108
2200	5.0	4.6	153	133	11.4	13.4	0.875	0.728	0.189	0.118	.0878	.0495	-.1265	-.0538
2215	4.7	4.4	157	140	11.0	13.8	0.722	0.841	0.150	0.124	.0561	.0554	-.0568	-.0769
2230	4.9	4.3	154	155	8.7	17.2	0.752	0.752	0.129	0.148	.0583	.0516	-.1194	-.0961
2245	5.2	4.7	152	149	7.5	13.0	0.612	0.432	0.126	0.100	.0167	.0043	-.0859	-.0701

APPENDIX B. TRANSFORMS AND HISTOGRAM PLOTS

Appendix B contains a printout of the GAUSq.XFM and Gausfit.XFM transforms developed using the Jandel Scientific Sigma Plot® program. These transforms were used to produce concentration histograms and calculate relevant puff dimension statistics. The transform printouts are followed by plots of the lateral and alongwind puff concentration histograms. The lateral histogram plots include a best fit curve, and estimates of the best fit sigma and the sigma obtained using the 16-84 percentile method (see Section 3.2.4).

```
jsv5R
;GAUSq.XFM
;Calculates sigmas for histogram data and provides a
;"best fit" sigma from a range of three sigma estimates calculated
;for Gaussian fits to the histogram with histogram area conserved.
; Calculations are done on user-
;entered class mark (position)  data entered in column 1 and
;concentration data in column 2.
;o = user-defined arbitrary origin
;x=class mark (center position) of each histogram column.
;d=distance from each x to o.
;N=sum of concentrations over histogram.
;y=concentration (f) for each histogram column.
;int=class interval:  user-defined histogram width.
min= -2100  ;user-defined min class mark
max= 5700  ;user-defined max class mark
int = 300  ; user-defined class interval
o = 300 ; user-defined origin
y0 = 113  ; user-entered max concentration from histogram
pi=3.1415926
x_col=1
y_col=2
x=col(x_col) ; user-entered class mark in column 1
y=col(y_col) ;user-entered concentration in column 2
N=total(y)  ;sum of histogram concentrations
cell(3,1)="sum conc:"
cell(3,2)= N
cell(3,3)="hist area:"
A = N*int   ; histogram area calculation.
cell(3,4) = A
col(4) = (x-o)/int  ; calculates distance d from user-selected origin,
col(5) = col(4)*col(4)  ; calculates d squared.
col(6) = col(2)*col(4)  ; product of d and concentration.
col(7) = col(2)*col(5)  ; product of d**2 and concentration.
fd = total(col(6))
; histogram mean position, xbar calculation:
xbar = o + int*(fd/N)
cell(3,5)= "xbar:"
cell (3,6)= xbar  ; histogram mean
;first (s1) histogram standard deviation calculation.
fd2 = total(col(7))
cell(3,7)=fd2
s1 = int*sqrt((fd2/N)-((fd/N)**2))
cell(3,8) = "s1, 1st est"
cell(3,9) = s1
;second (s2) histogram sd calculation.

cell(3,10)="s2,2nd est"
s2=A/(sqrt(2*pi)*y0)
cell(3,11)=s2
;find y1, the peak concentration from the data set
;that produced s1 and calculate s3, another equivalent
;area sigma between s1 and s2

y1=A/(sqrt(2*pi)*s1)
ynew=(y0+y1)/2
s3=A/(sqrt(2*pi)*ynew) ;s3 = intermediate sigma estimate
cell(3,12)="s3"
cell(3,13)=s3

;Calculate tau's, ordinates, and fits for the 3 sigmas
```

```
col(8)=(x-xbar)/s1  ;tau calc for s1
col(9)=(x-xbar)/s2  ;tau calc for s2
col(10)=(x-xbar)/s3 ;tau calc for s3
col(11)=exp(-(col(8)**2/2))  ;ordinate calc for s1
col(12)=exp(-(col(9)**2/2))  ;ordinate calc for s2
col(13)=exp(-(col(10)**2/2))  ;ordinate calc for s3
col(14)=col(11)*int*sqrt((N*(N-1))/(2*pi))/s1  ;fit for s1
col(15)=col(12)*int*sqrt((N*(N-1))/(2*pi))/s2  ;fit for s2
col(16)=col(13)*int*sqrt((N*(N-1))/(2*pi))/s3  ;fit for s3
;calculate total least square differences:
col(17)=sqrt((col(14)-col(2))**2)  ;difference fit 1 and histogram
col(18)=sqrt((col(15)-col(2))**2)  ;difference fit 2 and histogram
col(19)=sqrt((col(16)-col(2))**2)  ;difference fit 3 and historgram
ls1=total(col(17))
ls2=total(col(18))
ls3=total(col(19))
ls1p=(ls1/N)*100  ;fit 1 least sq error as % of total conc.
ls2p=(ls2/N)*100  ;fit 2 least sq error as % of total conc.
ls3p=(ls3/N)*100  ;fit 3 least sq error as % of total conc.
cell(3,14)="ls1 %:"
cell(3,15)=ls1p  ;display fit 1 ls error as % of A
cell(3,16)="ls2 %:"
cell(3,17)=ls2p
cell(3,18)="ls3%:"
cell(3,19)=ls3p
;Find the best fit sigma:
sig=if(ls1p>ls2p,s2,s1)  ;select the min of ls1p and ls2p
sx={ls1p,ls2p}
lsmin=min(sx)
sig1=if(ls3p<lsmin,s3,sig)   ;select the min of ls3p and sig
cell(3,20)="SIGMA:"
cell(3,21)=sig1
;Computation of coefficients of skewness and kurtosis:
;col(20)=col(5)*col(6)
;fd3=total(col(20))
;col(21)=col(5)*col(7)
;fd4=total(col(21))
;m3=fd3-3*fd*fd2+2*fd**3  ;skewness
;m4=fd4-4*fd*fd3+6*((fd**2)*fd2-3*fd**4  ;kurtosis
;sk=m3/(sig1)**3
;cell(3,22)="Coeff. SK:"
;cell(3,23)=sk
;K=m4/(sig1)**4
;cell(3,24)="Coeff. K:"
;cell(3,25)=K
```

```
jsv5R
;GAUSFIT.XFM
;Calculates moments and coefficients of skewness and kurtosis for histo
gram data.
;Calculations are done on user-
;entered class mark (position)  data entered in column 1 and
;concentration data in column 2.
;o = user-defined arbitrary origin
;x=class mark (center position) of each histogram column.
;d=distance from each x to o.
;N=sum of concentrations over histogram.
;y=concentration (f) for each histogram column.
;int=class interval:  user-defined histogram width.
min=13.9291  ;user-defined min class mark
max= 14.0187 ;user-defined max class mark
int = .00006945  ; user-defined class interval
o = 13.9  ; user-defined origin
y0 =3083.9 ; user-entered max concentration from histogram

pi=3.1415926
x_col=1
y_col=2
x=col(x_col) ; user-entered class mark in column 1
y=col(y_col) ;user-entered concentration in column 2

N=total(y)  ;sum of histogram concentrations
cell(3,1)="sum conc:"
cell(3,2)= N
cell(3,3)="hist area:"
A = N*int   ; histogram area calculation.
cell(3,4) = A
col(4) = (x-o)/int  ; calculates distance d from user-selected origin,
col(5) = col(4)*col(4)  ; calculates d squared.
col(6) = col(2)*col(4)  ; product of d and concentration.
col(7) = col(2)*col(5)  ; product of d**2 and concentration.
fd = total(col(6))
m1=fd/N
; histogram mean position, xbar calculation:
xbar = o + int*(fd/N)
cell(3,7)= "xbar:"
cell (3,8)= xbar  ; histogram mean
;first (s1) histogram standard deviation calculation.
fd2 = total(col(7))
m2=fd2/N
; Computation of coefficients of skewness and kurtosis:
col(8)=col(5)*col(6)
fd3=total(col(8))
m3=fd3/N
col(9)=col(5)*col(7)
fd4=total(col(9))
m4=fd4/N
mm2=m2-m1
```

```
mm3=m3-3*m1*m2+2*(m1)**3  ;third moment

mm4=m4-4*m1*m3+6*((m1)**2)*m2-3*(m1)**4  ;4th moment
sk=mm3/(mm2)**1.5   ;coeff of skewness
cell(3,9)="Coeff SK:"
cell(3,10)=sk
K=mm4/(mm2)**2
cell(3,11)="Coeff K:"
cell(3,12)=K
cell(3,13)=fd
cell(3,14)=fd2
cell(3,15)=fd3
cell(3,16)=fd4
cell(3,17)=mm2
cell(3,18)=mm3
cell(3,19)=mm4
```

Trial DSWA03, Line 1,Bag 1

8 November 1996, 0400-0415 PST

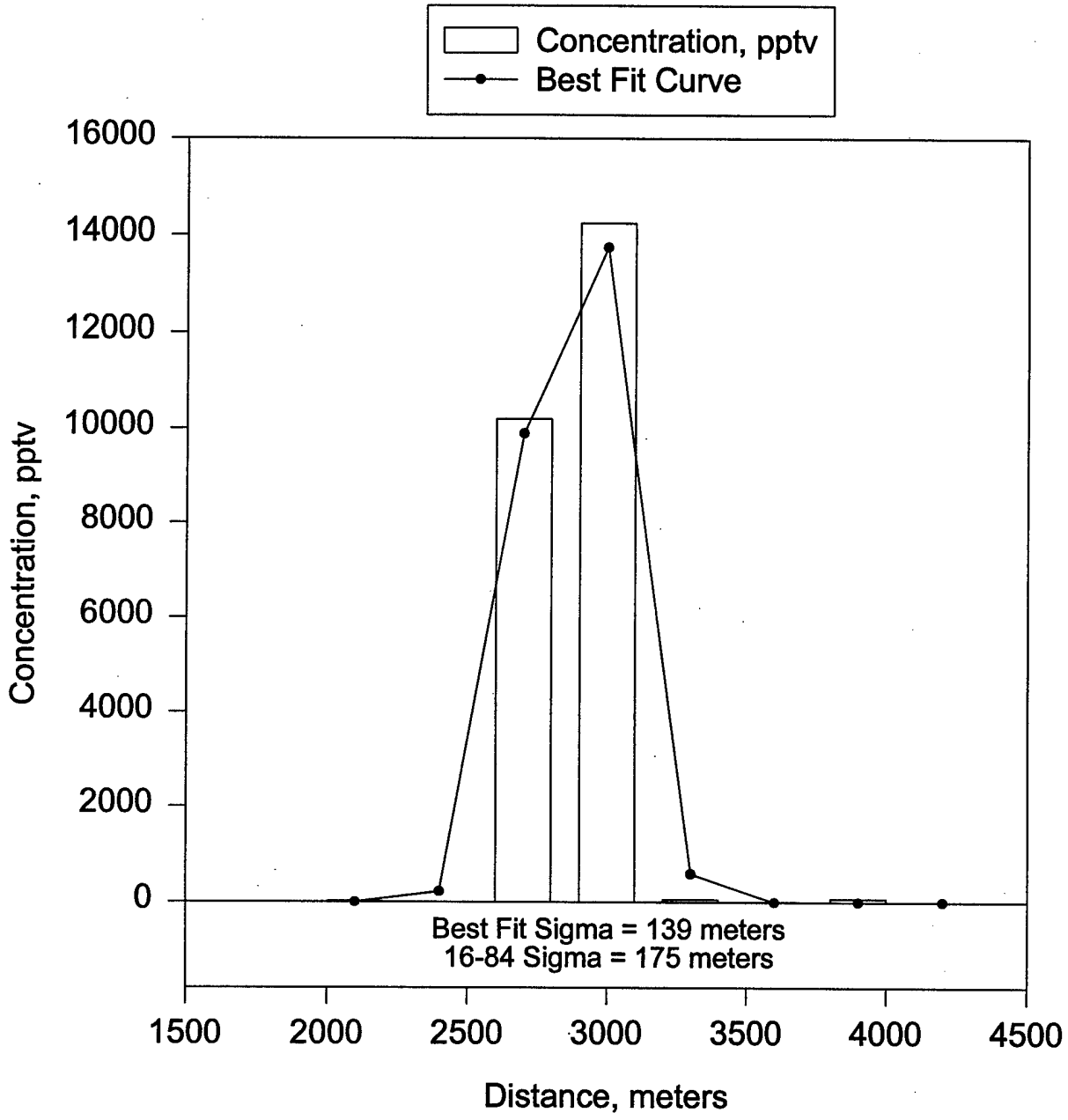

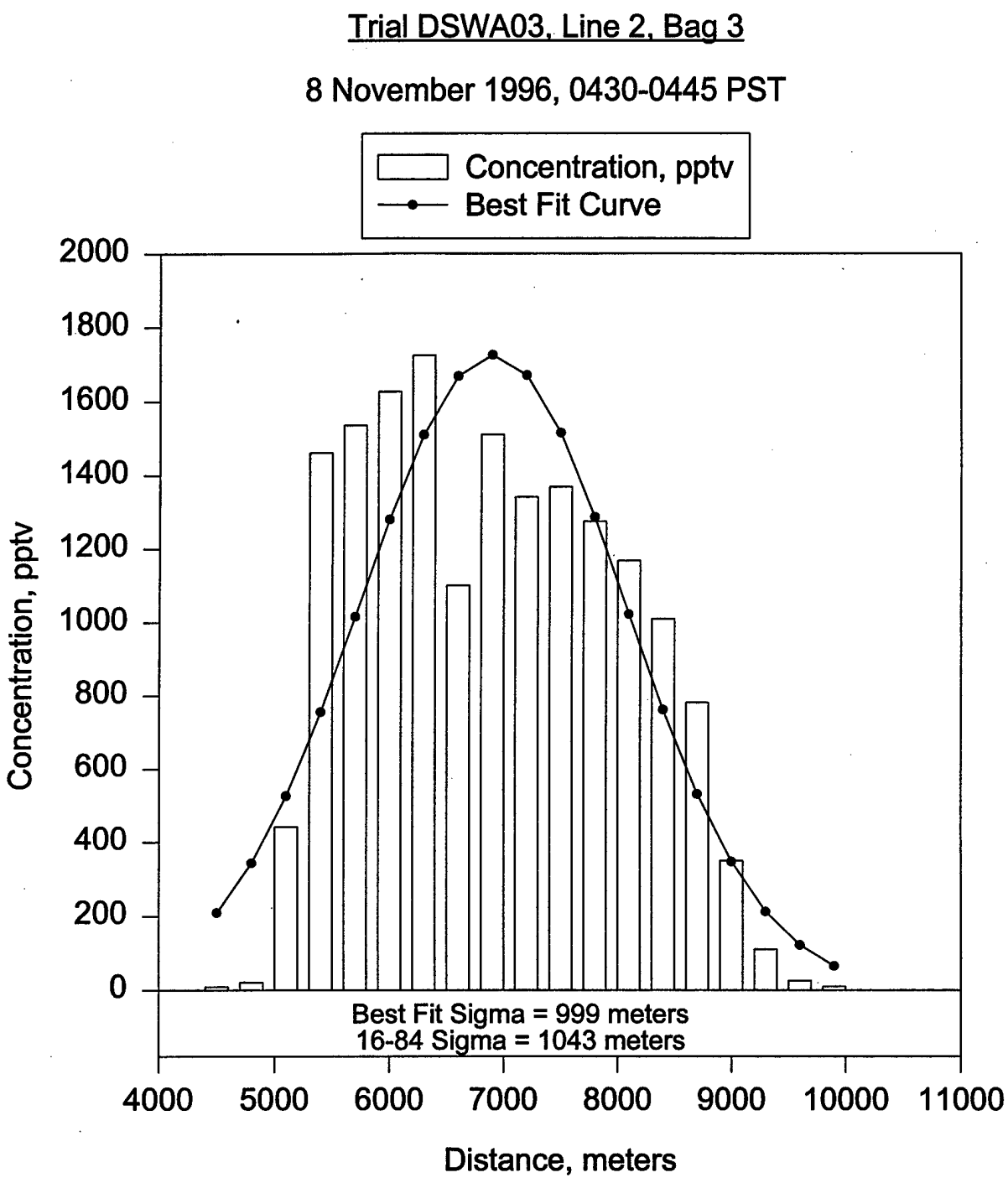
Trial DSWA03, Line 2, Bag 3
8 November 1996, 0430-0445 PST
Concentration, pptv
Best Fit Curve
2000
1800
1600
1400
1200
1000
800
600
400
200
0
Concentration, pptv
Best Fit Sigma = 999 meters
16-84 Sigma = 1043 meters
4000
5000
6000
7000
8000
9000
10000
11000
Distance, meters

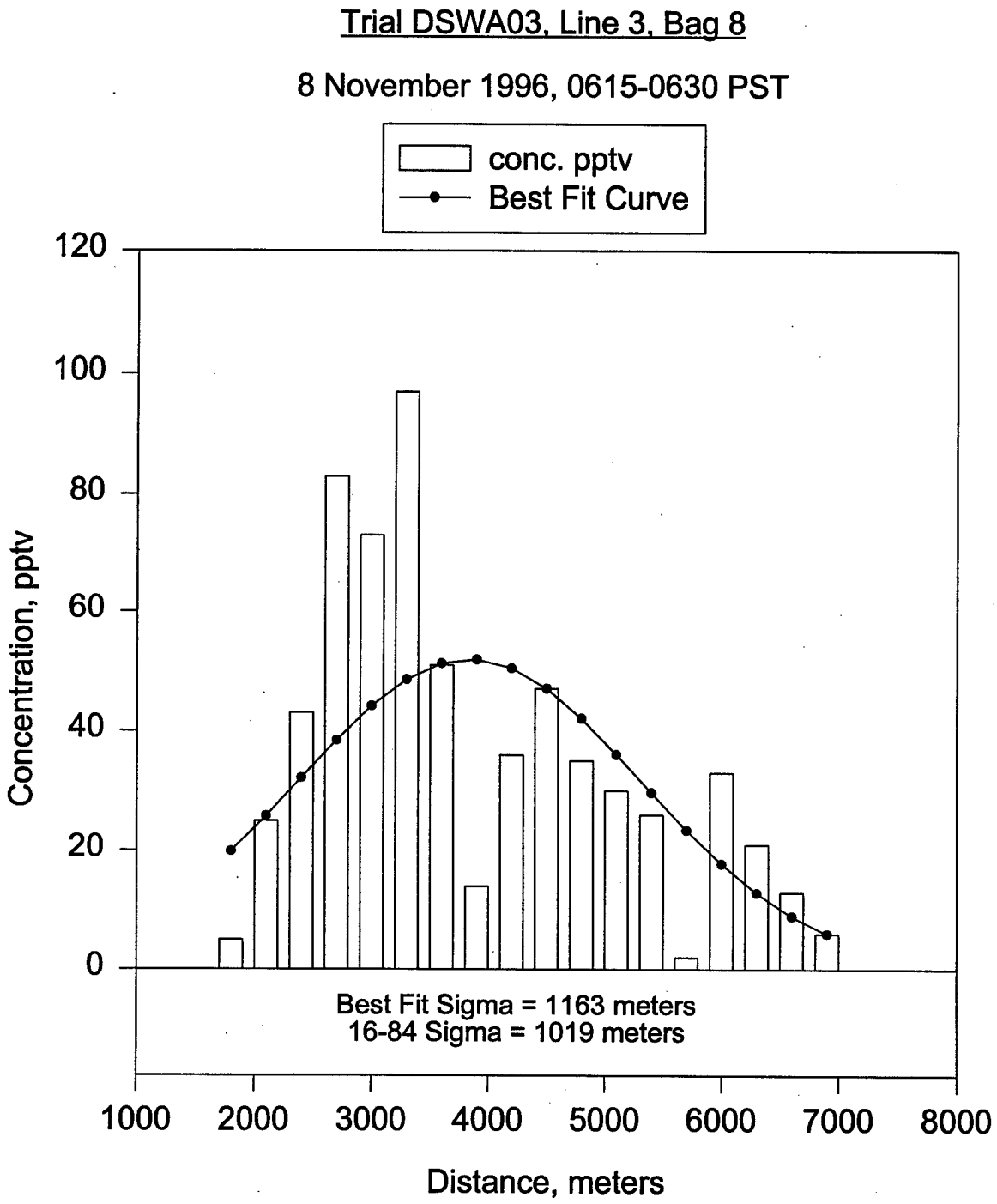
Trial DSWA03, Line 3, Bag 8
8 November 1996, 0615-0630 PST
conc. pptv
Best Fit Curve
120
100
80
60
40
20
0
Concentration, pptv
Best Fit Sigma = 1163 meters
16-84 Sigma = 1019 meters
1000
2000
3000
4000
5000
6000
7000
8000
Distance, meters

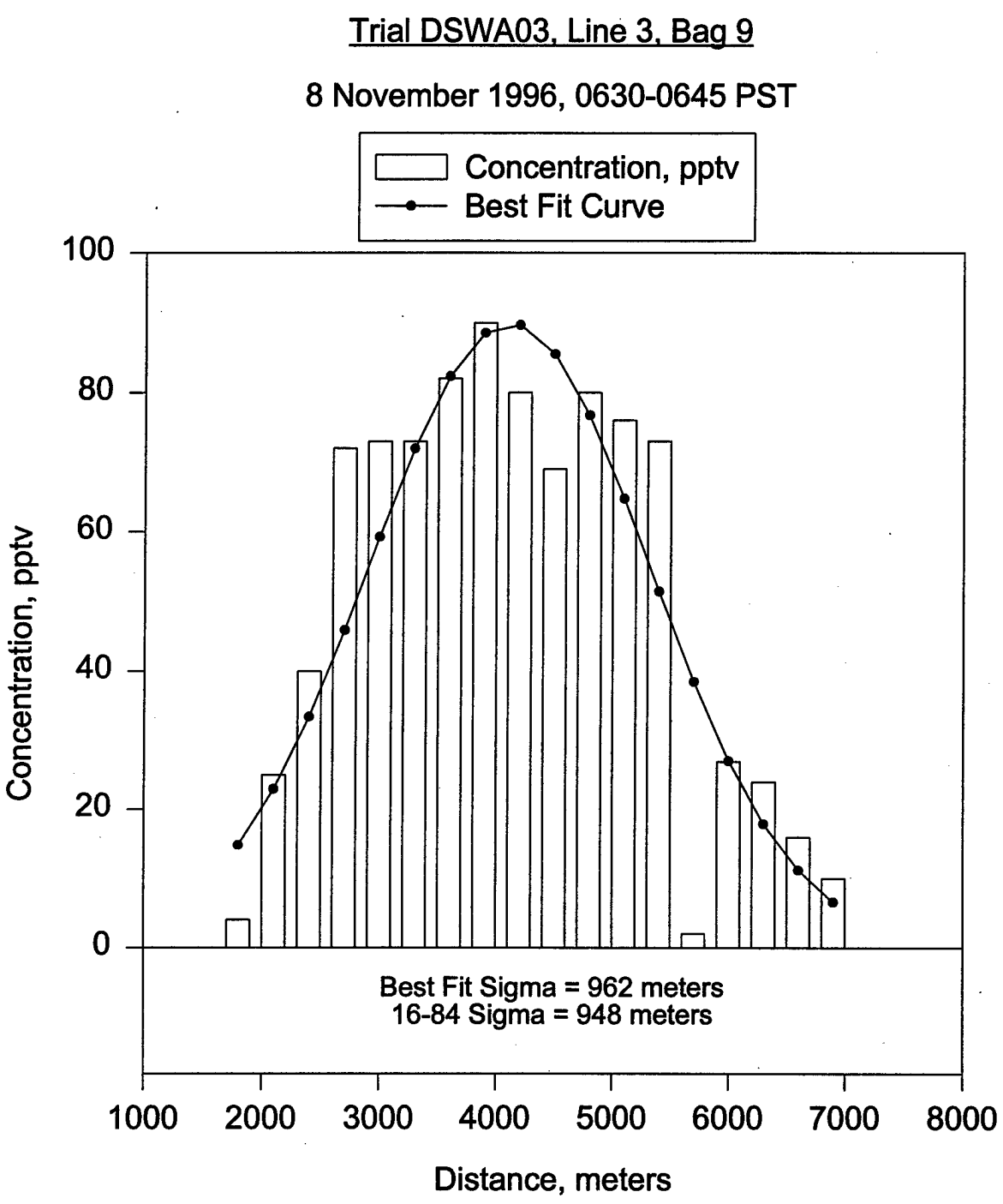
Trial DSWA03, Line 3, Bag 9
8 November 1996, 0630-0645 PST
Concentration, pptv
Best Fit Curve
100
80
60
40
20
0
Concentration, pptv
Best Fit Sigma = 962 meters
16-84 Sigma = 948 meters
1000
2000
3000
4000
5000
6000
7000
8000
Distance, meters

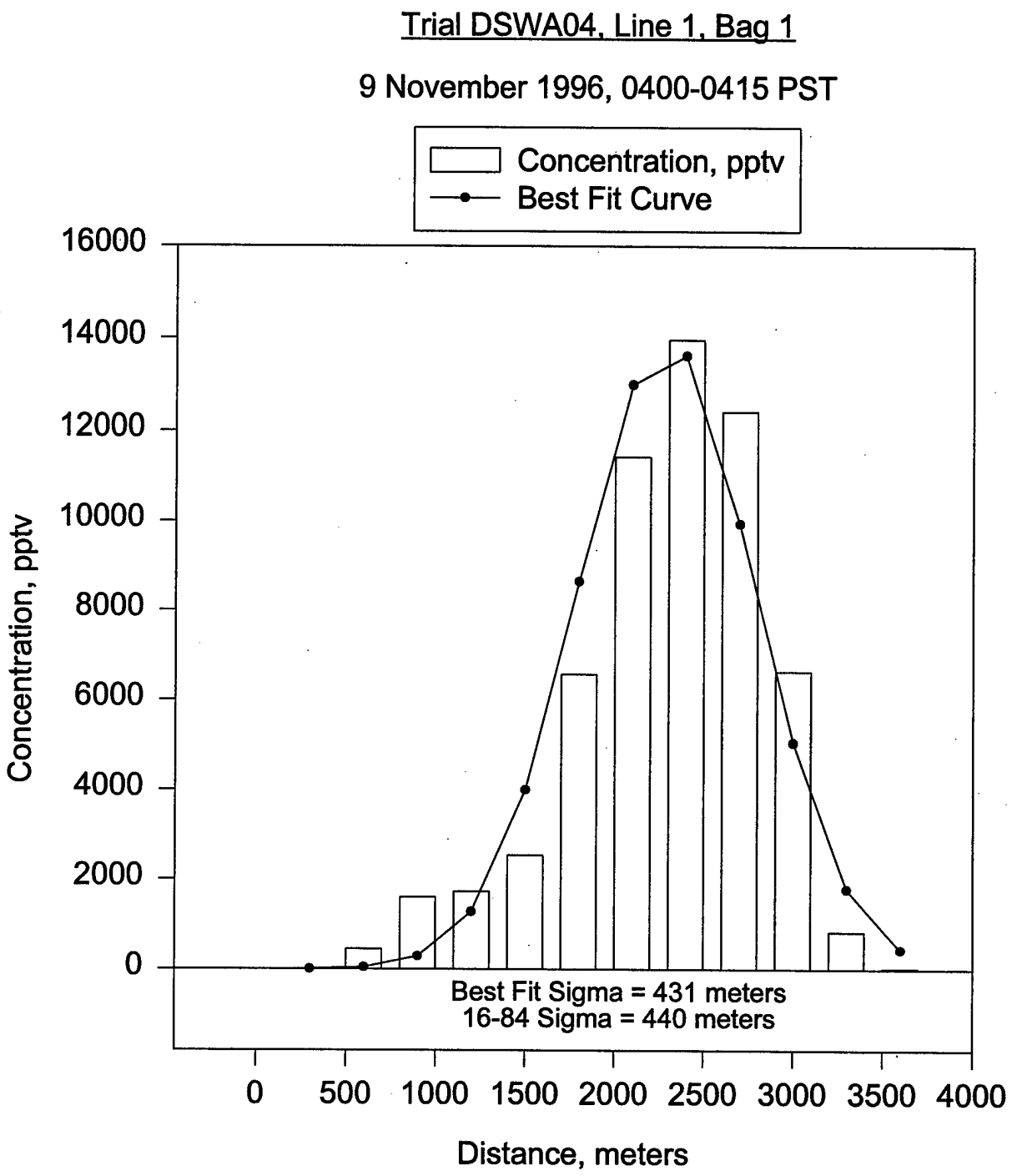
Trial DSWA04, Line 1, Bag 1
9 November 1996, 0400-0415 PST
Concentration, pptv
Best Fit Curve
16000
14000
12000
10000
8000
6000
4000
2000
0
Concentration, pptv
Best Fit Sigma = 431 meters
16-84 Sigma = 440 meters
0
500
1000
1500
2000
2500
3000
3500
4000
Distance, meters

Trial DSWA04, Line 2, Bag 3

9 November 1996, 0430-0445 PST

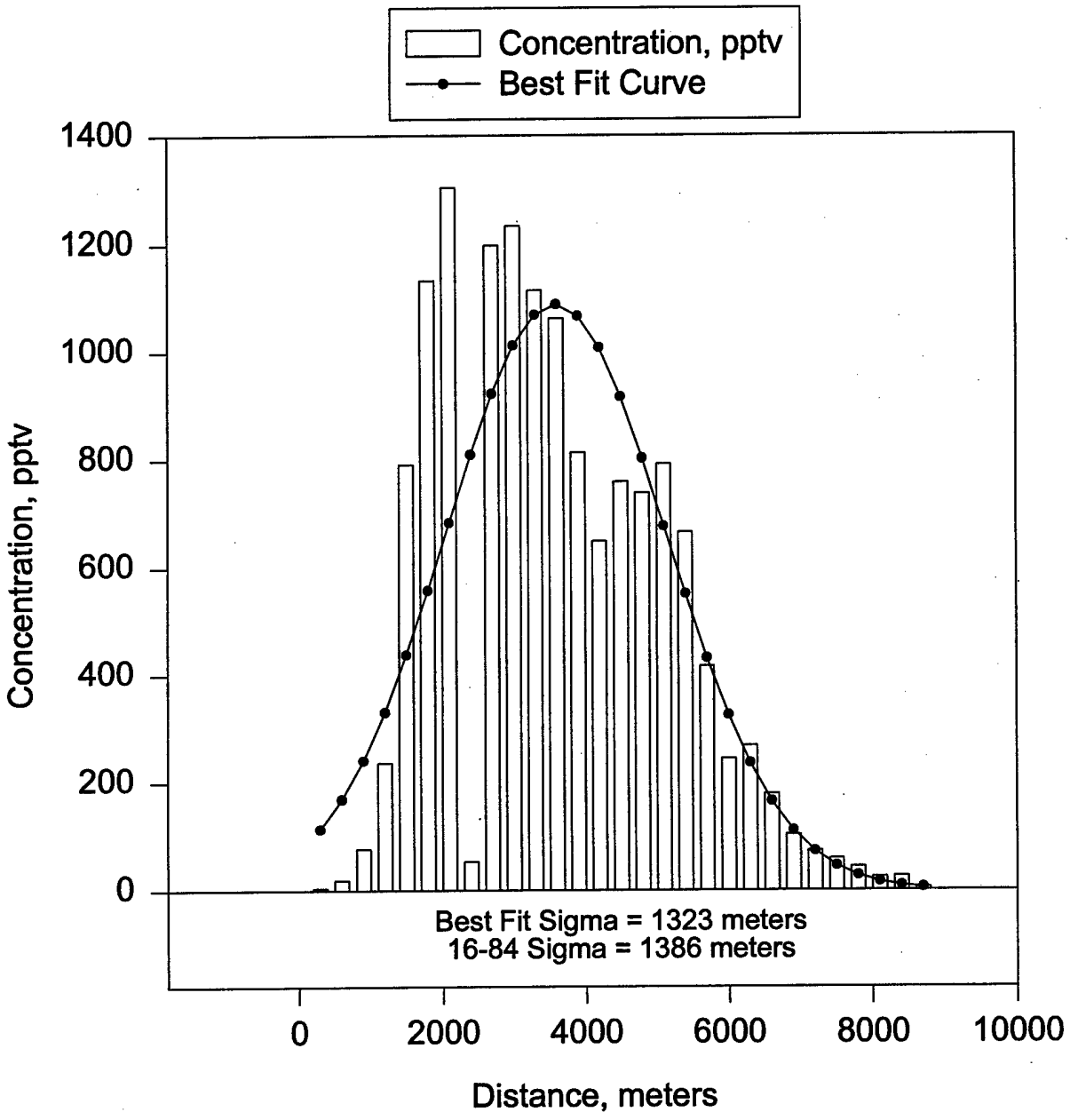

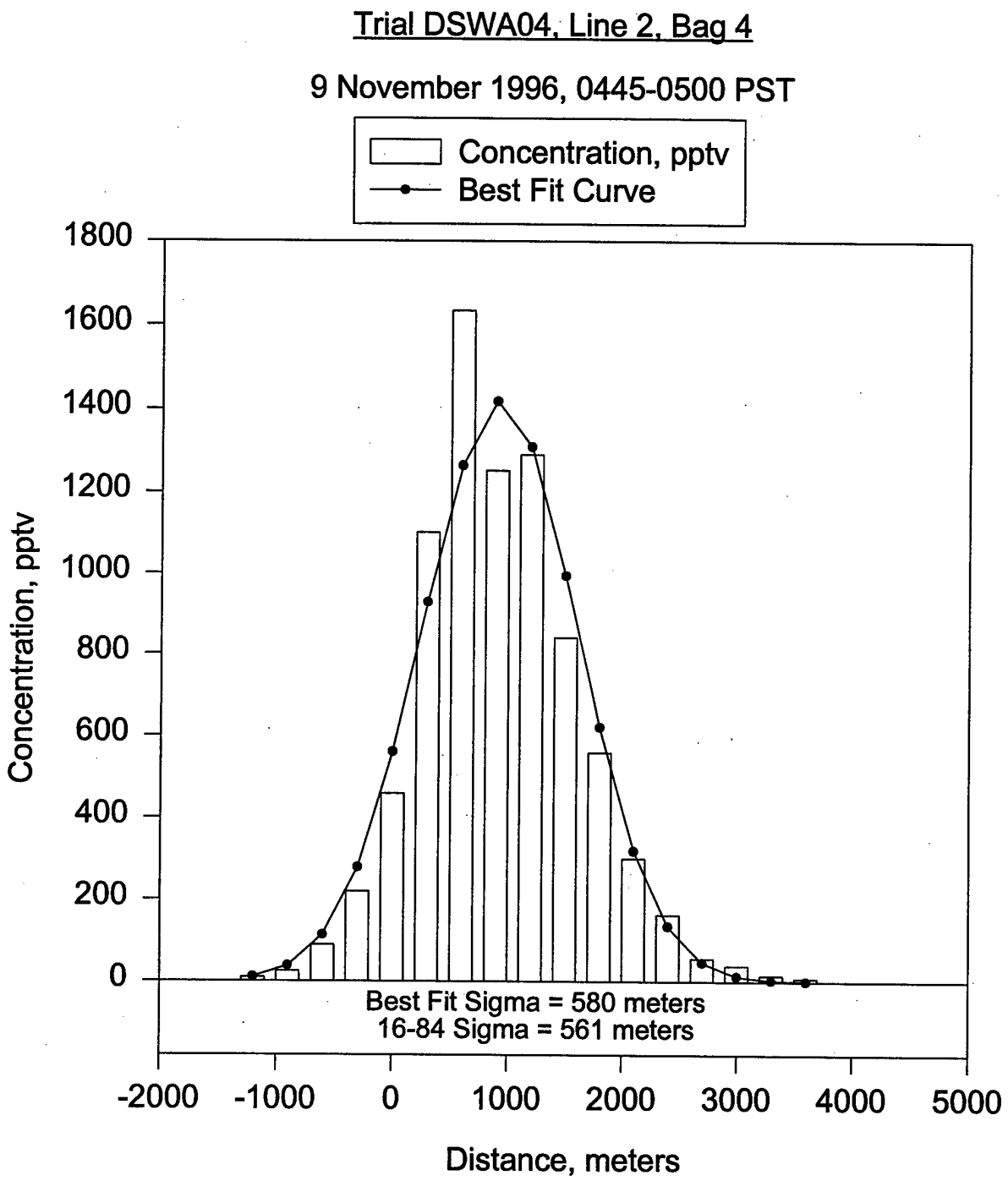
Trial DSWA04, Line 2, Bag 4
9 November 1996, 0445-0500 PST
Concentration, pptv
Best Fit Curve
1800
1600
1400
1200
1000
800
600
400
200
0
Concentration, pptv
Best Fit Sigma = 580 meters
16-84 Sigma = 561 meters
-2000
-1000
0
1000
2000
3000
4000
5000
Distance, meters

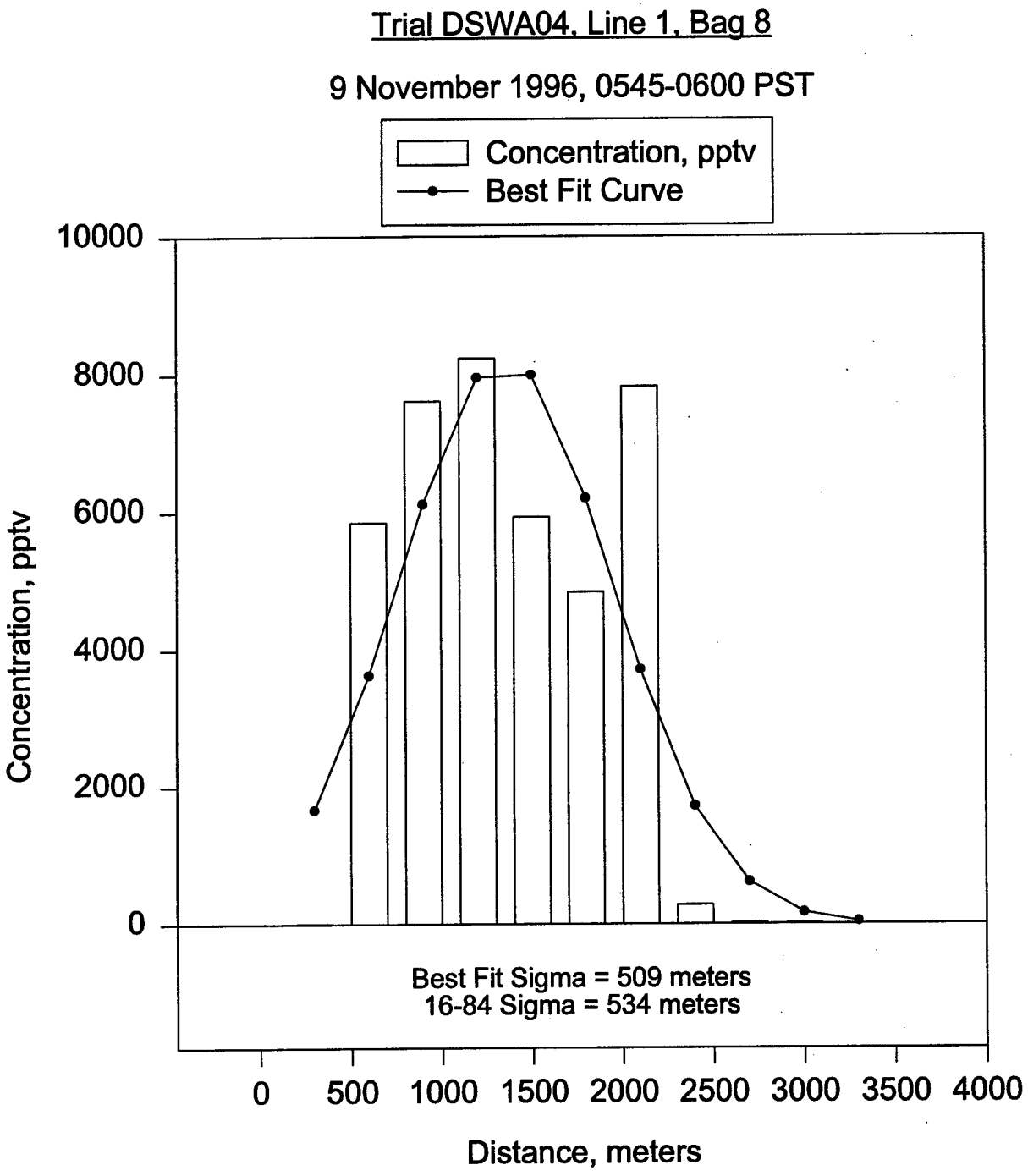
Trial DSWA04, Line 1, Bag 8
9 November 1996, 0545-0600 PST
Concentration, pptv
Best Fit Curve
10000
8000
6000
4000
2000
0
Concentration, pptv
Best Fit Sigma = 509 meters
16-84 Sigma = 534 meters
0
500
1000
1500
2000
2500
3000
3500
4000
Distance, meters

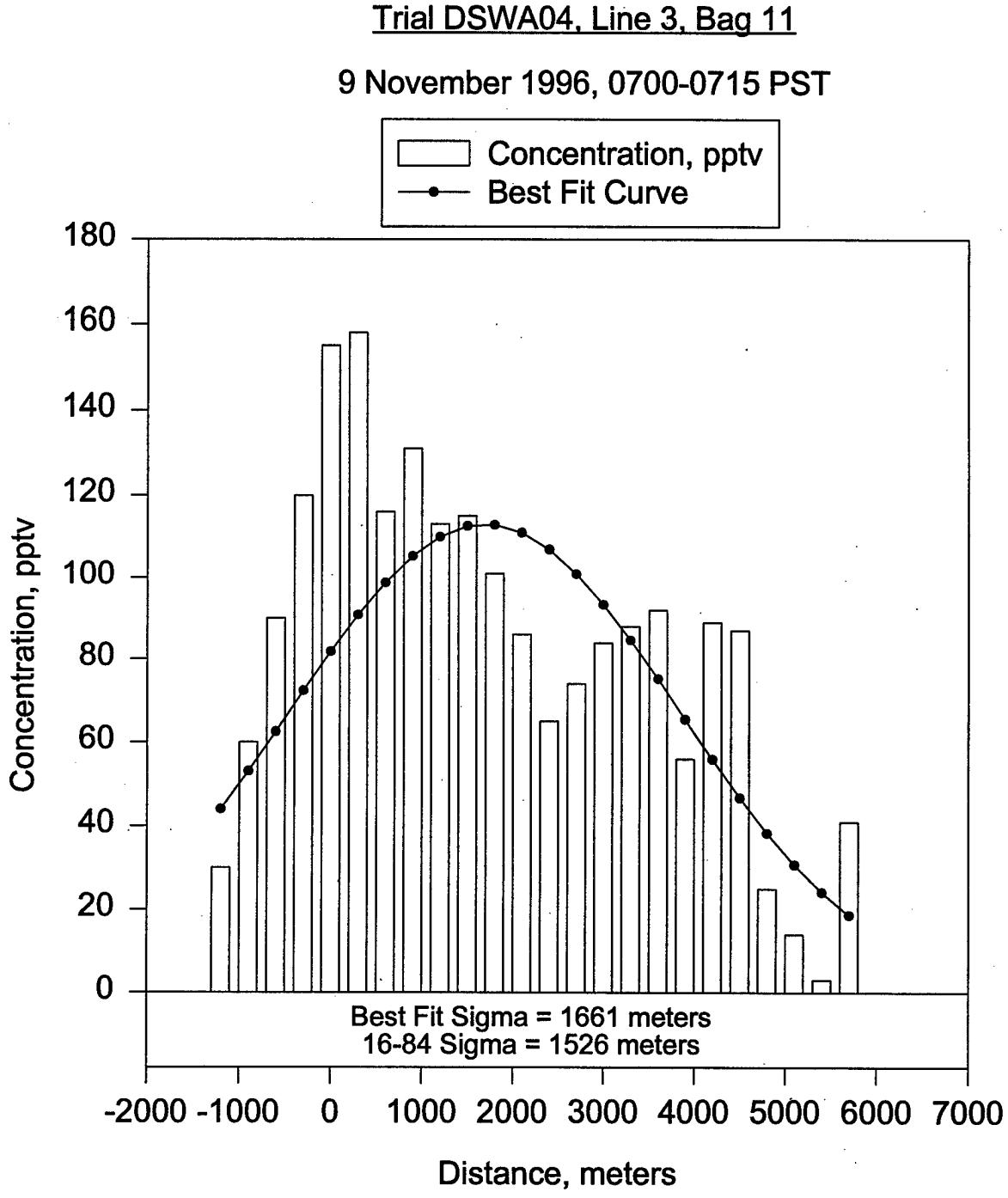
Trial DSWA04, Line 3, Bag 11
9 November 1996, 0700-0715 PST
Concentration, pptv
Best Fit Curve
180
160
140
120
100
80
60
40
20
0
Concentration, pptv
Best Fit Sigma = 1661 meters
16-84 Sigma = 1526 meters
-2000 -1000 0 1000 2000 3000 4000 5000 6000 7000
Distance, meters

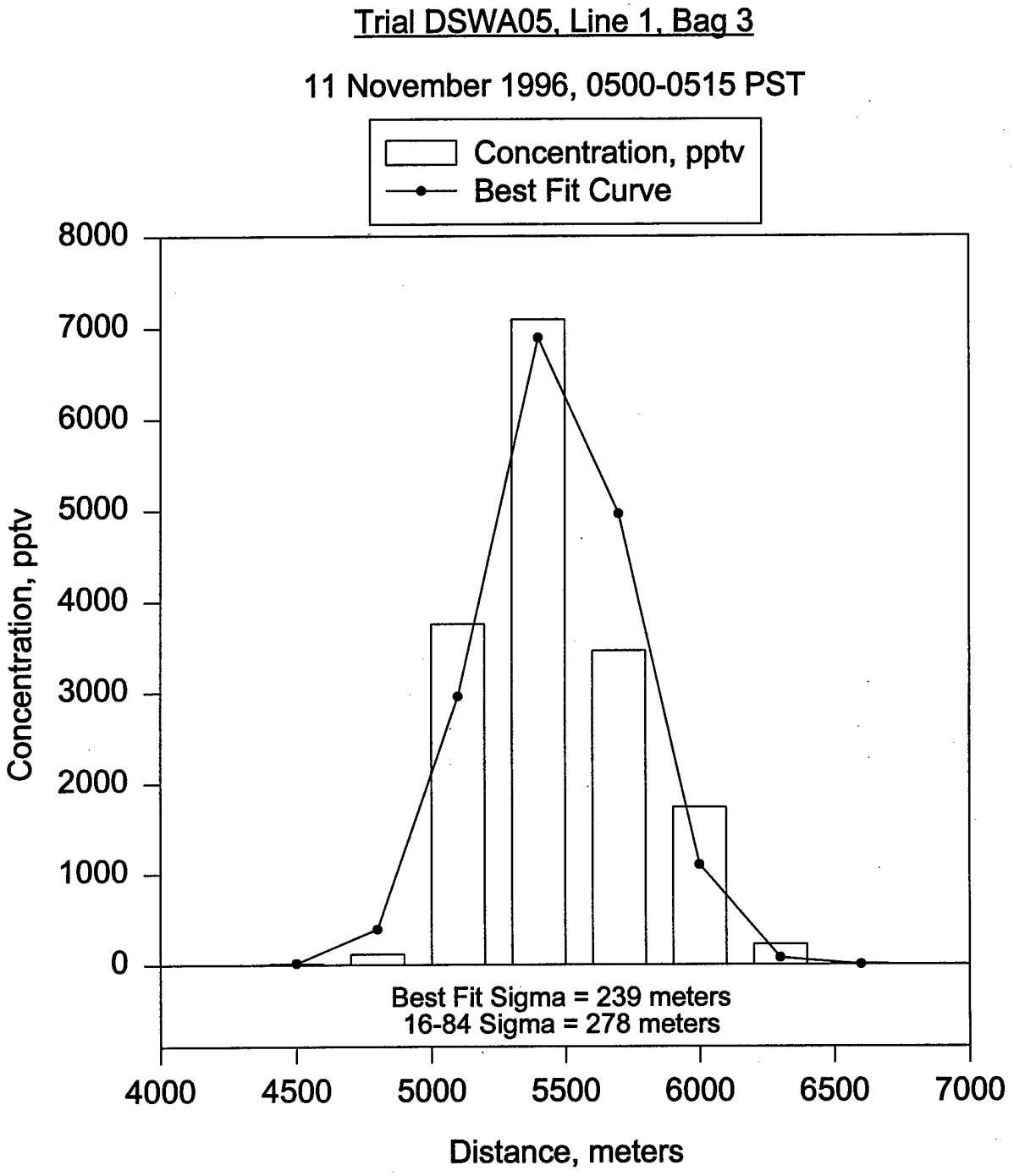
Trial DSWA05, Line 1, Bag 3
11 November 1996, 0500-0515 PST
Concentration, pptv
Best Fit Curve
8000
7000
6000
5000
4000
3000
2000
1000
0
Concentration, pptv
Best Fit Sigma = 239 meters
16-84 Sigma = 278 meters
4000
4500
5000
5500
6000
6500
7000
Distance, meters

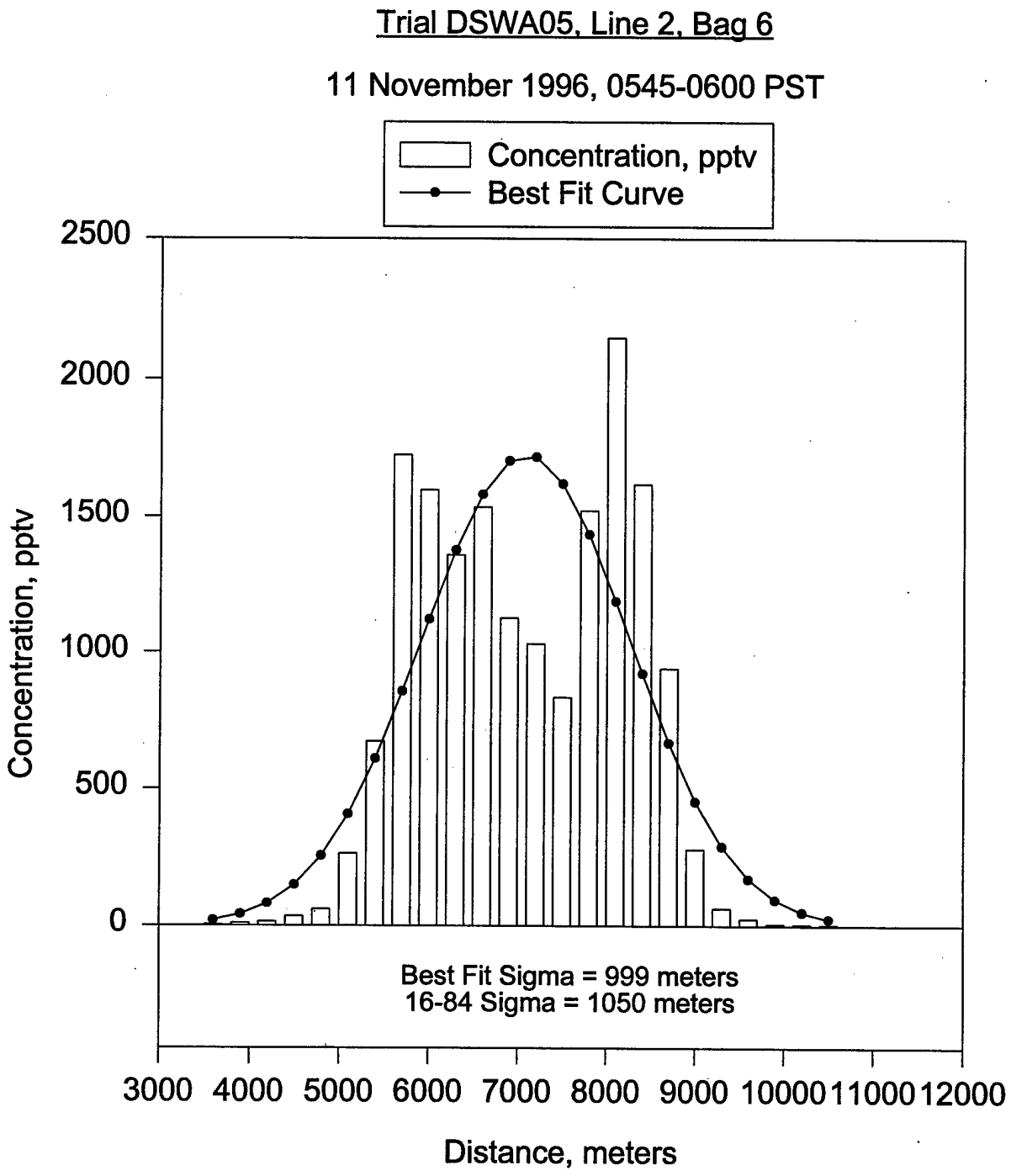
Trial DSWA05, Line 2, Bag 6
11 November 1996, 0545-0600 PST
Concentration, pptv
Best Fit Curve
2500
2000
1500
1000
500
0
Concentration, pptv
Best Fit Sigma = 999 meters
16-84 Sigma = 1050 meters
3000 4000 5000 6000 7000 8000 9000 10000 11000 12000
Distance, meters

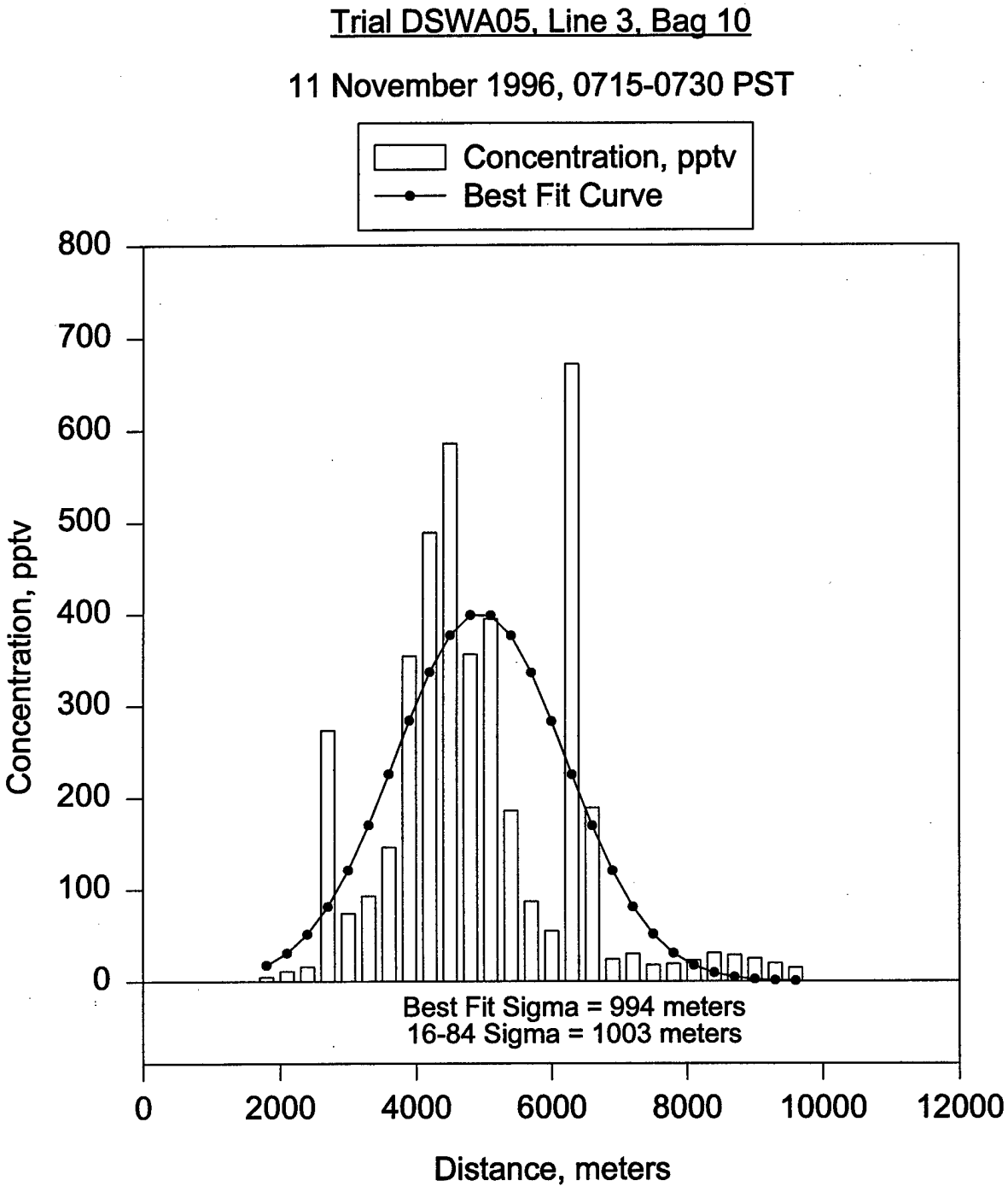
Trial DSWA05, Line 3, Bag 10
11 November 1996, 0715-0730 PST
Concentration, pptv
Best Fit Curve
800
700
600
500
400
300
200
100
0
Concentration, pptv
Best Fit Sigma = 994 meters
16-84 Sigma = 1003 meters
0
2000
4000
6000
8000
10000
12000
Distance, meters

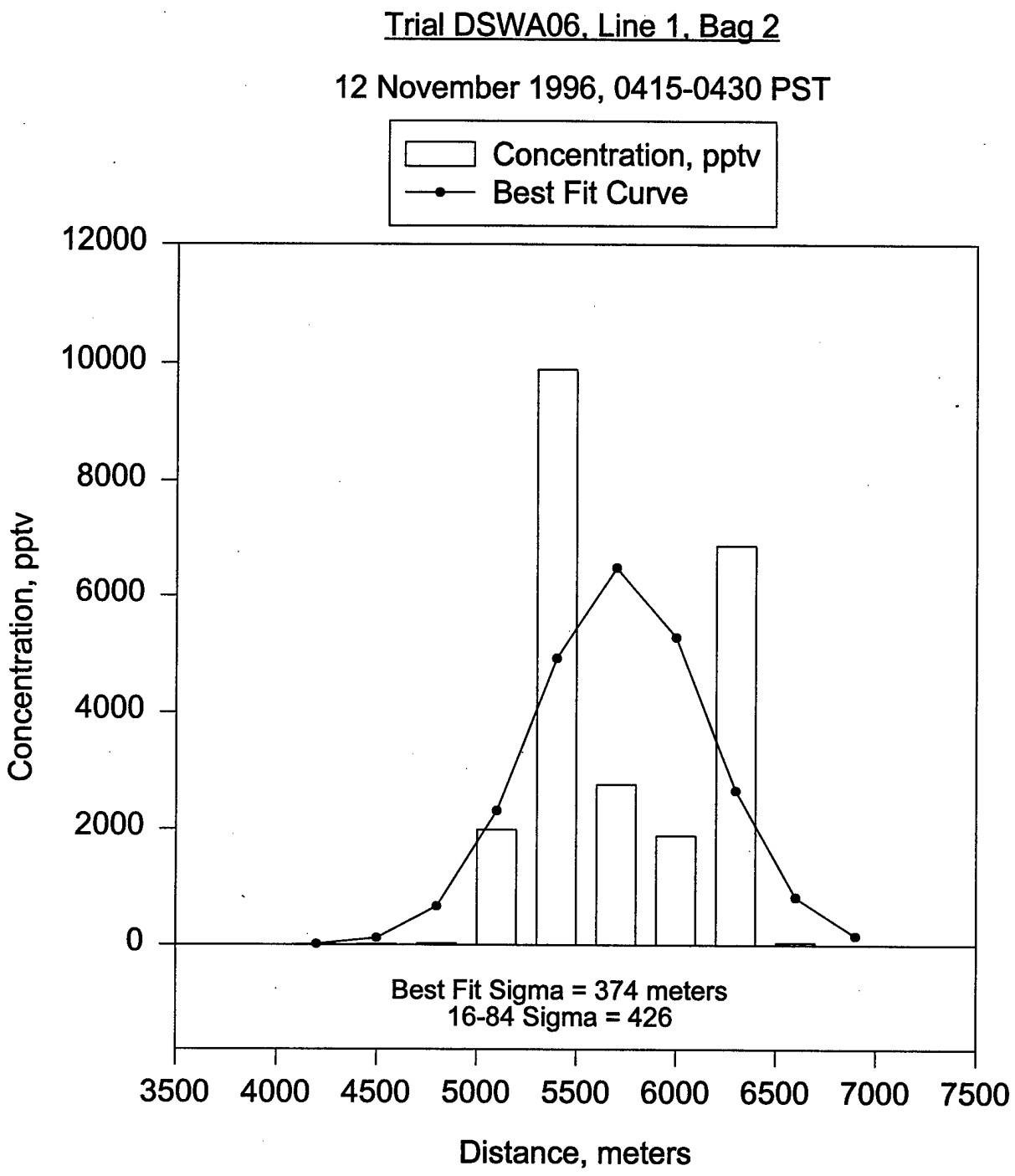
Trial DSWA06, Line 1, Bag 2
12 November 1996, 0415-0430 PST
Concentration, pptv
Best Fit Curve
12000
10000
8000
6000
4000
2000
0
Concentration, pptv
Best Fit Sigma = 374 meters
16-84 Sigma = 426
3500
4000
4500
5000
5500
6000
6500
7000
7500
Distance, meters

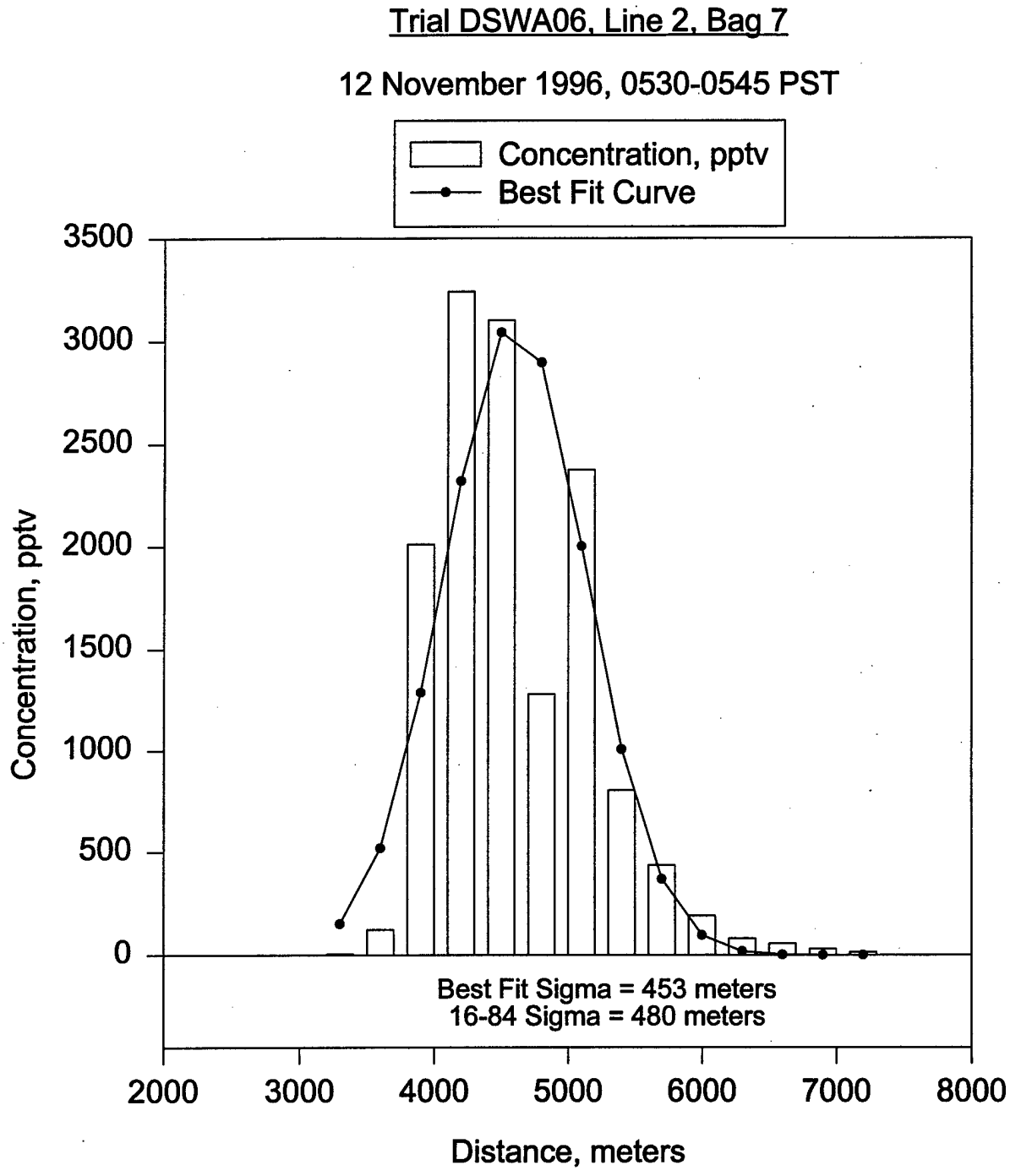
Trial DSWA06, Line 2, Bag 7
12 November 1996, 0530-0545 PST
Concentration, pptv
Best Fit Curve
3500
3000
2500
2000
1500
1000
500
0
Concentration, pptv
Best Fit Sigma = 453 meters
16-84 Sigma = 480 meters
2000
3000
4000
5000
6000
7000
8000
Distance, meters

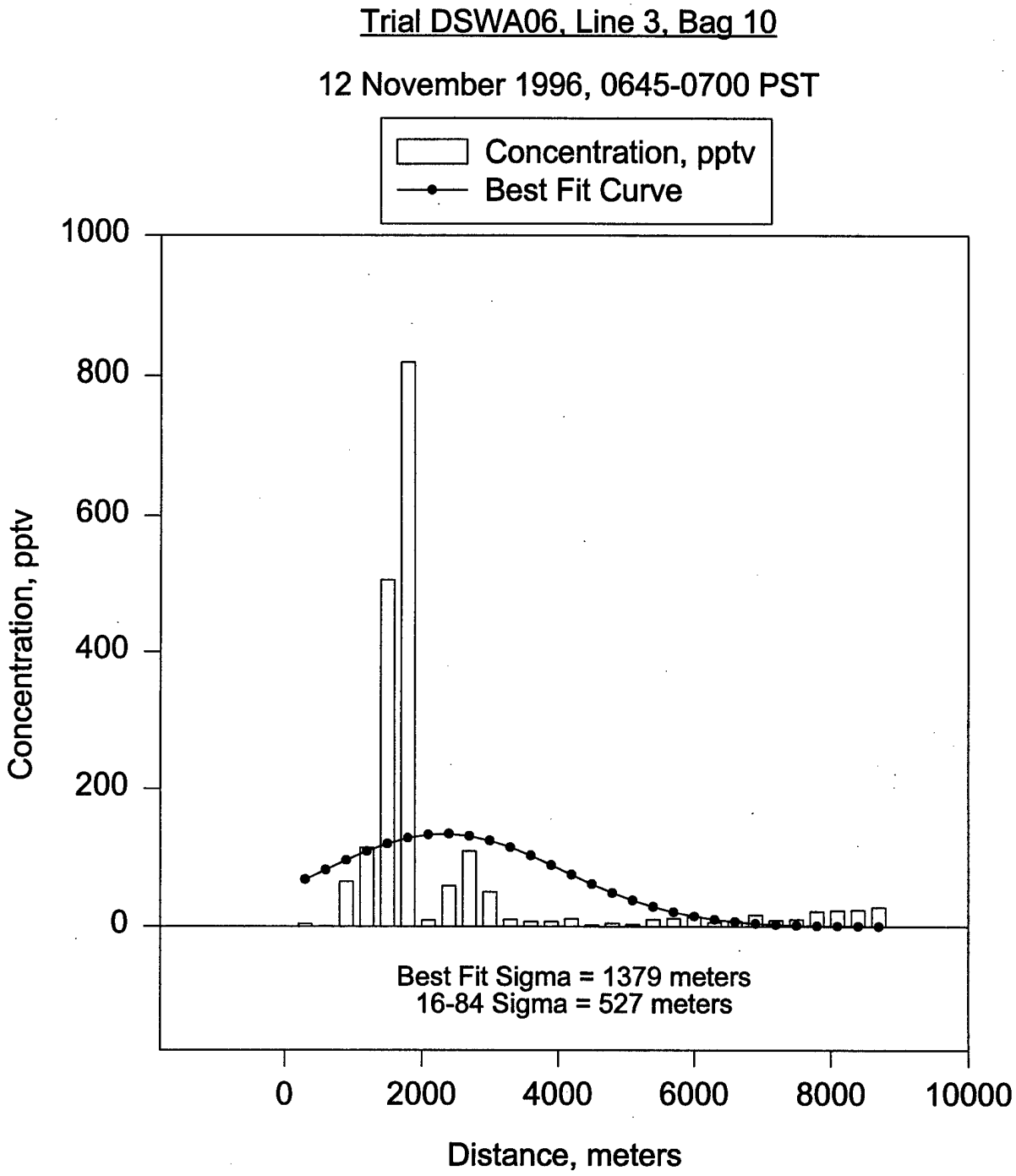
Trial DSWA06, Line 3, Bag 10
12 November 1996, 0645-0700 PST
Concentration, pptv
Best Fit Curve
1000
800
600
400
200
0
Concentration, pptv
Best Fit Sigma = 1379 meters
16-84 Sigma = 527 meters
0
2000
4000
6000
8000
10000
Distance, meters

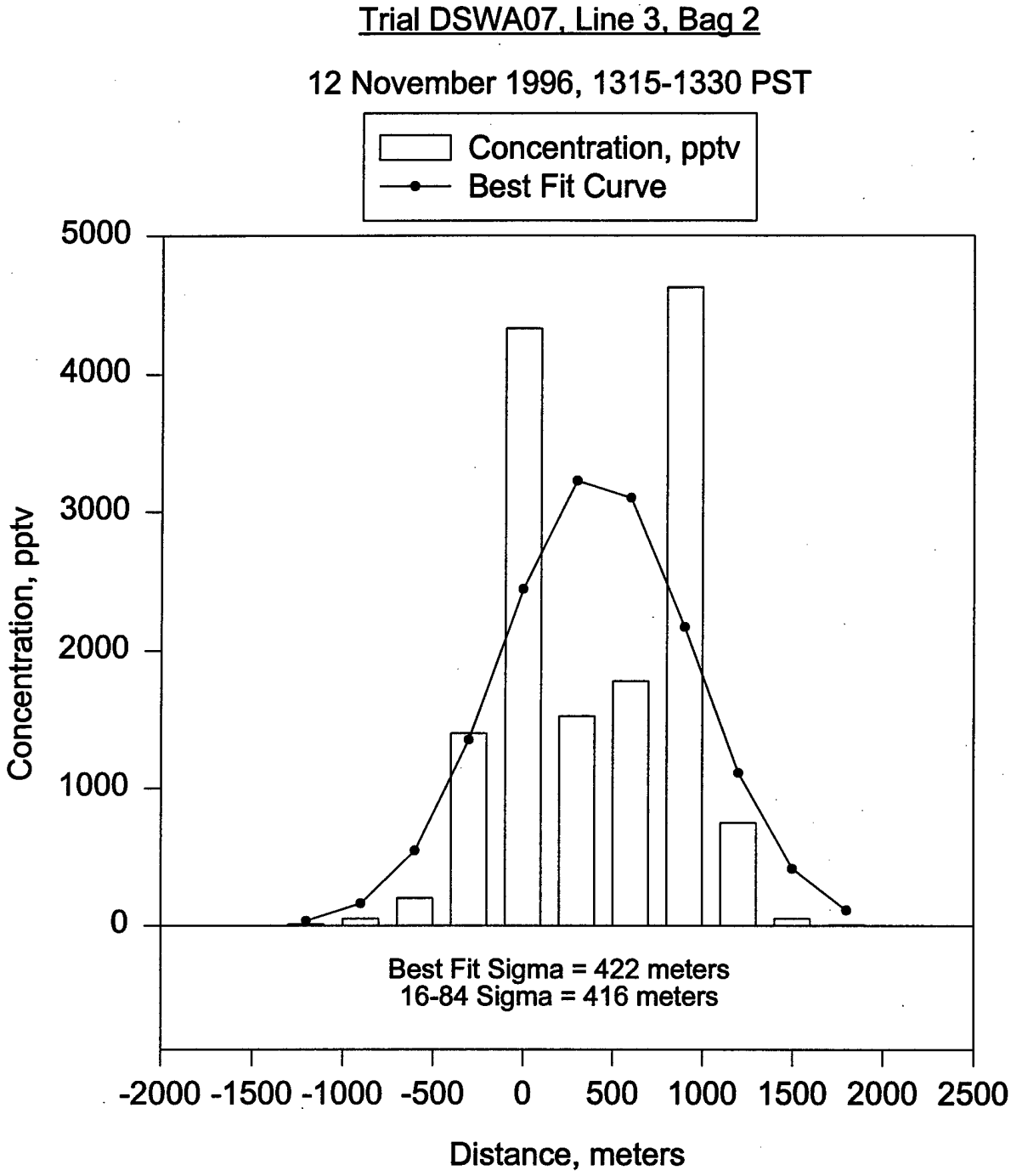
Trial DSWA07, Line 3, Bag 2
12 November 1996, 1315-1330 PST
Concentration, pptv
Best Fit Curve
5000
4000
3000
2000
1000
0
Concentration, pptv
Best Fit Sigma = 422 meters
16-84 Sigma = 416 meters
-2000 -1500 -1000 -500 0 500 1000 1500 2000 2500
Distance, meters

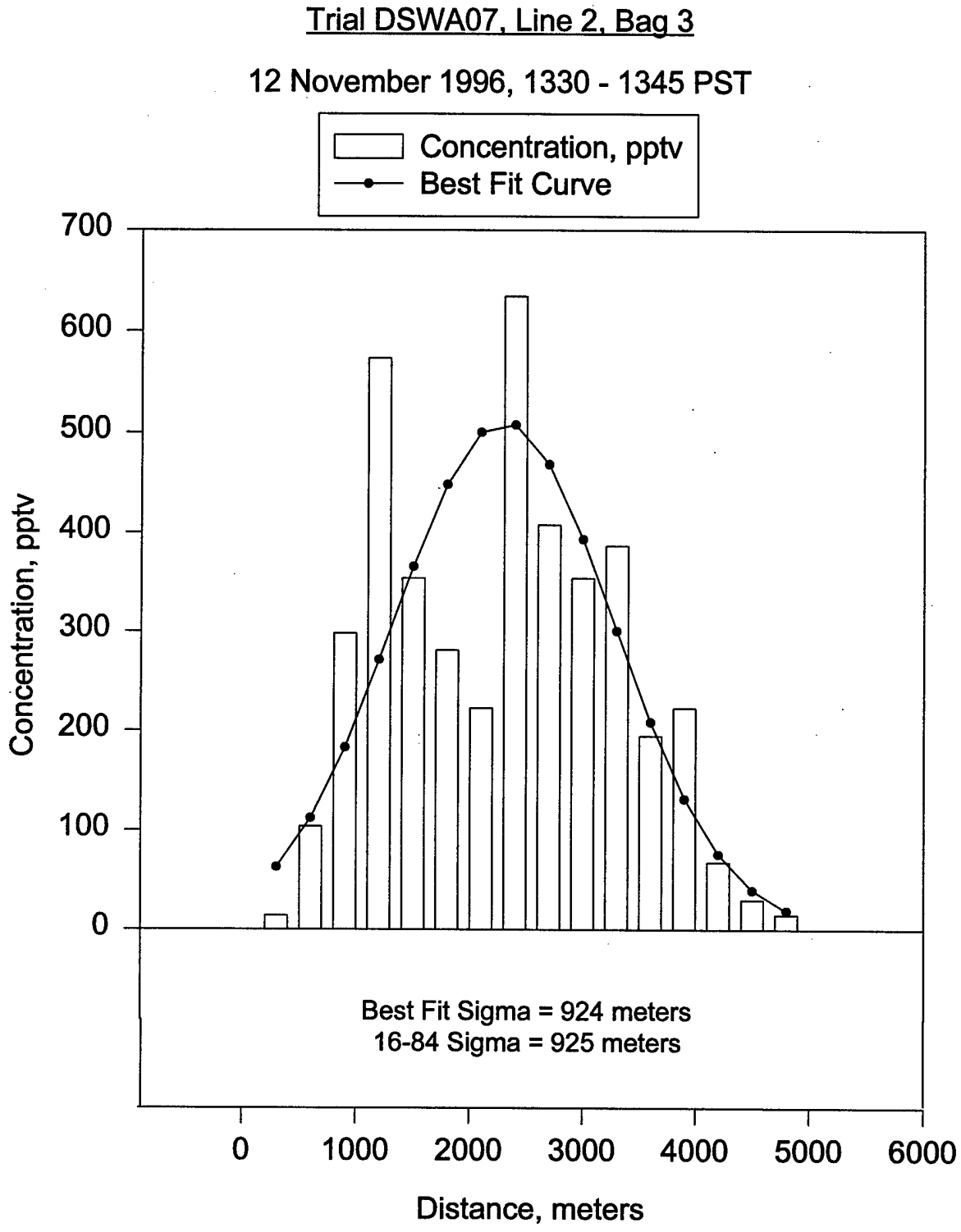
Trial DSWA07, Line 2, Bag 3
12 November 1996, 1330 - 1345 PST
Concentration, pptv
Best Fit Curve
700
600
500
400
300
200
100
0
Concentration, pptv
Best Fit Sigma = 924 meters
16-84 Sigma = 925 meters
0
1000
2000
3000
4000
5000
6000
Distance, meters

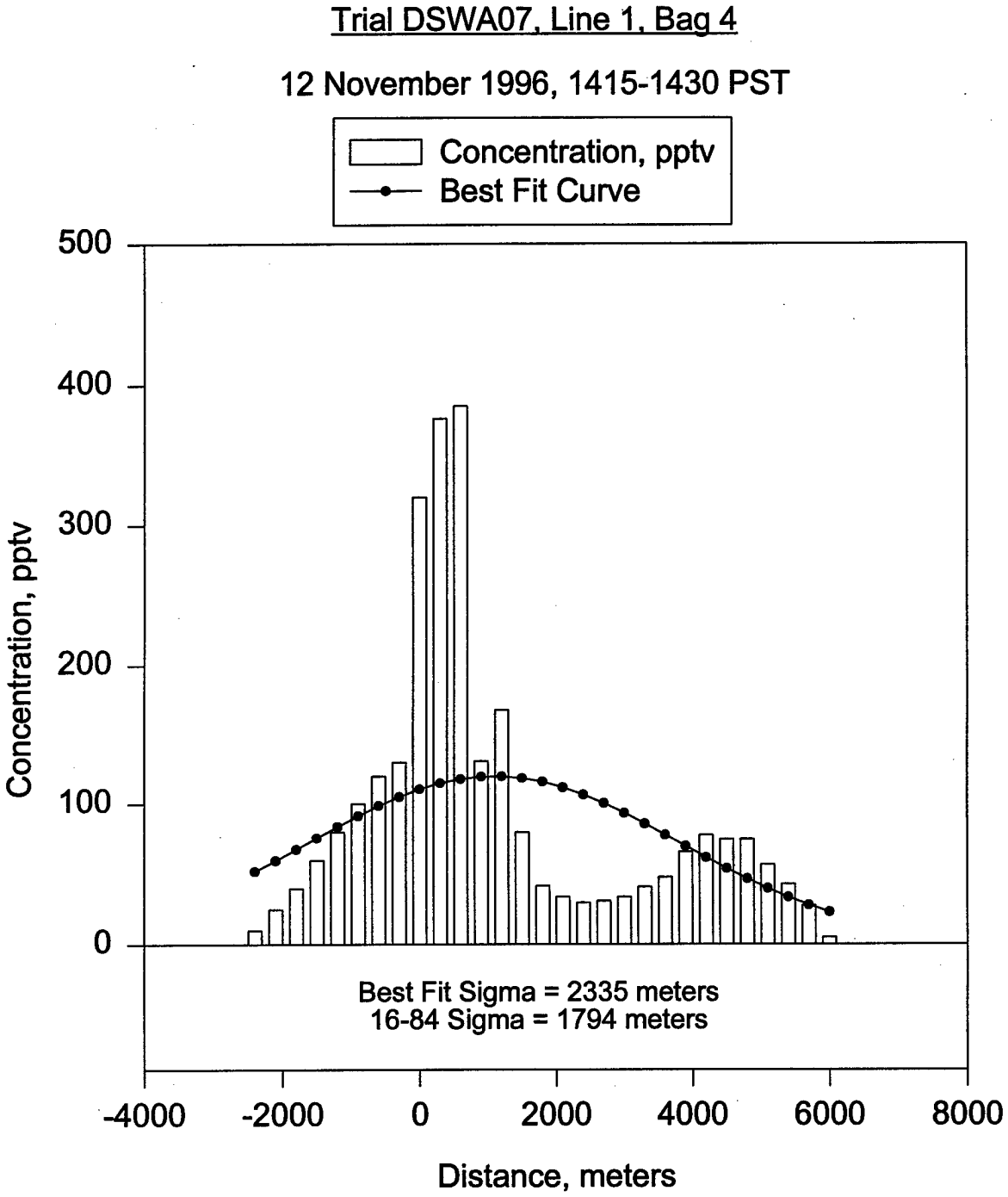
Trial DSWA07, Line 1, Bag 4
12 November 1996, 1415-1430 PST
Concentration, pptv
Best Fit Curve
500
400
300
200
100
0
Concentration, pptv
Best Fit Sigma = 2335 meters
16-84 Sigma = 1794 meters
-4000
-2000
0
2000
4000
6000
8000
Distance, meters

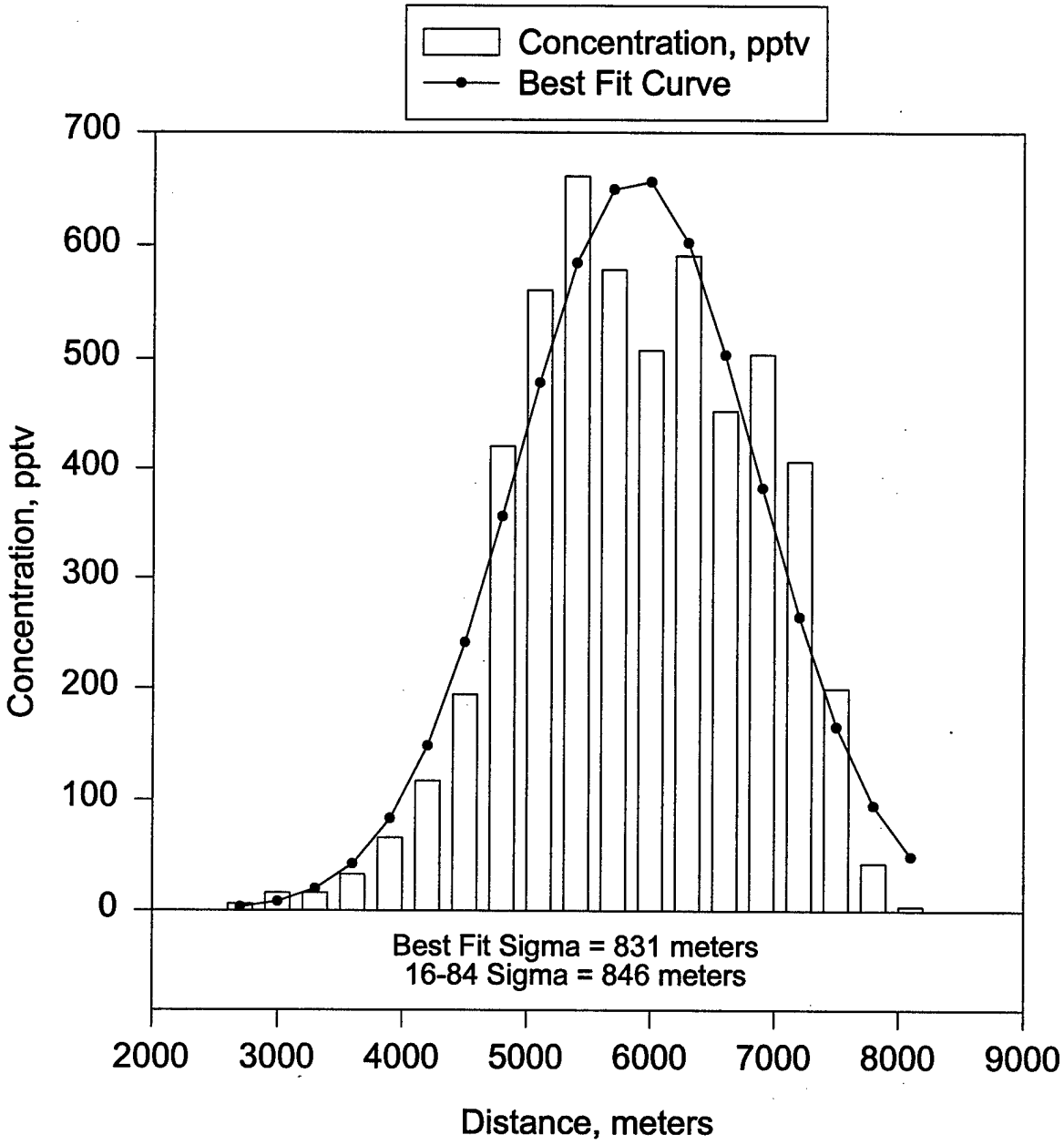
Trial DSWA09, Line 2, Bag 4
13 November 1996, 1445 - 1500 PST
Concentration, pptv
Best Fit Curve
700
600
500
400
300
200
100
0
Concentration, pptv
Best Fit Sigma = 831 meters
16-84 Sigma = 846 meters
2000
3000
4000
5000
6000
7000
8000
9000
Distance, meters

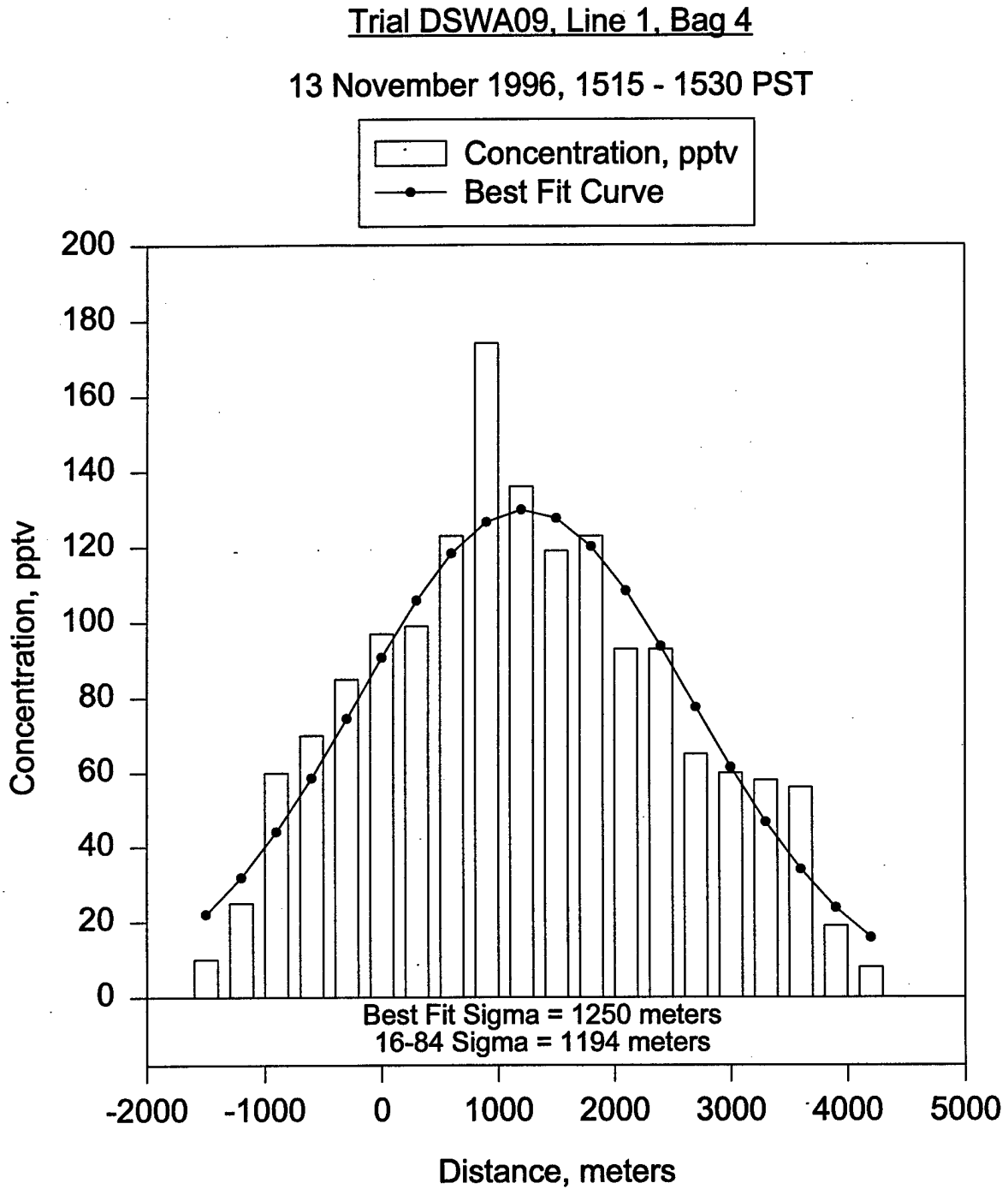
Trial DSWA09, Line 1, Bag 4
13 November 1996, 1515 - 1530 PST
Concentration, pptv
Best Fit Curve
200
180
160
140
120
100
80
60
40
20
0
Concentration, pptv
Best Fit Sigma = 1250 meters
16-84 Sigma = 1194 meters
-2000
-1000
0
1000
2000
3000
4000
5000
Distance, meters

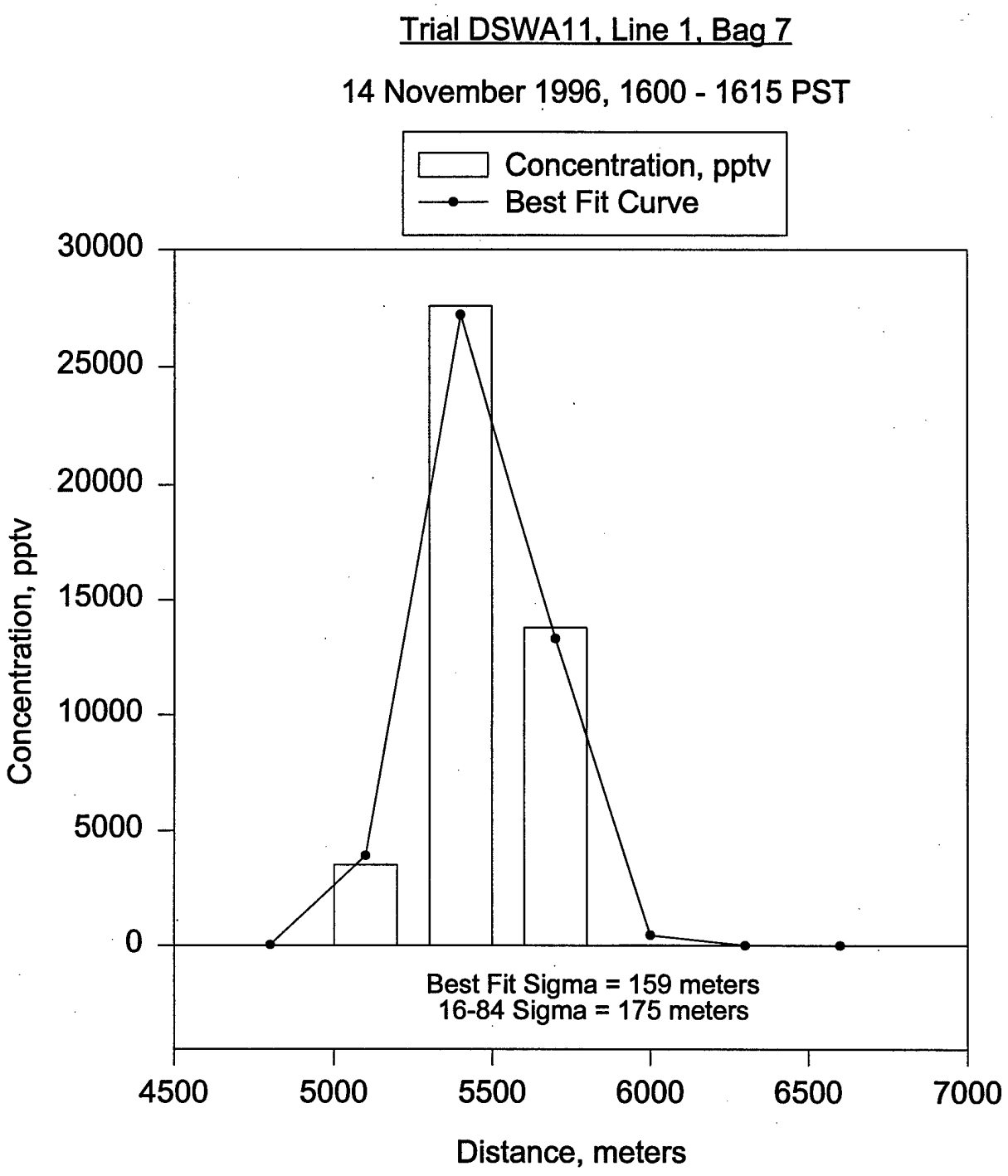
Trial DSWA11, Line 1, Bag 7
14 November 1996, 1600 - 1615 PST
Concentration, pptv
Best Fit Curve
30000
25000
20000
15000
10000
5000
0
Concentration, pptv
Best Fit Sigma = 159 meters
16-84 Sigma = 175 meters
4500
5000
5500
6000
6500
7000
Distance, meters

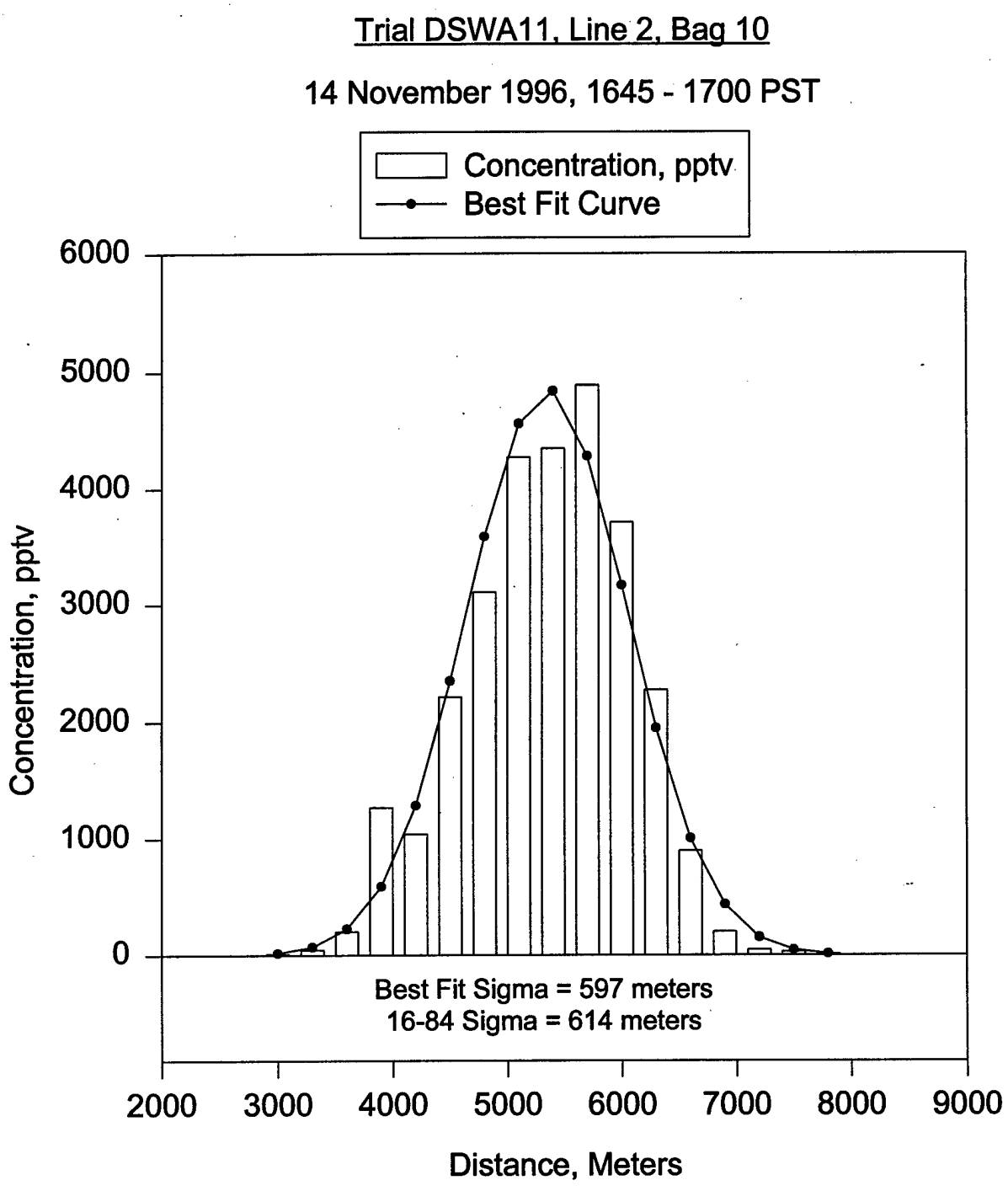
Trial DSWA11, Line 2, Bag 10
14 November 1996, 1645 - 1700 PST
Concentration, pptv
Best Fit Curve
6000
5000
4000
3000
2000
1000
0
Concentration, pptv
Best Fit Sigma = 597 meters
16-84 Sigma = 614 meters
2000
3000
4000
5000
6000
7000
8000
9000
Distance, Meters

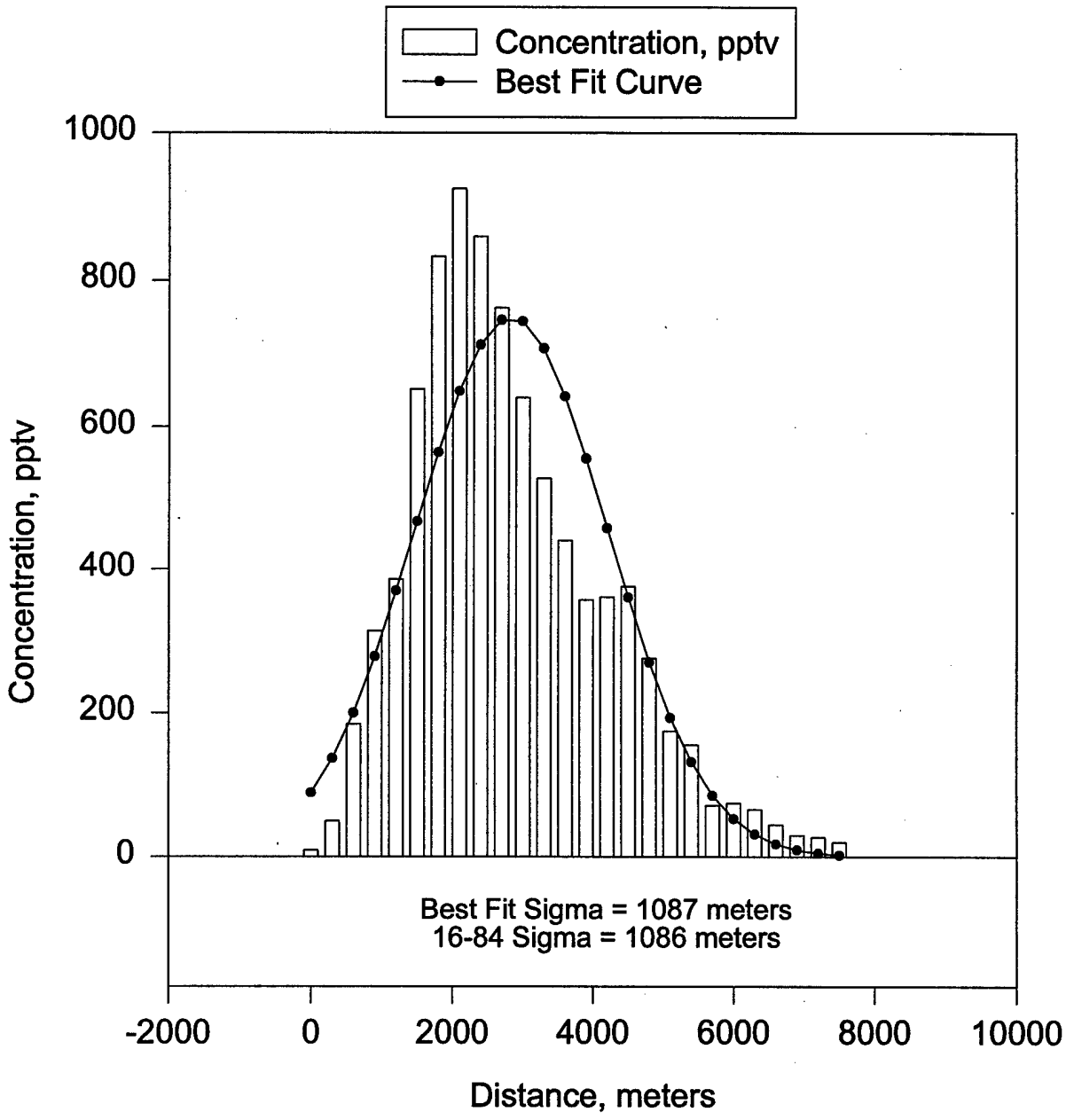
Trial DSWA11, Line 3, Bag 11
14 November 1996, 1730 - 1745 PST
Concentration, pptv
Best Fit Curve
1000
800
600
400
200
0
Concentration, pptv
Best Fit Sigma = 1087 meters
16-84 Sigma = 1086 meters
-2000
0
2000
4000
6000
8000
10000
Distance, meters

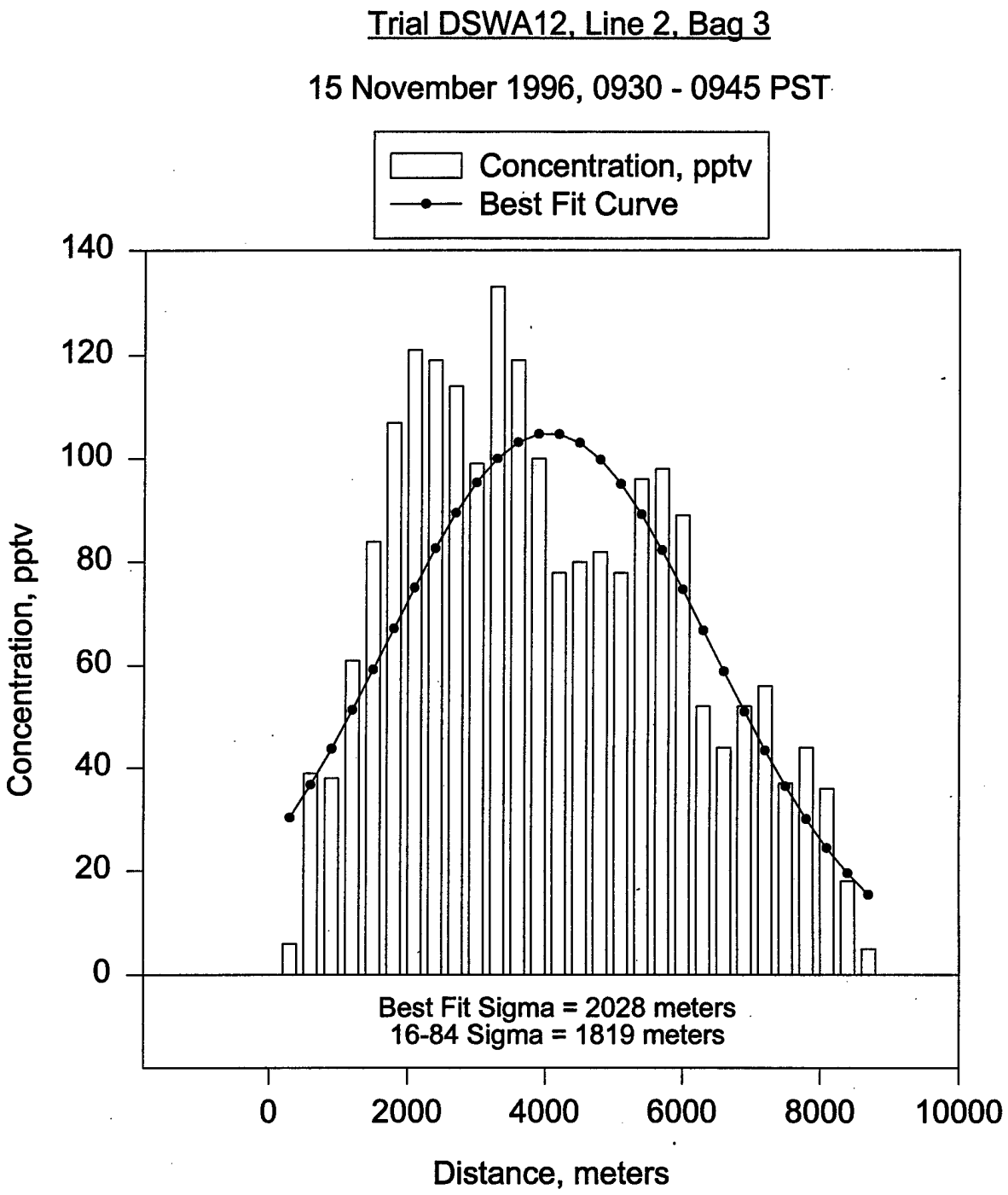
Trial DSWA12, Line 2, Bag 3
15 November 1996, 0930 - 0945 PST
Concentration, pptv
Best Fit Curve
140
120
100
80
60
40
20
0
Concentration, pptv
Best Fit Sigma = 2028 meters
16-84 Sigma = 1819 meters
0
2000
4000
6000
8000
10000
Distance, meters

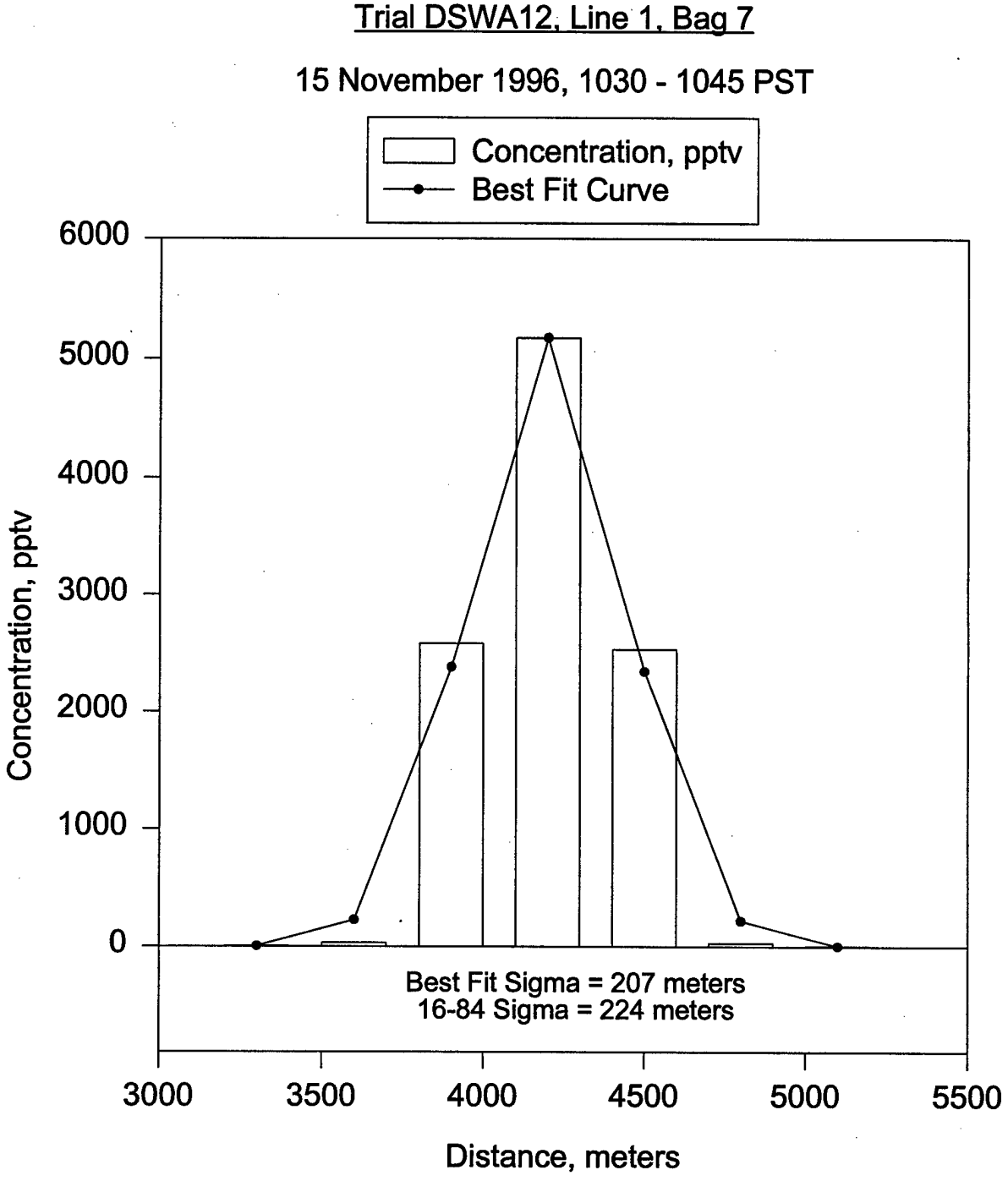
Trial DSWA12, Line 1, Bag 7
15 November 1996, 1030 - 1045 PST
Concentration, pptv
Best Fit Curve
6000
5000
4000
3000
2000
1000
0
Concentration, pptv
Best Fit Sigma = 207 meters
16-84 Sigma = 224 meters
3000
3500
4000
4500
5000
5500
Distance, meters

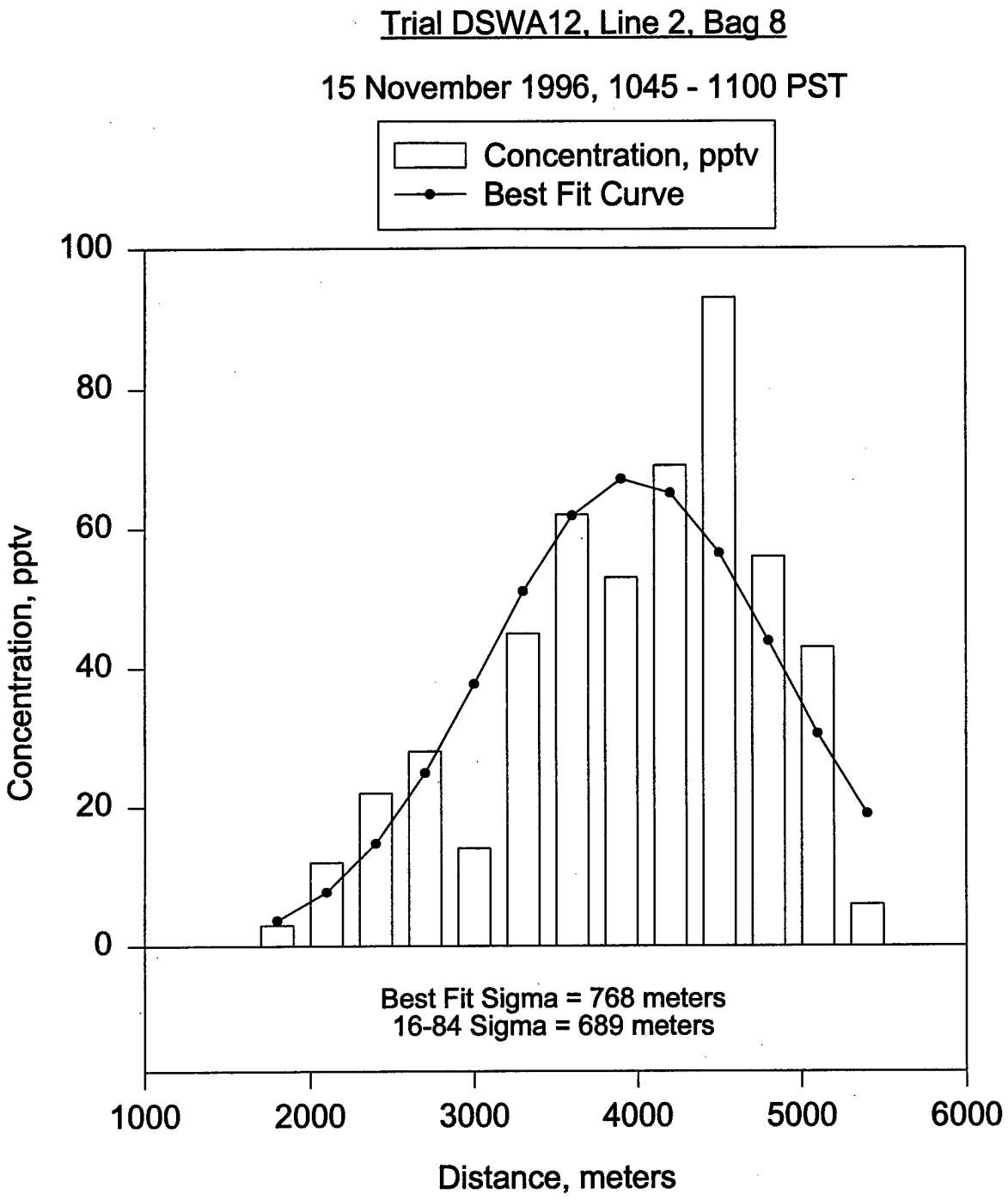
Trial DSWA12, Line 2, Bag 8
15 November 1996, 1045 - 1100 PST
Concentration, pptv
Best Fit Curve
100
80
60
40
20
0
Concentration, pptv
Best Fit Sigma = 768 meters
16-84 Sigma = 689 meters
1000
2000
3000
4000
5000
6000
Distance, meters

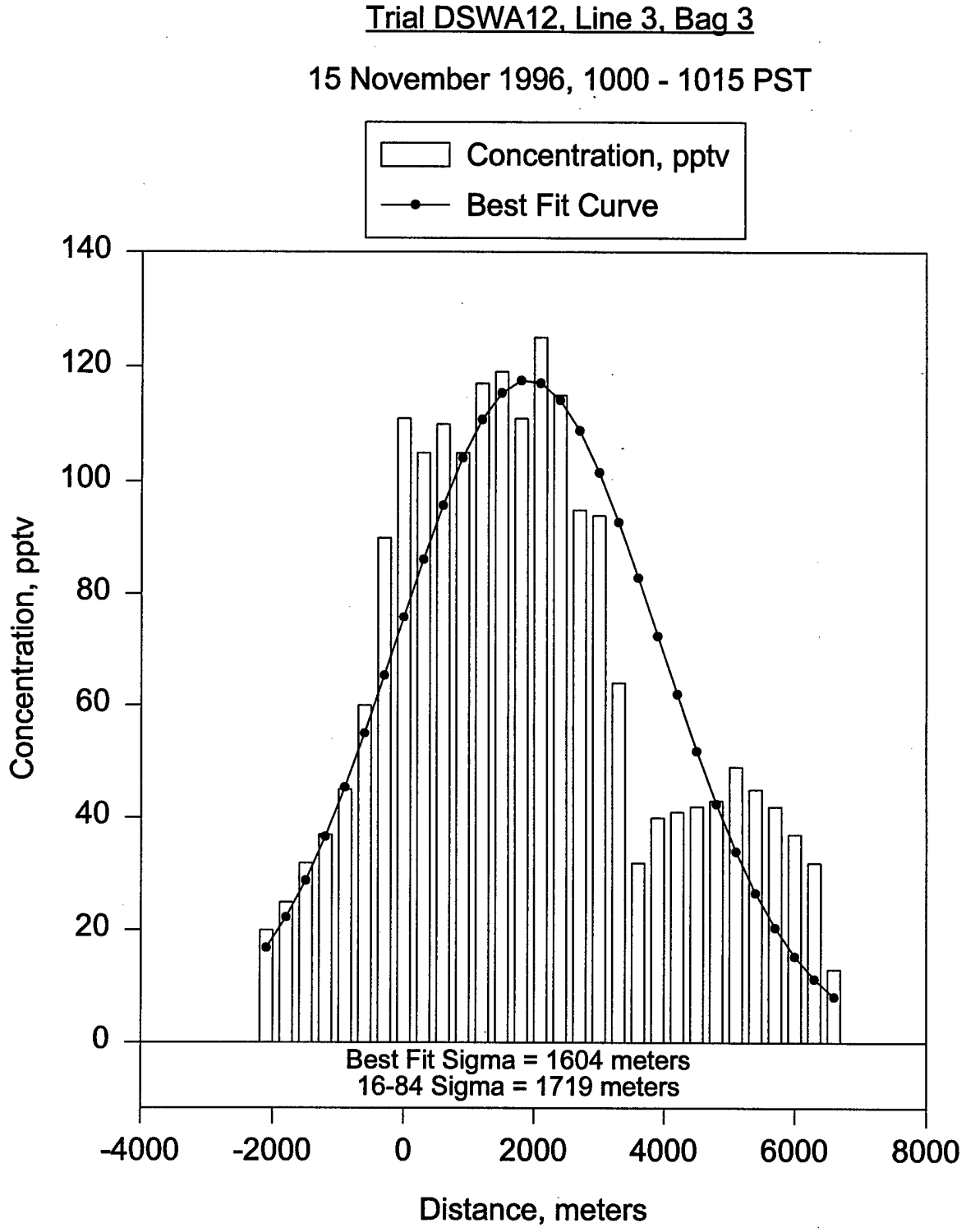
Trial DSWA12, Line 3, Bag 3
15 November 1996, 1000 - 1015 PST
Concentration, pptv
Best Fit Curve
140
120
100
80
60
40
20
0
Concentration, pptv
Best Fit Sigma = 1604 meters
16-84 Sigma = 1719 meters
-4000
-2000
0
2000
4000
6000
8000
Distance, meters

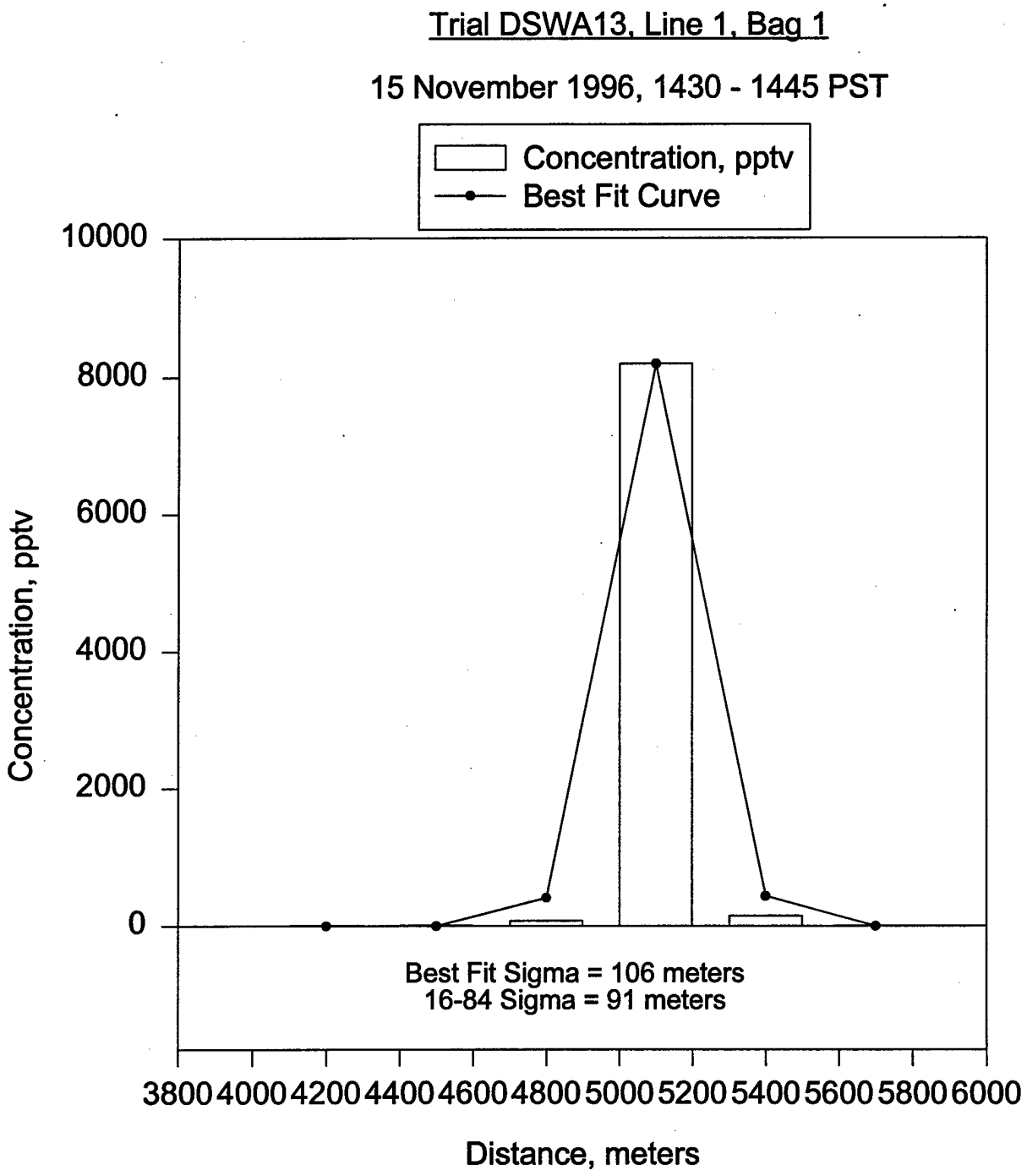
Trial DSWA13, Line 1, Bag 1
15 November 1996, 1430 - 1445 PST
Concentration, pptv
Best Fit Curve
10000
8000
6000
4000
2000
0
Concentration, pptv
Best Fit Sigma = 106 meters
16-84 Sigma = 91 meters
3800 4000 4200 4400 4600 4800 5000 5200 5400 5600 5800 6000
Distance, meters

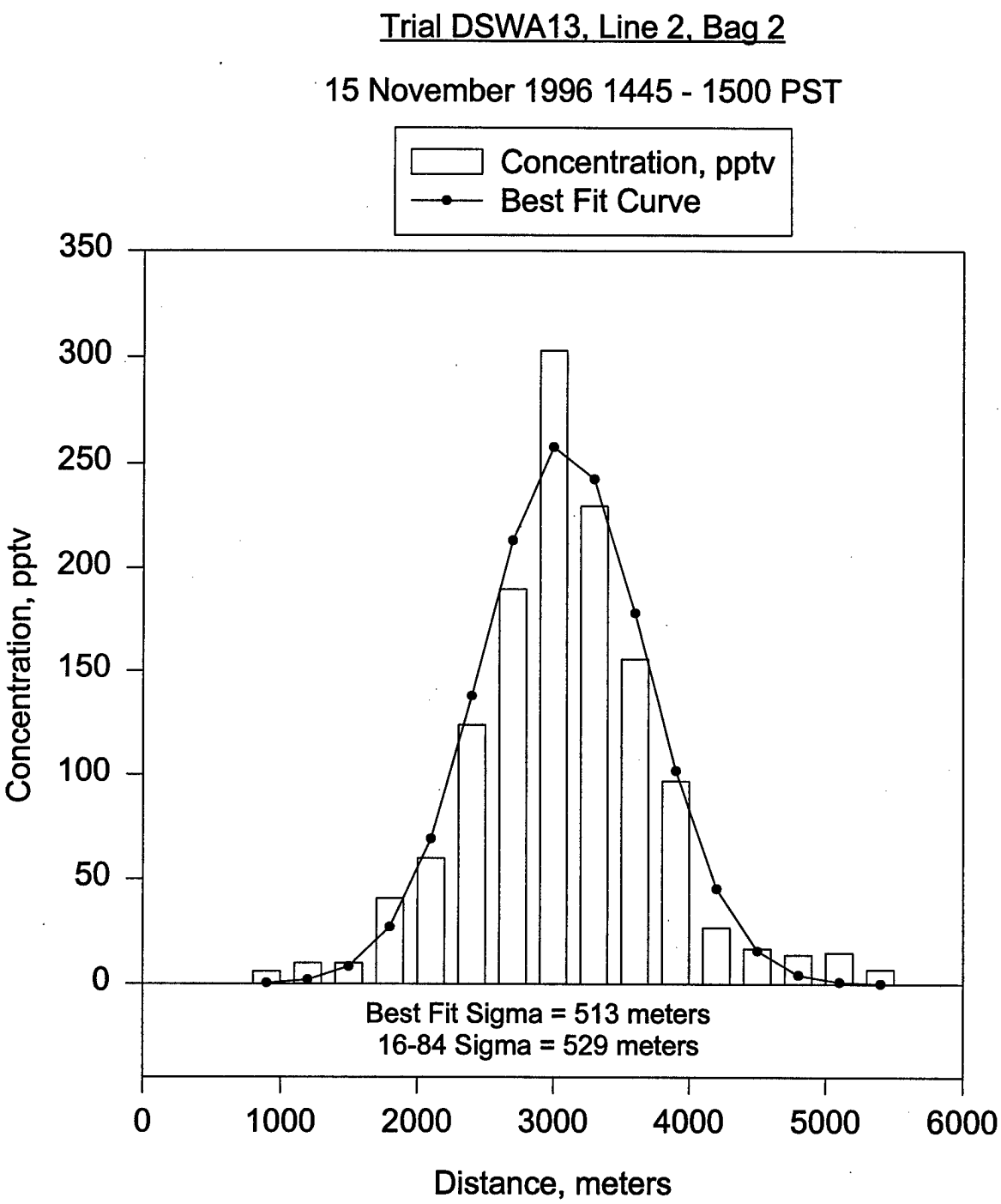
Trial DSWA13, Line 2, Bag 2
15 November 1996 1445 - 1500 PST
Concentration, pptv
Best Fit Curve
350
300
250
200
150
100
50
0
Concentration, pptv
Best Fit Sigma = 513 meters
16-84 Sigma = 529 meters
0
1000
2000
3000
4000
5000
6000
Distance, meters

Trial DSWA13, Line 3, Bag 1

15 November 1996, 1500 - 1515 PST

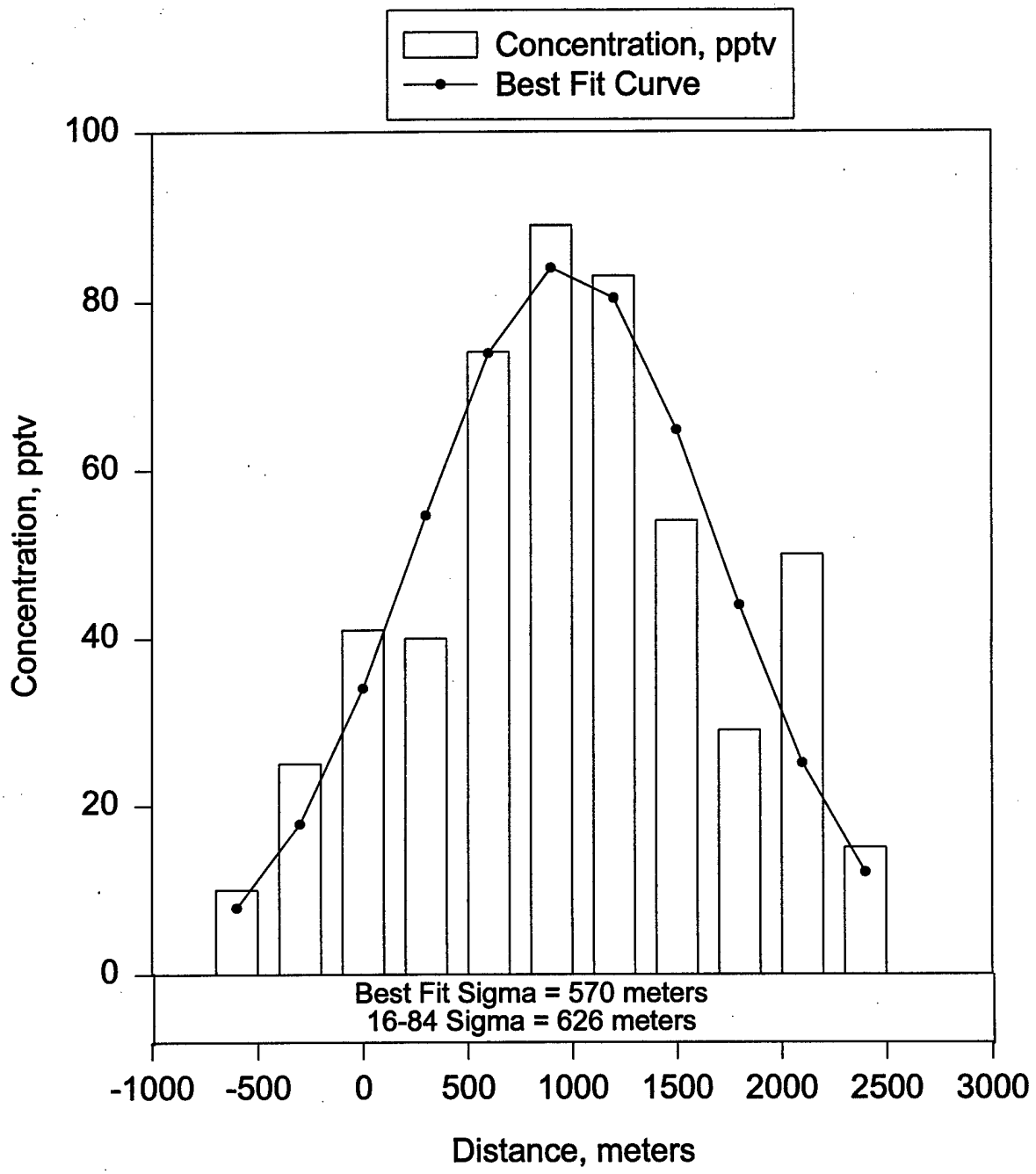

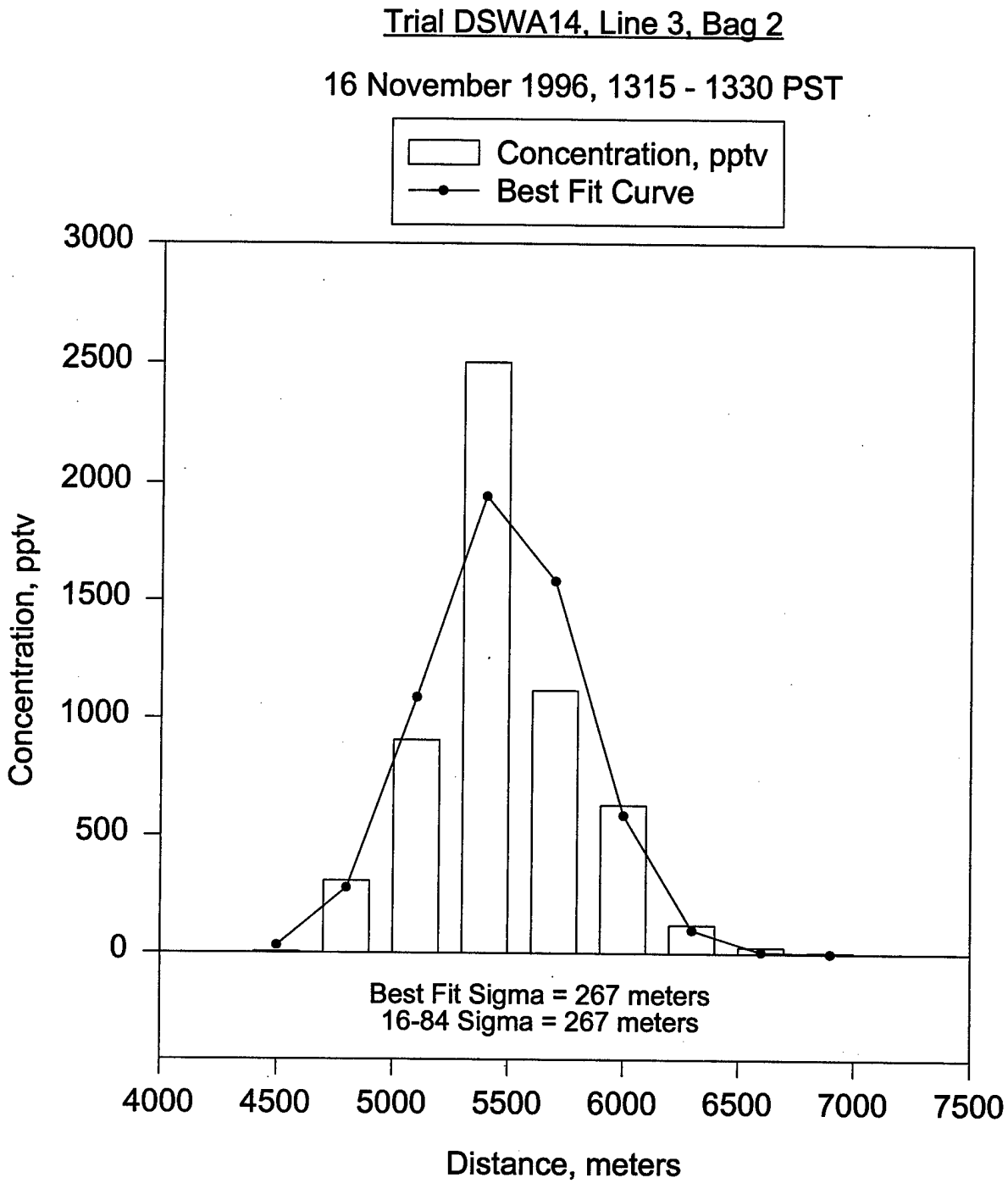
Trial DSWA14, Line 3, Bag 2
16 November 1996, 1315 - 1330 PST
Concentration, pptv
Best Fit Curve
3000
2500
2000
1500
1000
500
0
Concentration, pptv
Best Fit Sigma = 267 meters
16-84 Sigma = 267 meters
4000
4500
5000
5500
6000
6500
7000
7500
Distance, meters

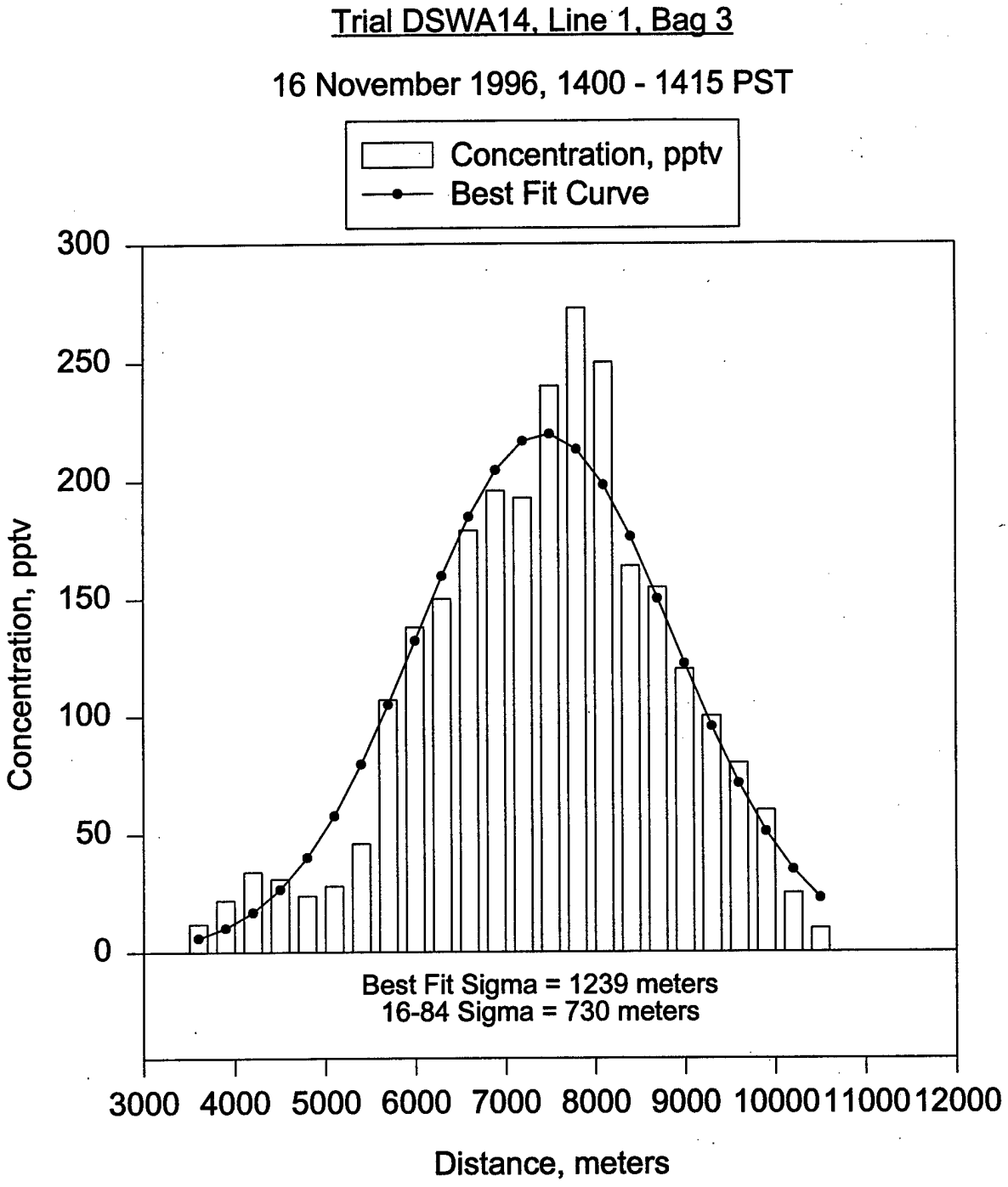
Trial DSWA14, Line 1, Bag 3
16 November 1996, 1400 - 1415 PST
Concentration, pptv
Best Fit Curve
300
250
200
150
100
50
0
Concentration, pptv
Best Fit Sigma = 1239 meters
16-84 Sigma = 730 meters
3000 4000 5000 6000 7000 8000 9000 10000 11000 12000
Distance, meters

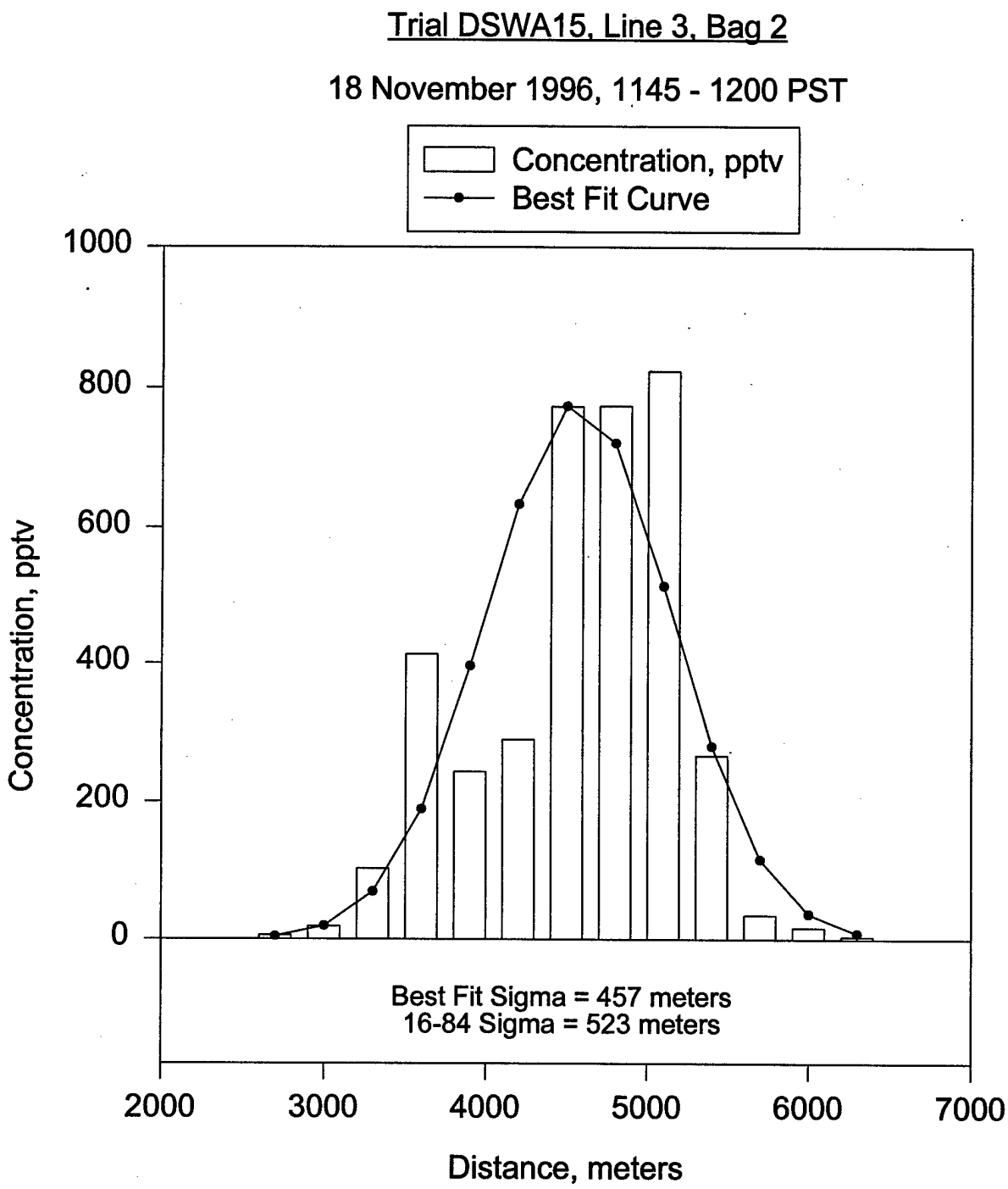
Trial DSWA15, Line 3, Bag 2
18 November 1996, 1145 - 1200 PST
Concentration, pptv
Best Fit Curve
1000
800
600
400
200
0
Concentration, pptv
Best Fit Sigma = 457 meters
16-84 Sigma = 523 meters
2000
3000
4000
5000
6000
7000
Distance, meters

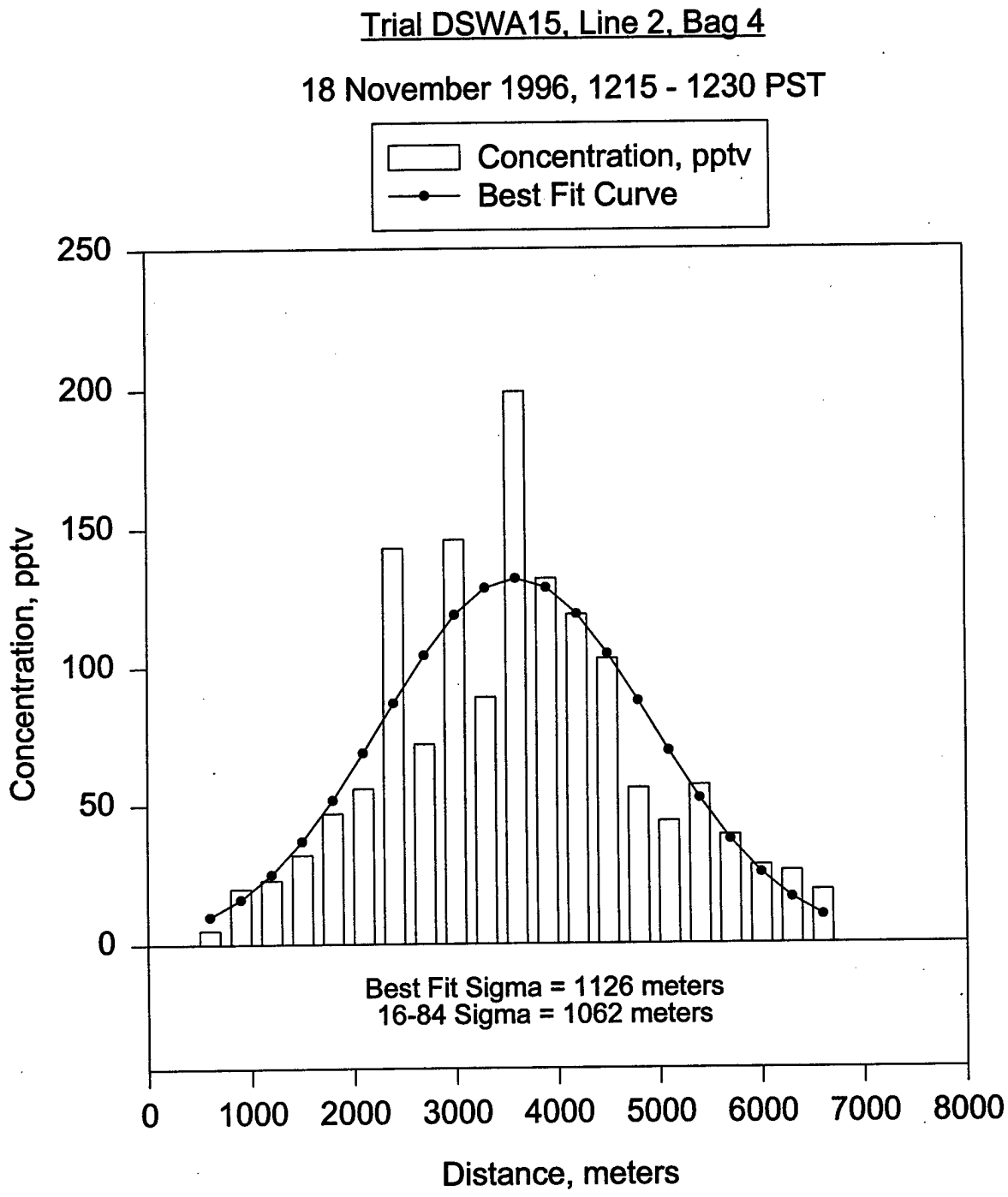
Trial DSWA15, Line 2, Bag 4
18 November 1996, 1215 - 1230 PST
Concentration, pptv
Best Fit Curve
250
200
150
100
50
0
Concentration, pptv
Best Fit Sigma = 1126 meters
16-84 Sigma = 1062 meters
0
1000
2000
3000
4000
5000
6000
7000
8000
Distance, meters

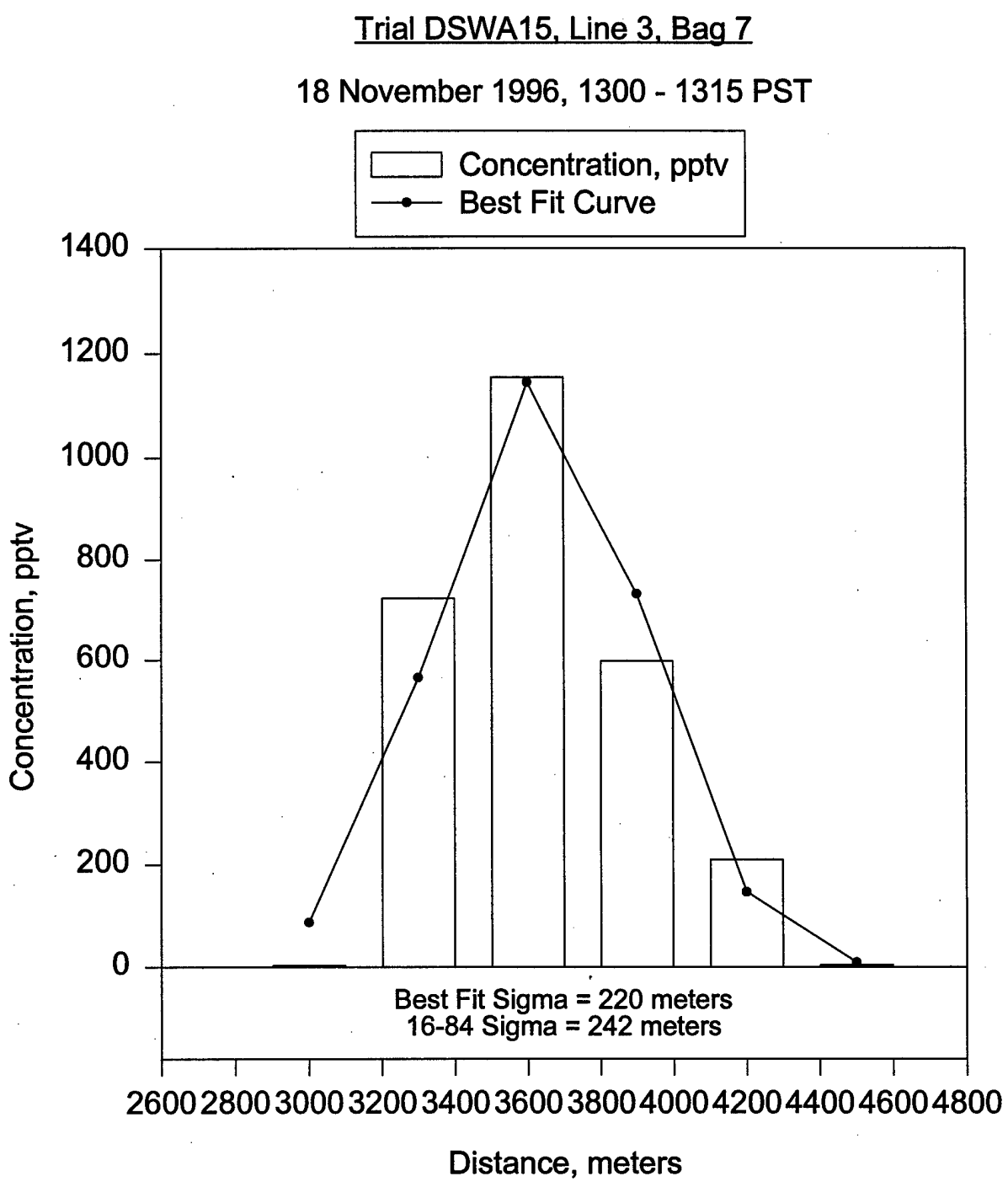
Trial DSWA15, Line 3, Bag 7
18 November 1996, 1300 - 1315 PST
Concentration, pptv
Best Fit Curve
1400
1200
1000
800
600
400
200
0
Concentration, pptv
Best Fit Sigma = 220 meters
16-84 Sigma = 242 meters
2600 2800 3000 3200 3400 3600 3800 4000 4200 4400 4600 4800
Distance, meters

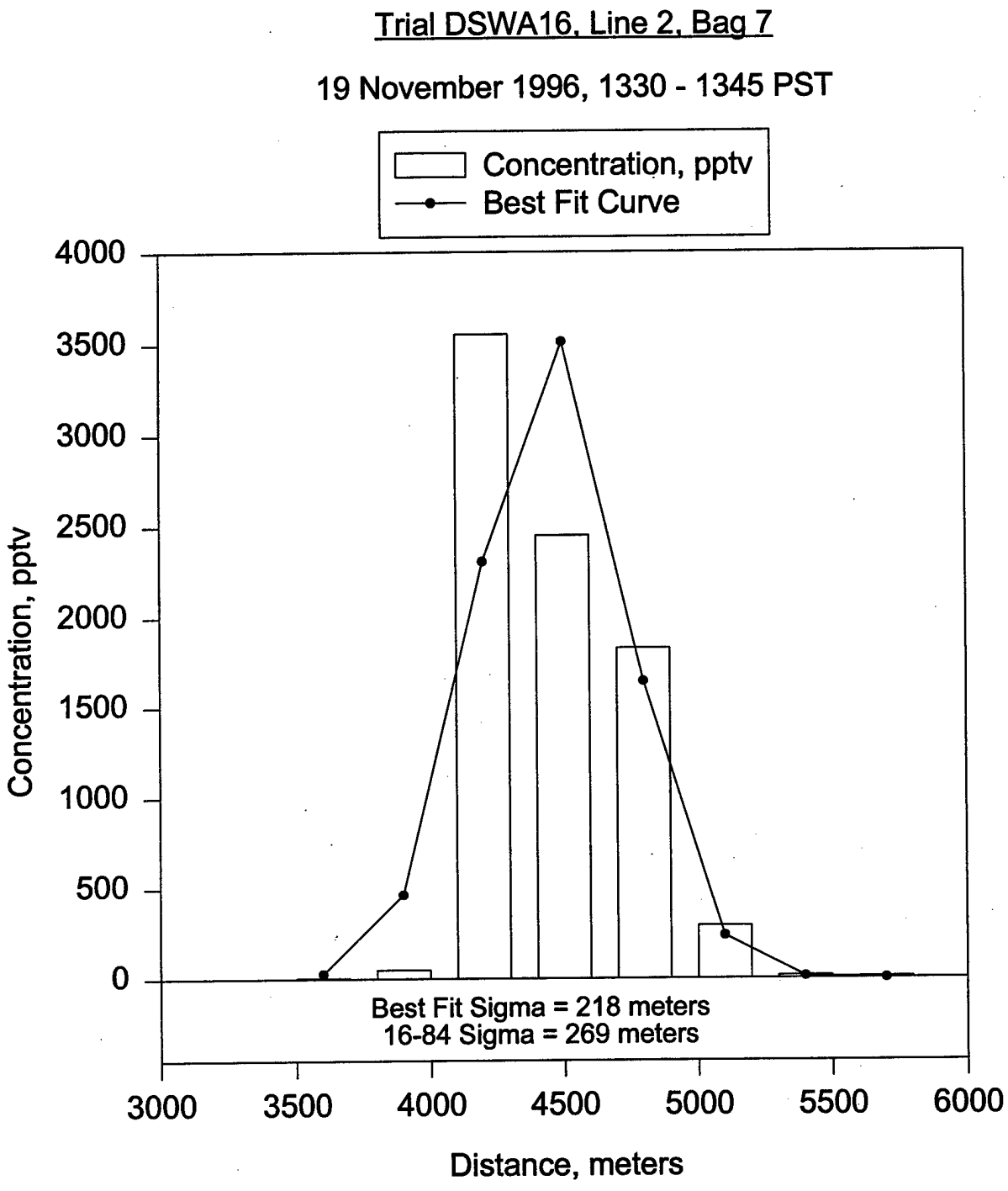
Trial DSWA16, Line 2, Bag 7
19 November 1996, 1330 - 1345 PST
Concentration, pptv
Best Fit Curve
4000
3500
3000
2500
2000
1500
1000
500
0
Concentration, pptv
Best Fit Sigma = 218 meters
16-84 Sigma = 269 meters
3000
3500
4000
4500
5000
5500
6000
Distance, meters

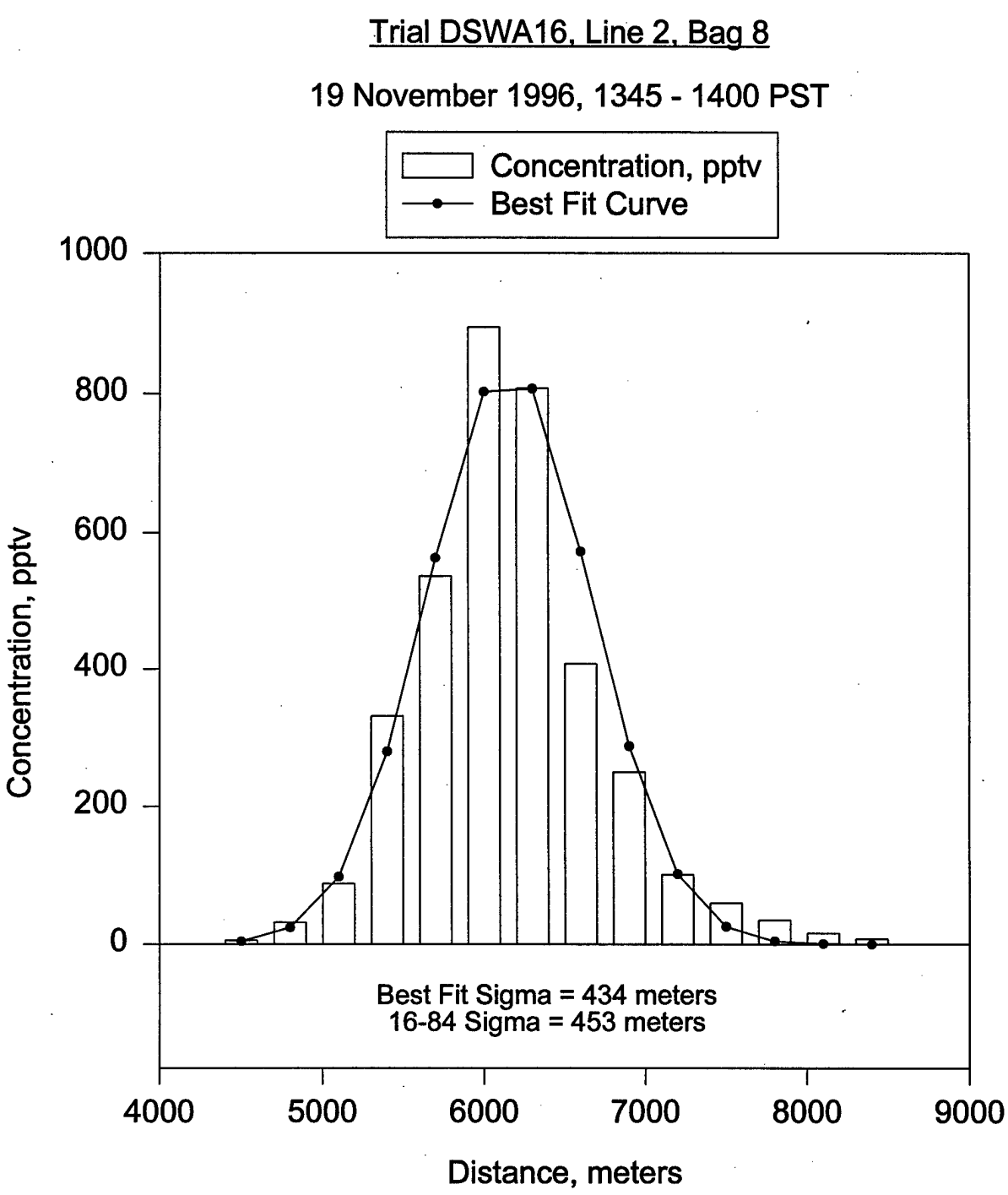
Trial DSWA16, Line 2, Bag 8
19 November 1996, 1345 - 1400 PST
Concentration, pptv
Best Fit Curve
1000
800
600
400
200
0
Concentration, pptv
Best Fit Sigma = 434 meters
16-84 Sigma = 453 meters
4000
5000
6000
7000
8000
9000
Distance, meters

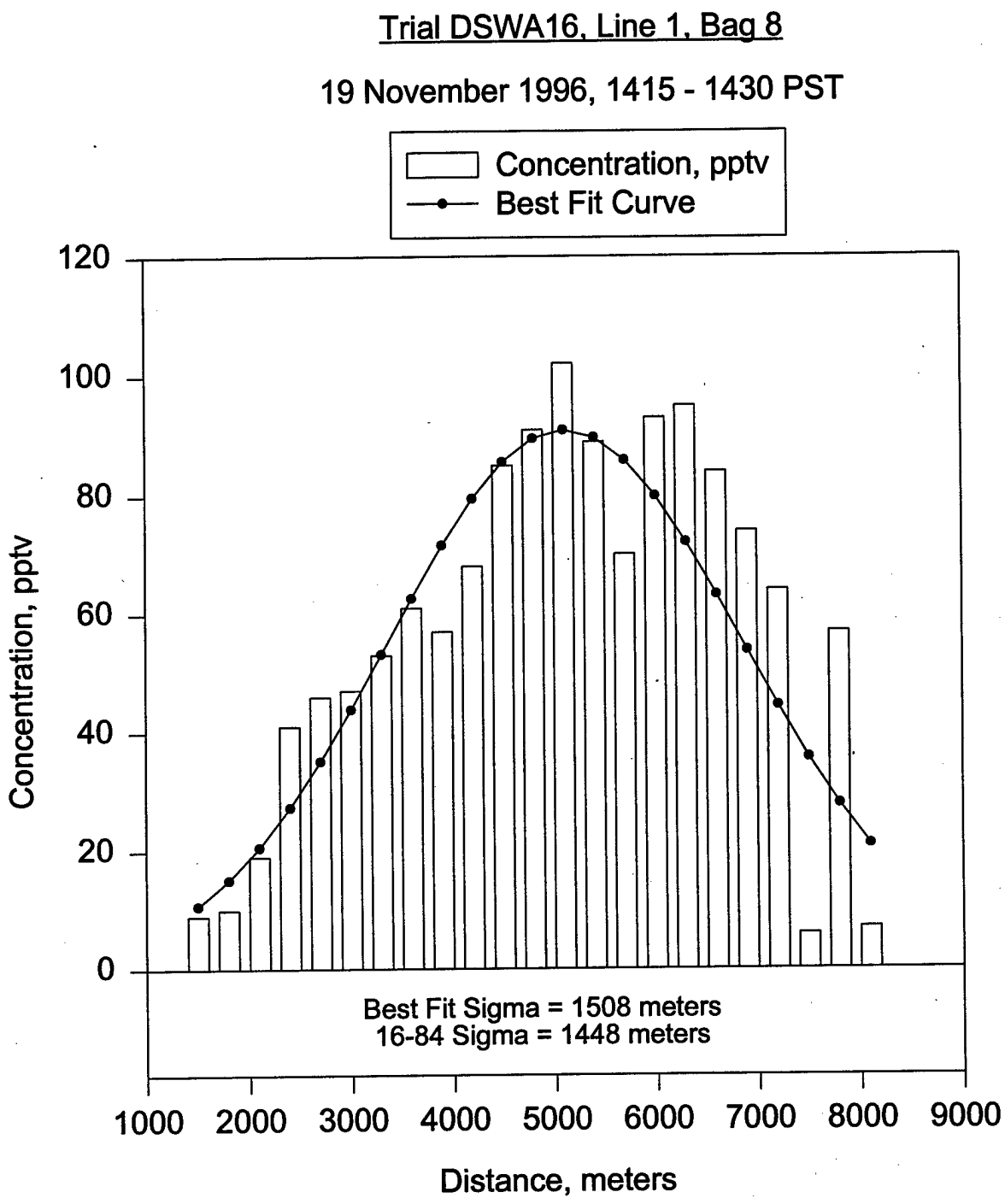
Trial DSWA16, Line 1, Bag 8
19 November 1996, 1415 - 1430 PST
Concentration, pptv
Best Fit Curve
120
100
80
60
40
20
0
Concentration, pptv
Best Fit Sigma = 1508 meters
16-84 Sigma = 1448 meters
1000
2000
3000
4000
5000
6000
7000
8000
9000
Distance, meters

Trial DSWA17, Line 2, Bag 3

20 November 1996, 1230 - 1245 PST

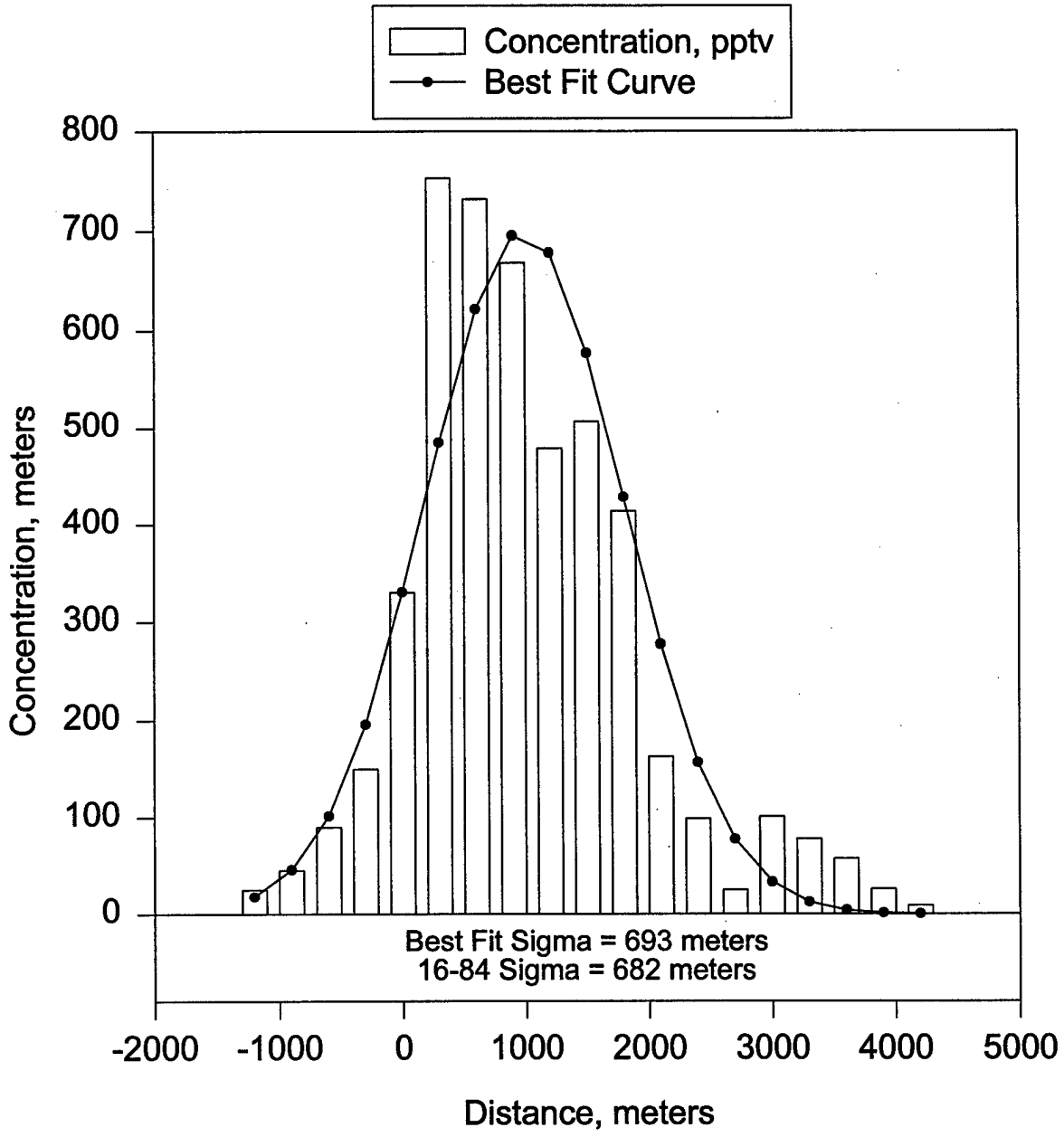

Trial DSWA17, Line 1, Bag 9

20 November 1996, 1430 - 1445 PST

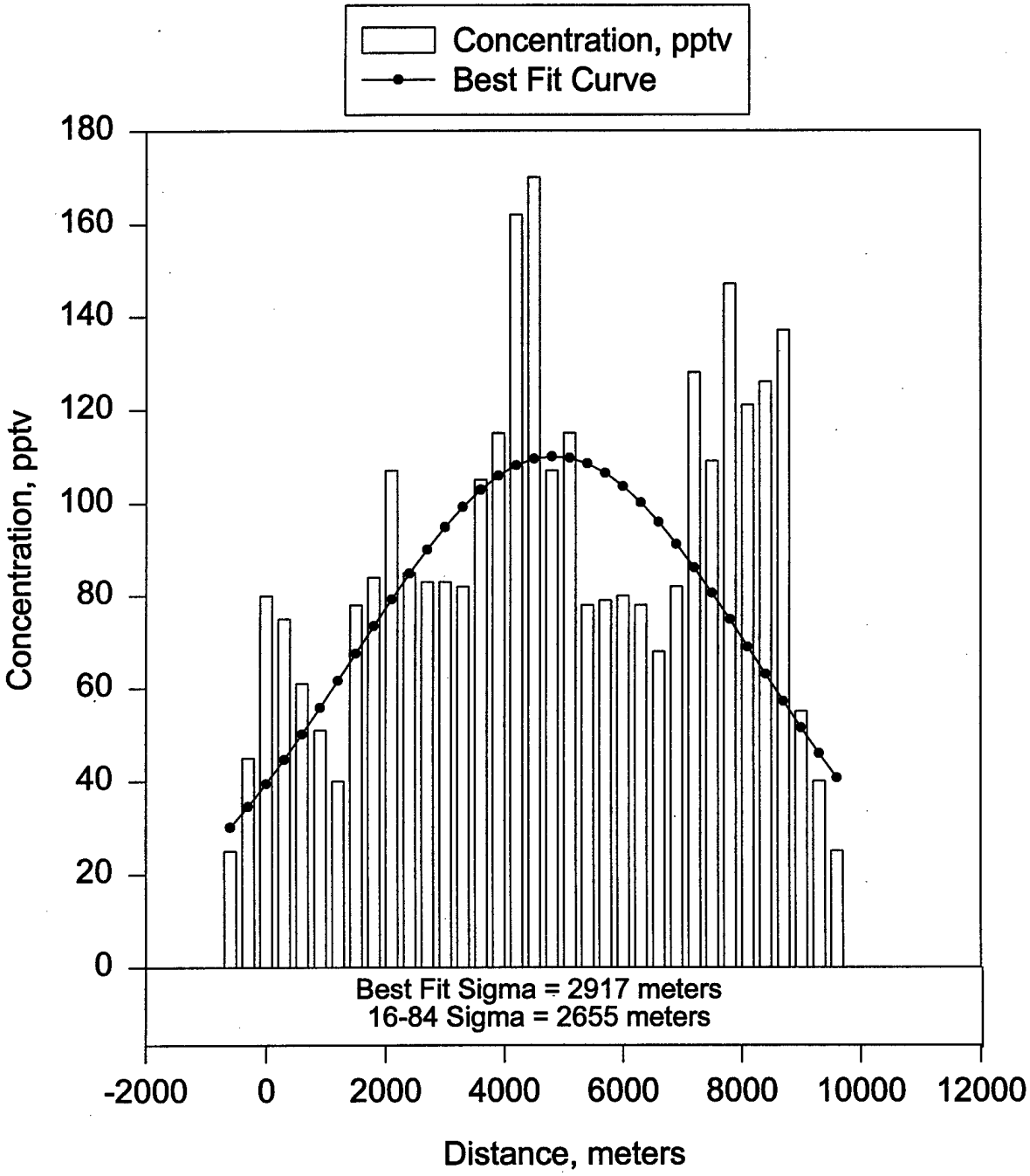

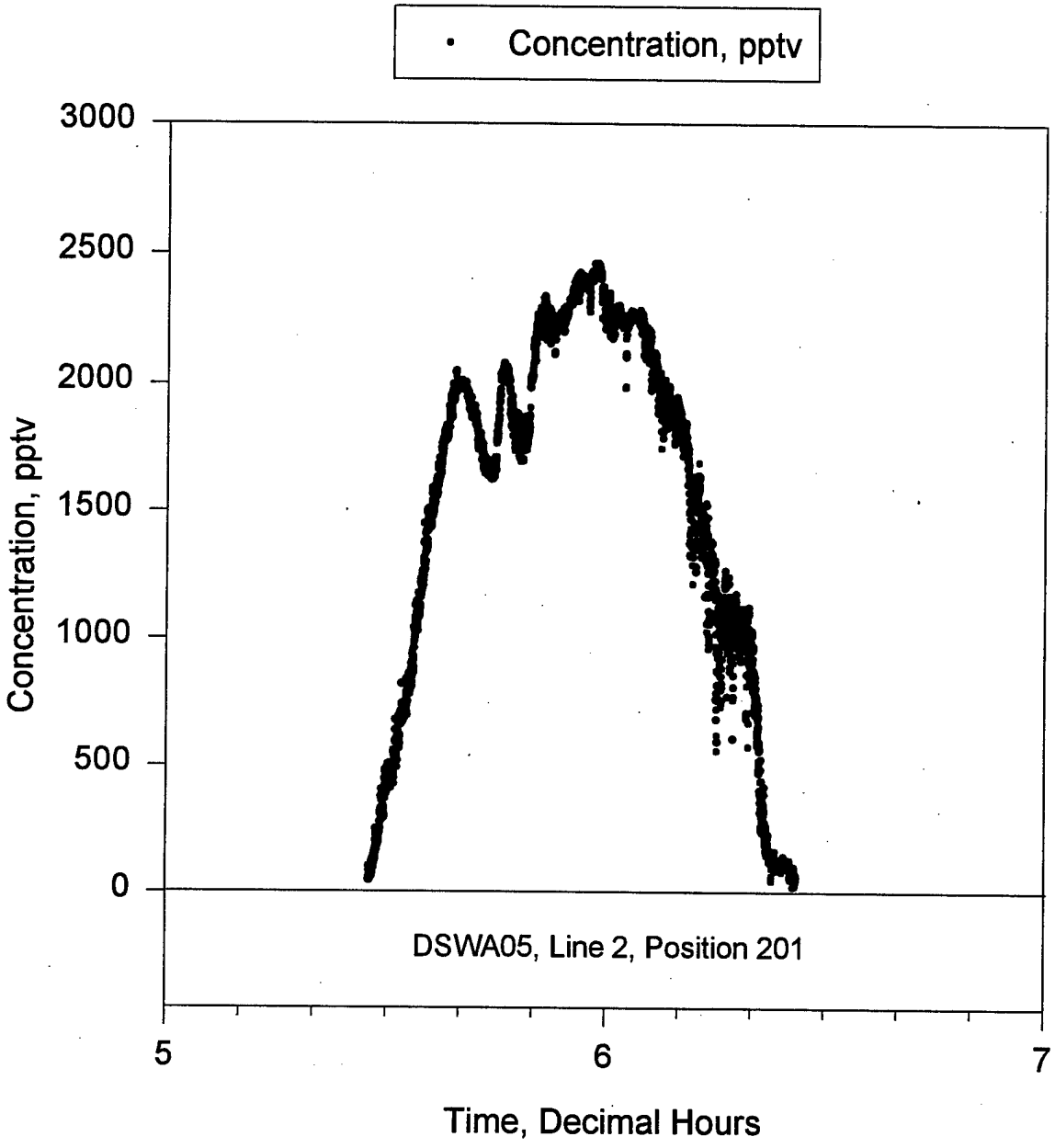
Concentration, pptv
3000
2500
2000
1500
1000
500
0
Concentration, pptv
DSWA05, Line 2, Position 201
5
6
7
Time, Decimal Hours

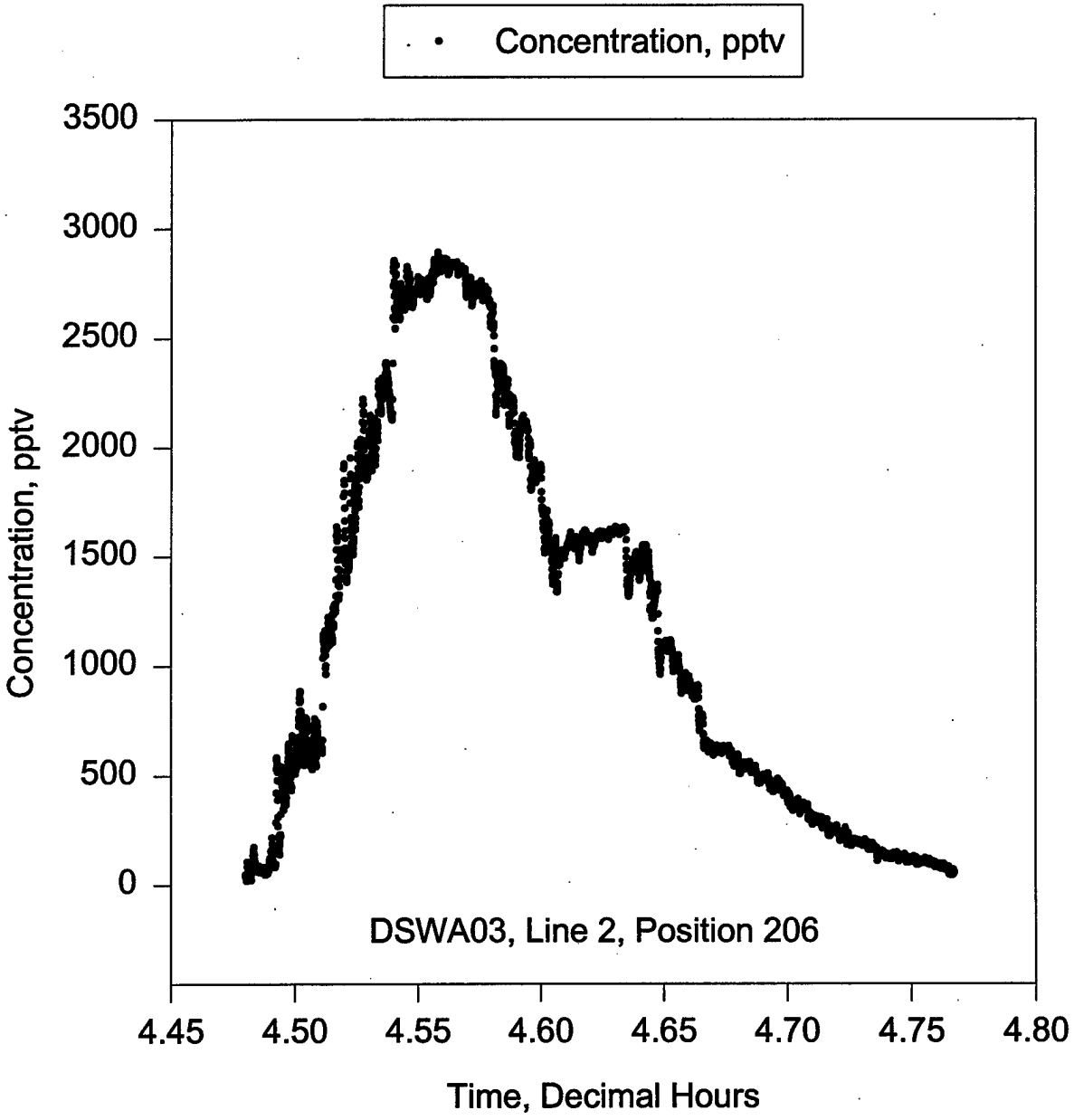
Concentration, pptv
3500
3000
2500
2000
1500
1000
500
0
Concentration, pptv
DSWA03, Line 2, Position 206
4.45
4.50
4.55
4.60
4.65
4.70
4.75
4.80
Time, Decimal Hours

DA4V2.SPW

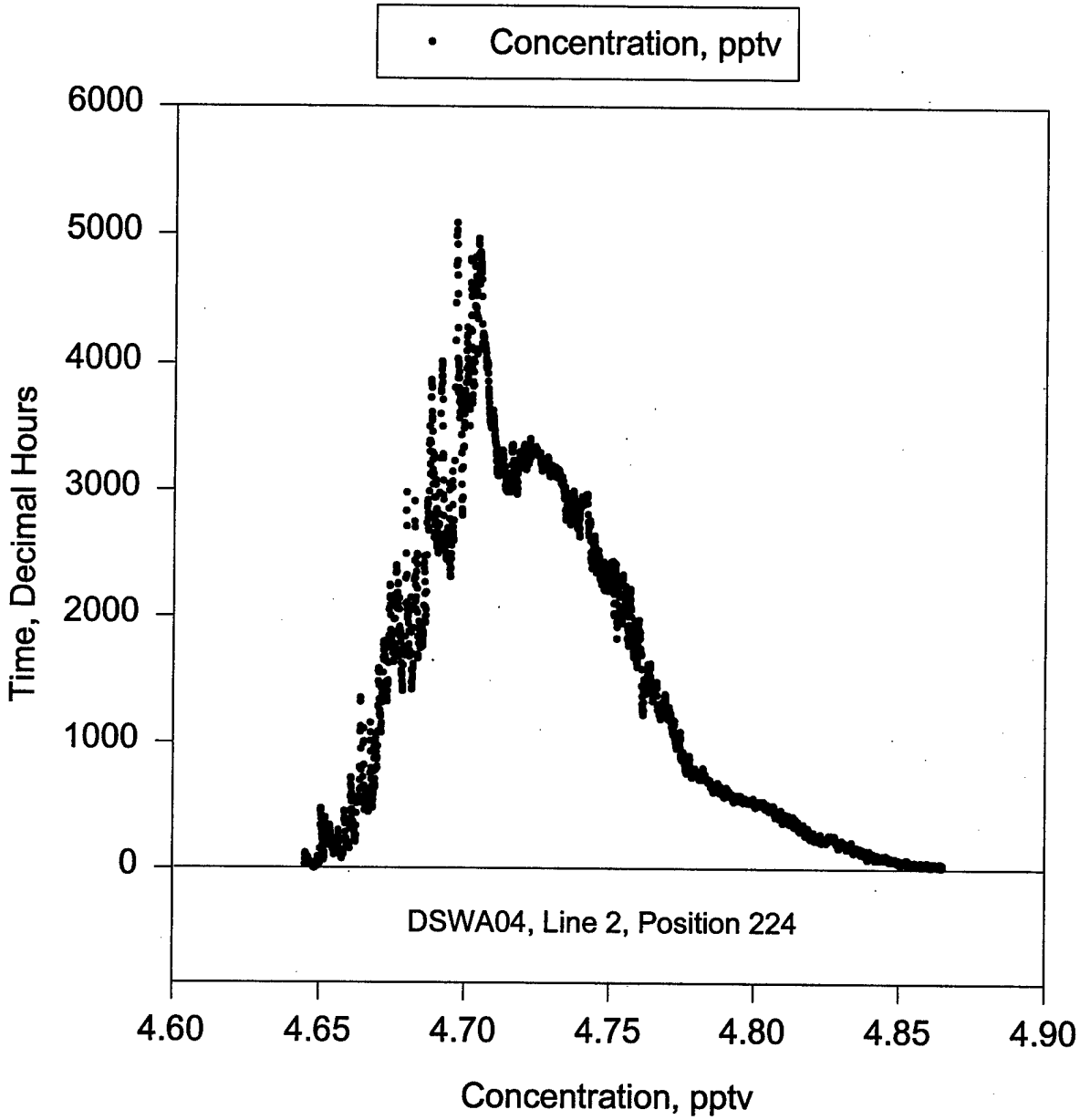
Concentration, pptv
6000
5000
4000
3000
2000
1000
0
Time, Decimal Hours
DSWA04, Line 2, Position 224
4.60
4.65
4.70
4.75
4.80
4.85
4.90
Concentration, pptv

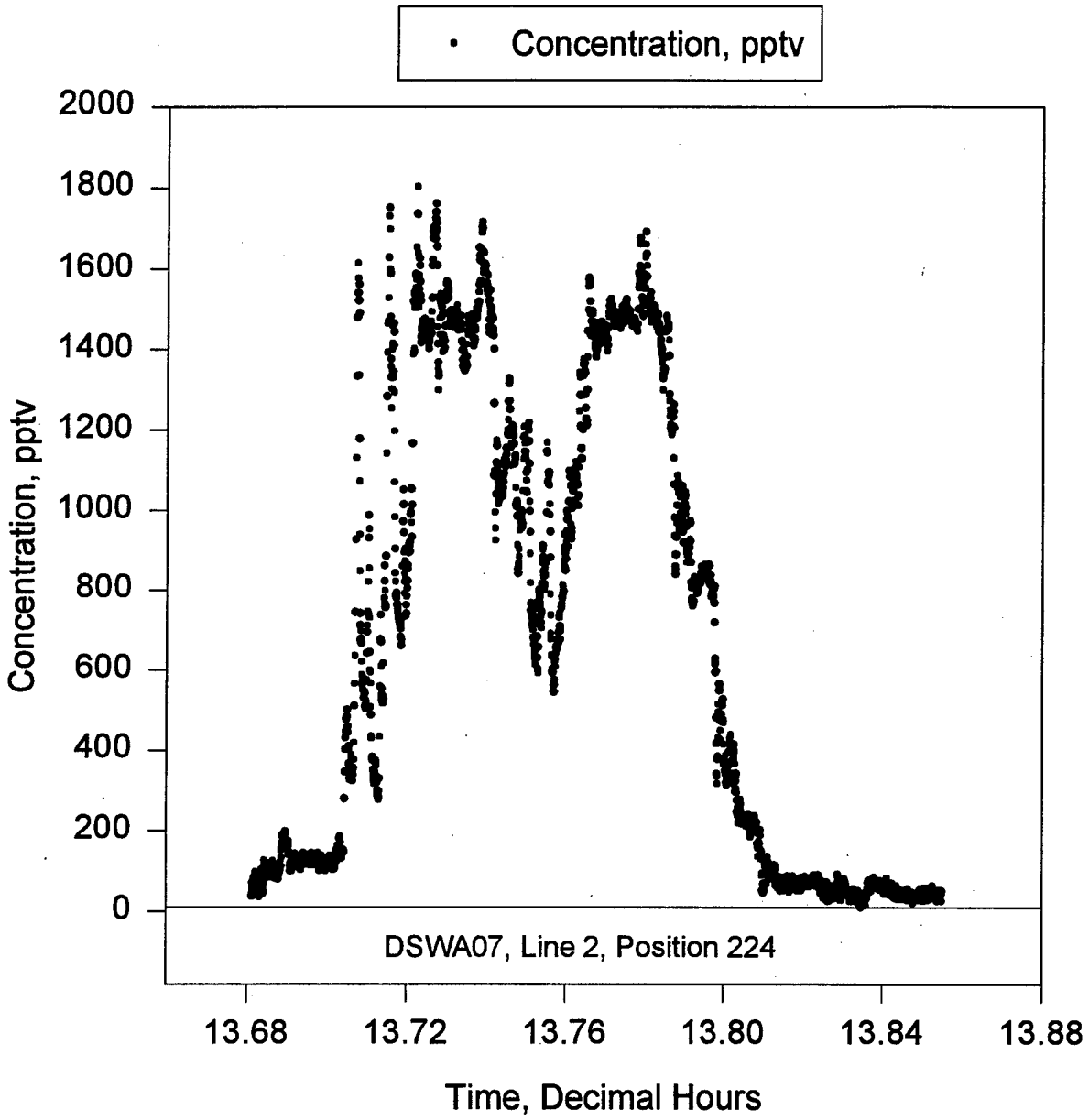
Concentration, pptv
2000
1800
1600
1400
1200
1000
800
600
400
200
0
Concentration, pptv
DSWA07, Line 2, Position 224
13.68
13.72
13.76
13.80
13.84
13.88
Time, Decimal Hours

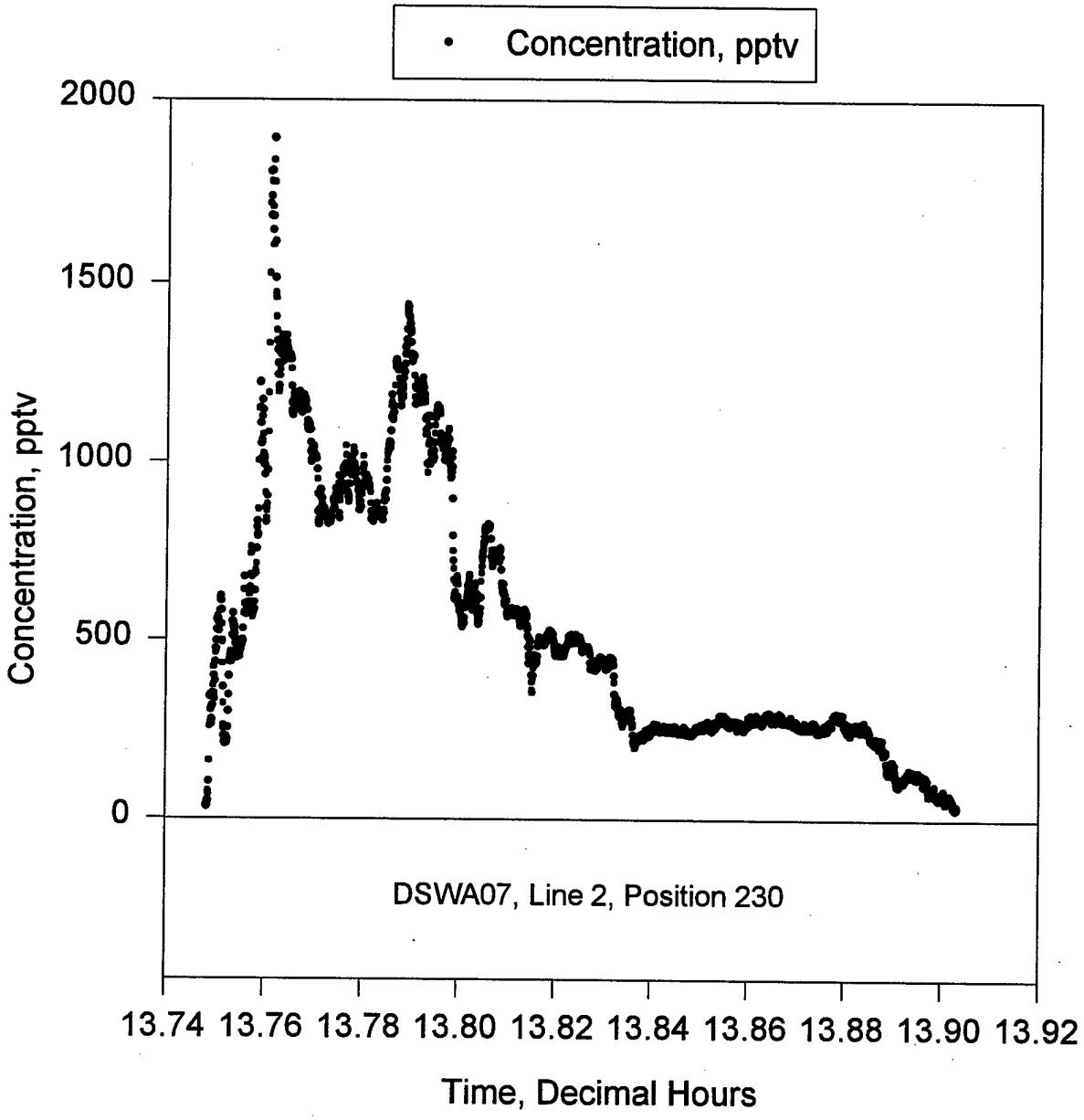
Concentration, pptv
2000
1500
1000
500
0
Concentration, pptv
DSWA07, Line 2, Position 230
13.74 13.76 13.78 13.80 13.82 13.84 13.86 13.88 13.90 13.92
Time, Decimal Hours

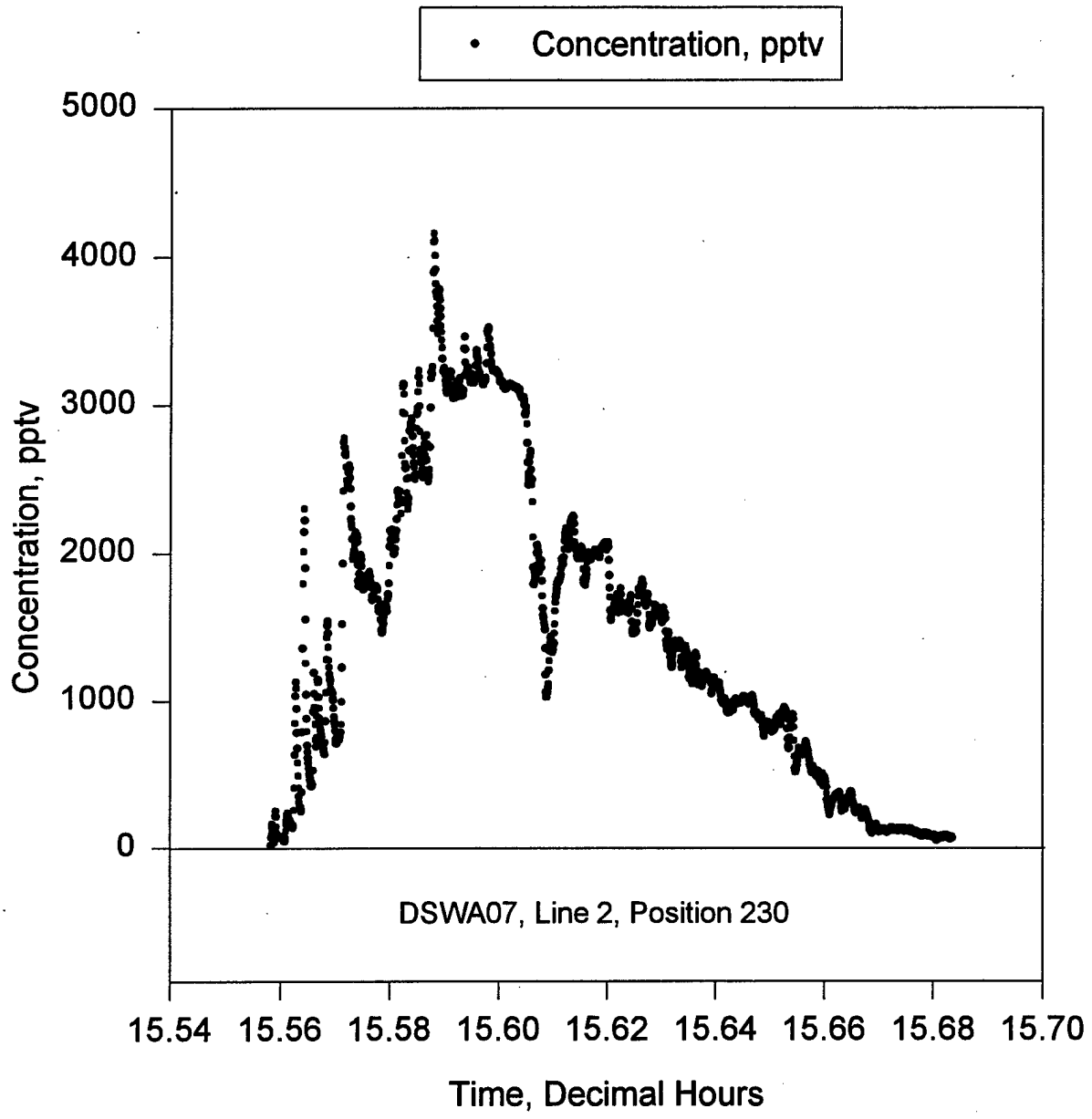
Concentration, pptv
5000
4000
3000
2000
1000
0
Concentration, pptv
DSWA07, Line 2, Position 230
15.54
15.56
15.58
15.60
15.62
15.64
15.66
15.68
15.70
Time, Decimal Hours

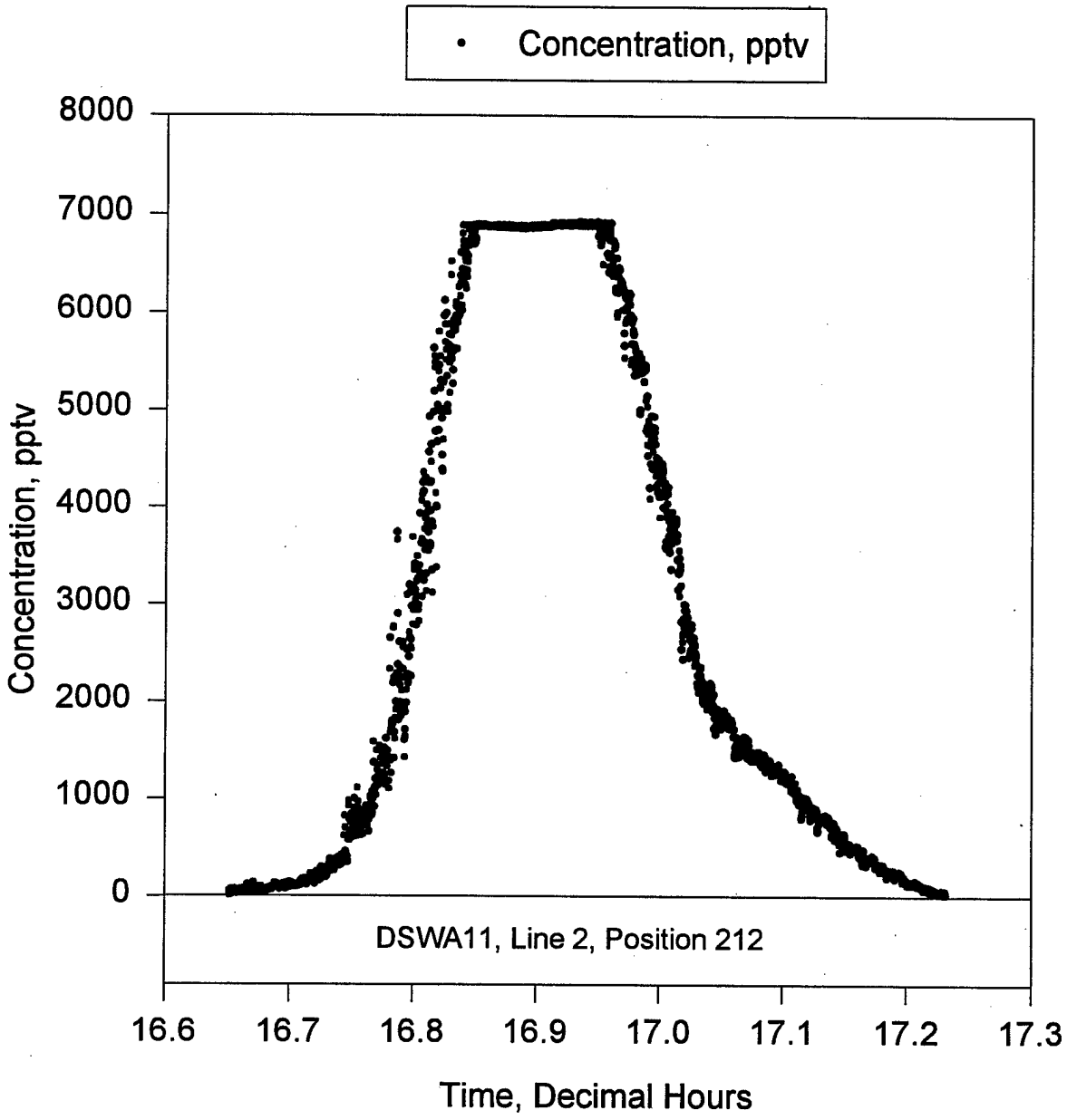
Concentration, pptv
8000
7000
6000
5000
4000
3000
2000
1000
0
Concentration, pptv
DSWA11, Line 2, Position 212
16.6
16.7
16.8
16.9
17.0
17.1
17.2
17.3
Time, Decimal Hours

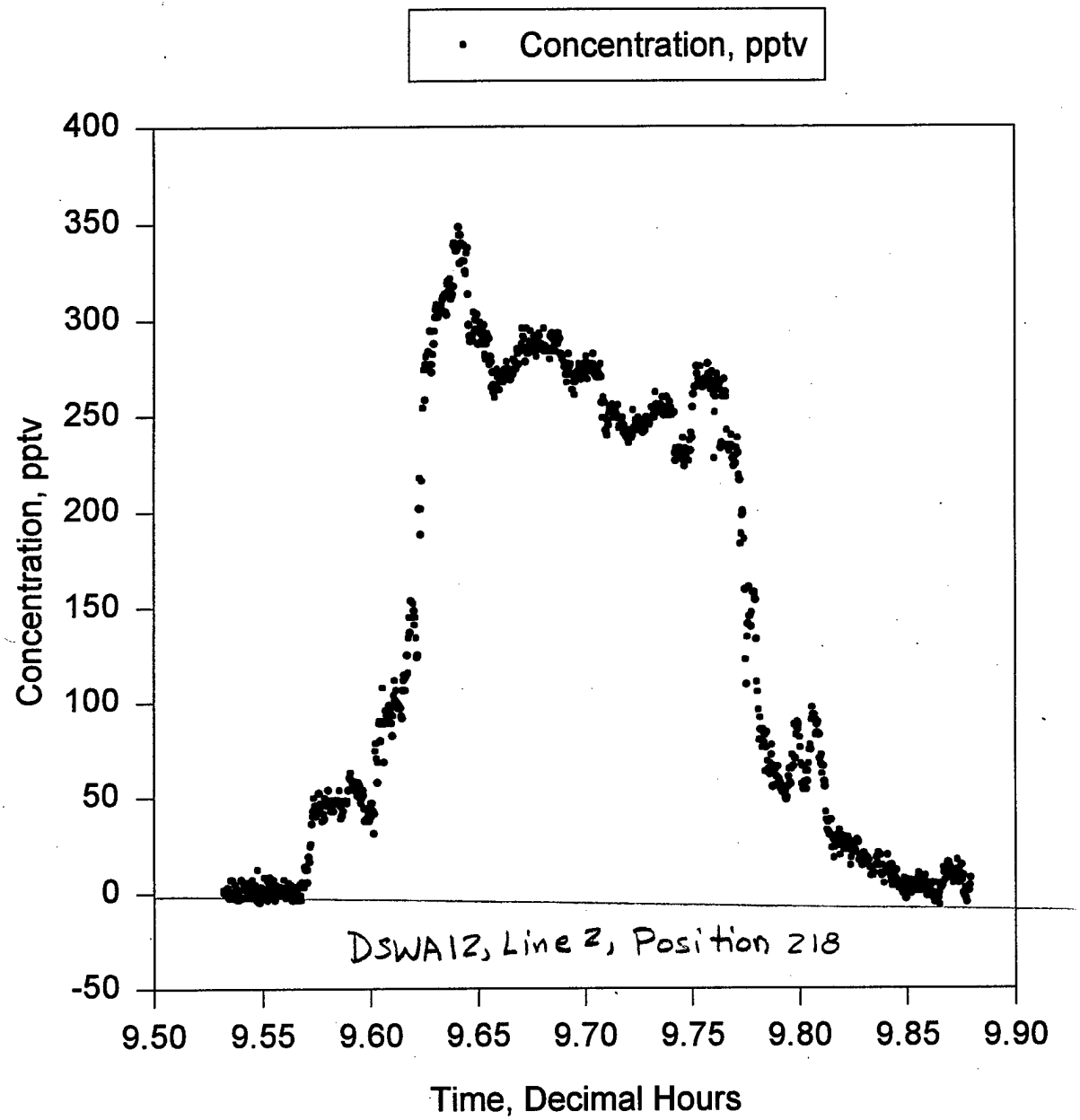
Concentration, pptv
400
350
300
250
200
150
100
50
0
-50
Concentration, pptv
DSWA12, Line 2, Position 218
9.50
9.55
9.60
9.65
9.70
9.75
9.80
9.85
9.90
Time, Decimal Hours

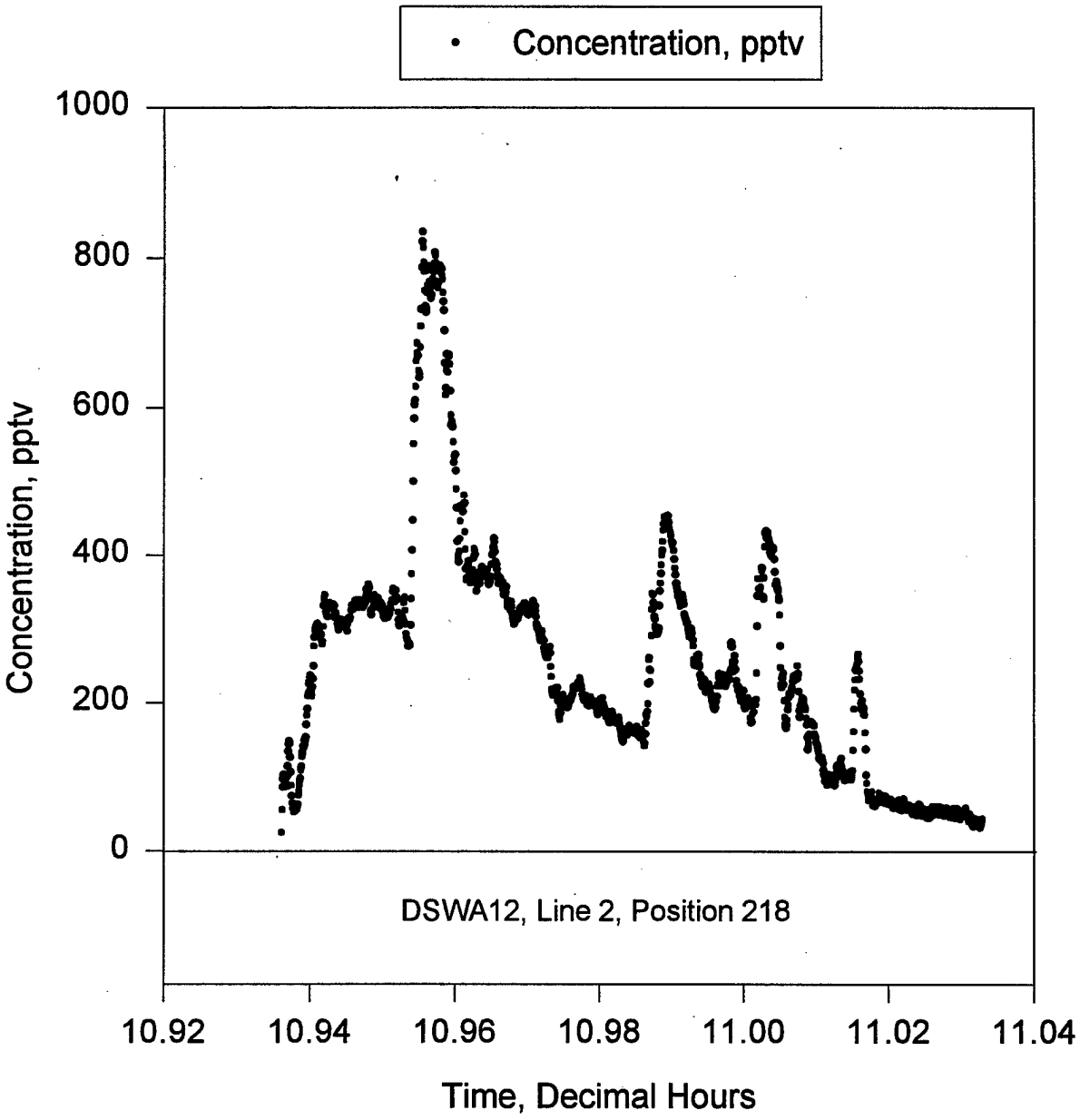
Concentration, pptv
1000
800
600
400
200
0
Concentration, pptv
DSWA12, Line 2, Position 218
10.92
10.94
10.96
10.98
11.00
11.02
11.04
Time, Decimal Hours

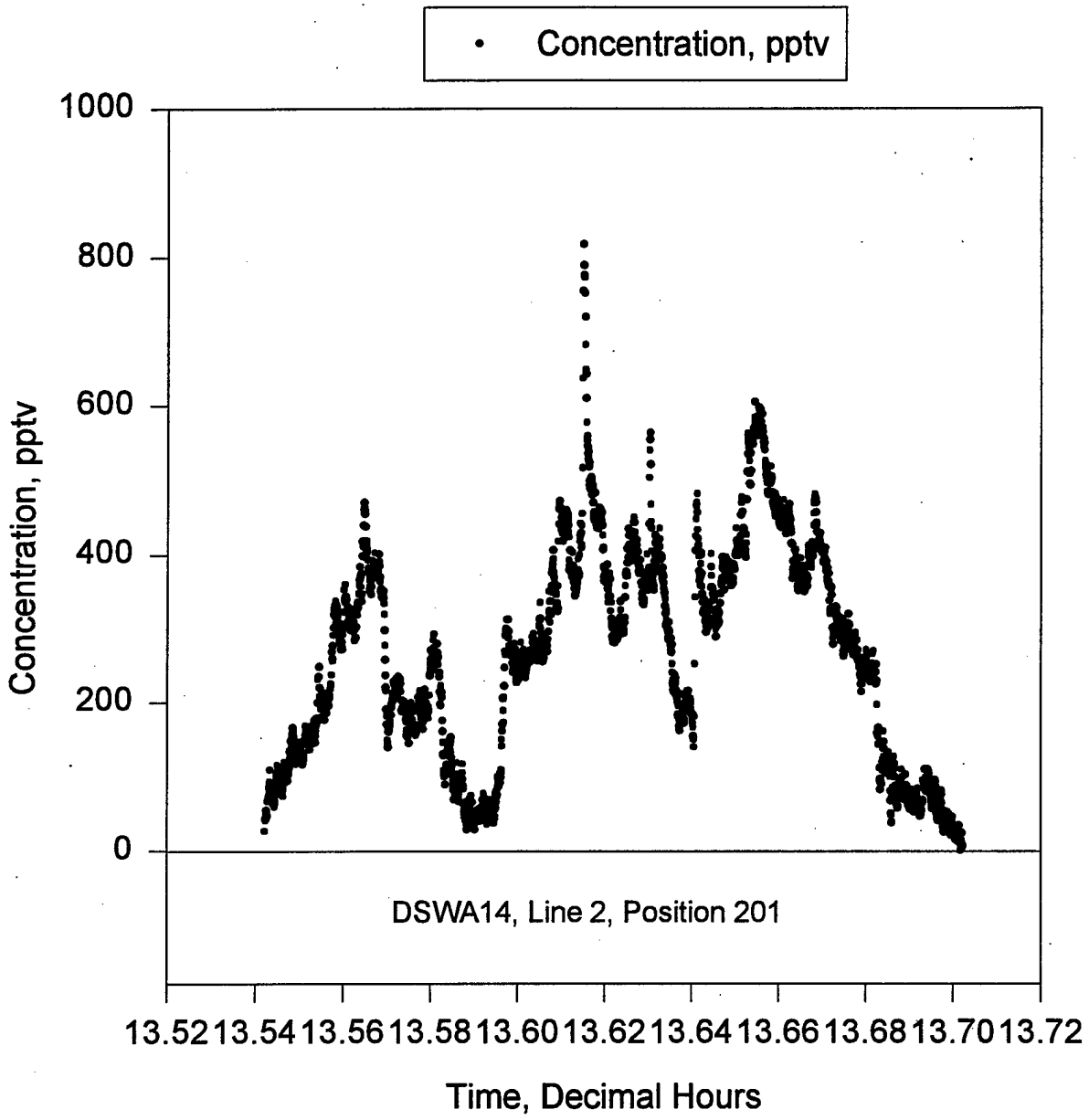
Concentration, pptv
1000
800
600
400
200
0
Concentration, pptv
DSWA14, Line 2, Position 201
13.52 13.54 13.56 13.58 13.60 13.62 13.64 13.66 13.68 13.70 13.72
Time, Decimal Hours

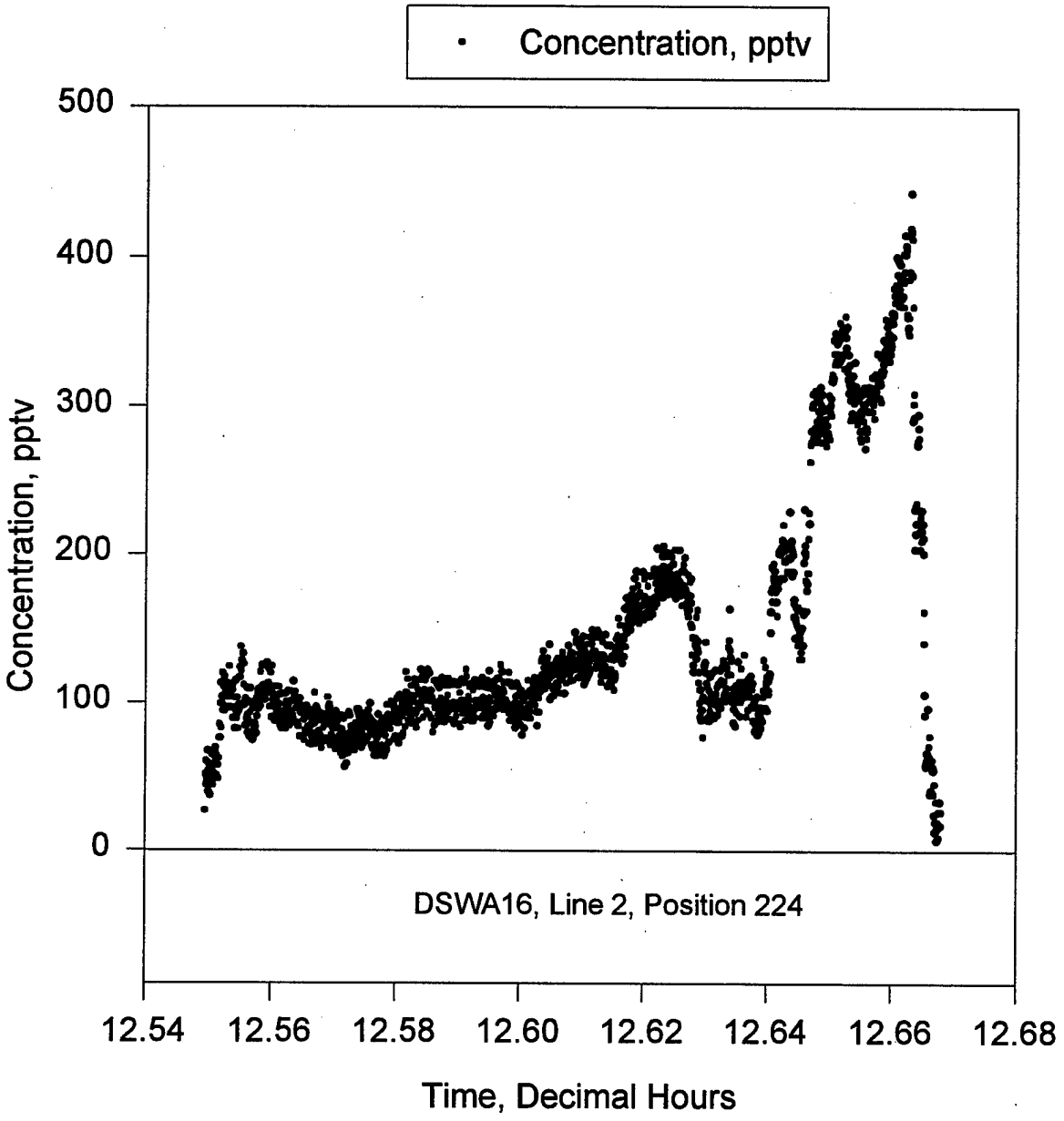
Concentration, pptv
500
400
300
200
100
0
Concentration, pptv
DSWA16, Line 2, Position 224
12.54
12.56
12.58
12.60
12.62
12.64
12.66
12.68
Time, Decimal Hours

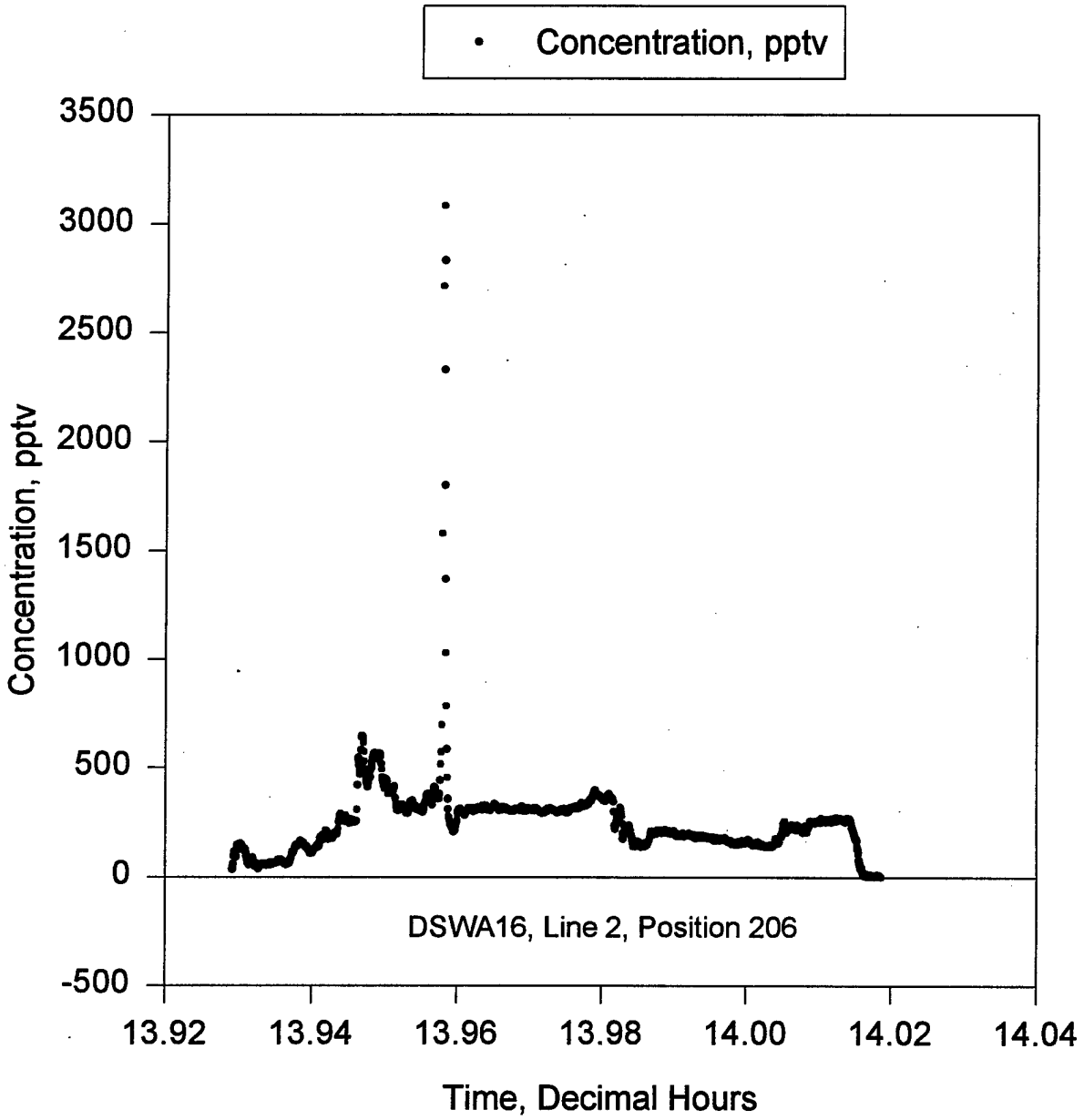
Concentration, pptv
3500
3000
2500
2000
1500
1000
500
0
-500
Concentration, pptv
DSWA16, Line 2, Position 206
13.92
13.94
13.96
13.98
14.00
14.02
14.04
Time, Decimal Hours

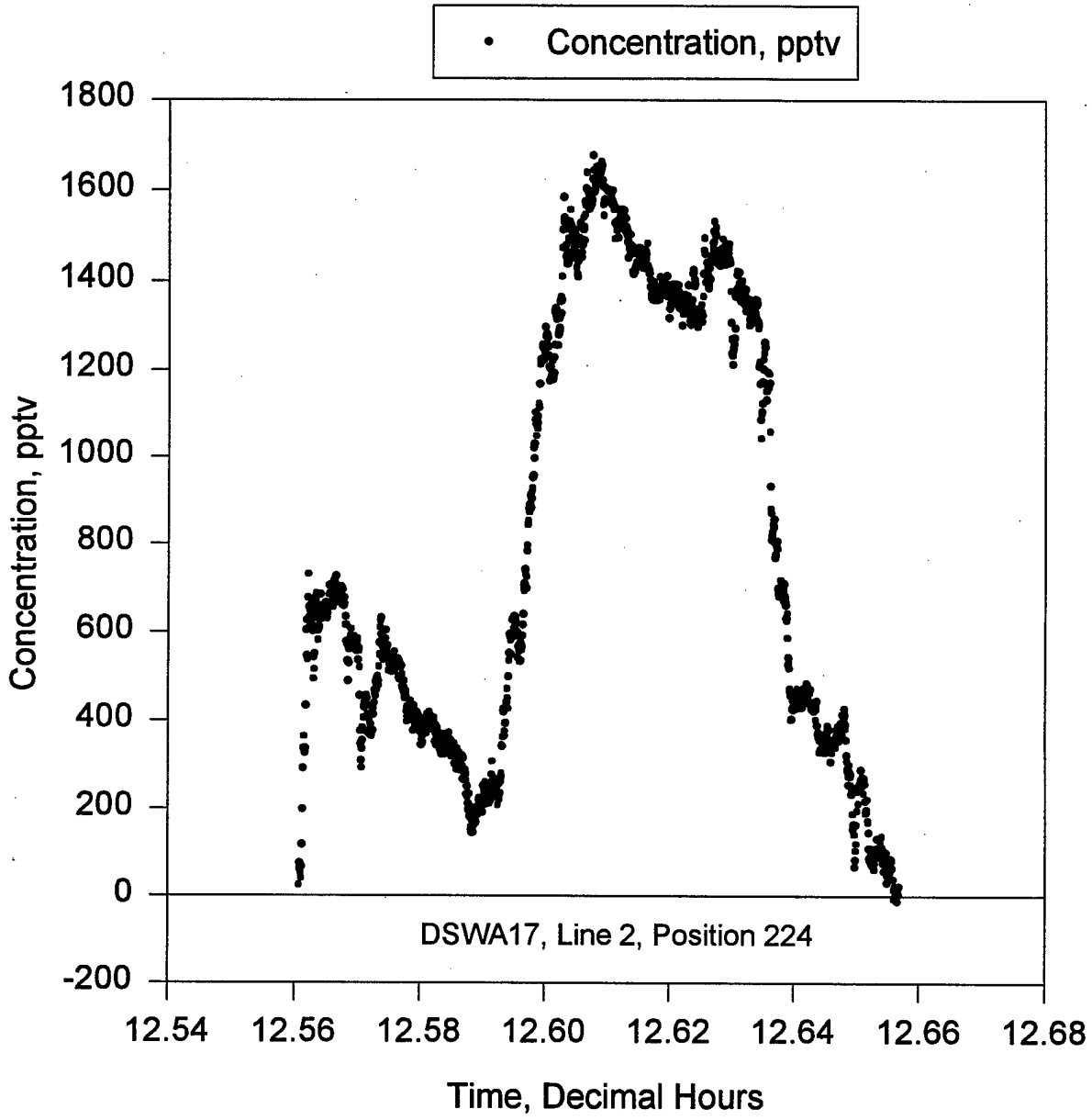
Concentration, pptv
1800
1600
1400
1200
1000
800
600
400
200
0
-200
Concentration, pptv
DSWA17, Line 2, Position 224
12.54
12.56
12.58
12.60
12.62
12.64
12.66
12.68
Time, Decimal Hours

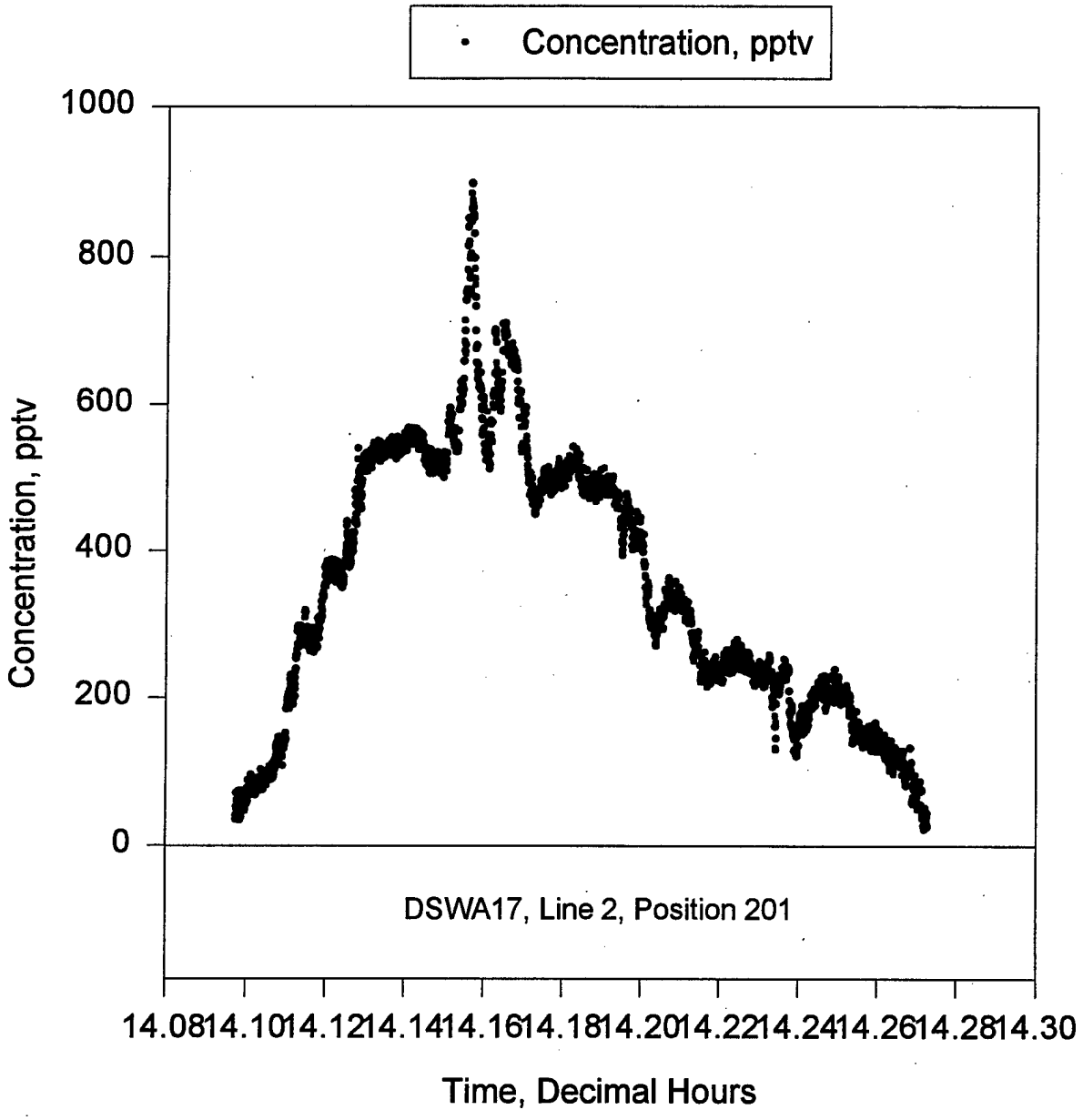
Concentration, pptv
1000
800
600
400
200
0
Concentration, pptv
DSWA17, Line 2, Position 201
14.08
14.10
14.12
14.14
14.16
14.18
14.20
14.22
14.24
14.26
14.28
14.30
Time, Decimal Hours

Blank Page

APPENDIX C. SULFUR HEXAFLUORIDE MASS CALCULATION PROCEDURE

The sulfur hexafluoride mass calculation procedure described in Appendix C was contributed by Dr. William Espander of Logicon RDA.

Logicon RDA
SYSTEMS TECHNOLOGY OPERATION
2600 Yale Boulevard S.E.
Post Office Box 9377
Albuquerque, NM 87119-9377

Tel: 505 842-8911
Fax: 505 242-2249

6 January 1997

To: Dugway Proving Ground (Dr. C. Biltoft, WD-M)
West Desert Test Center Meteorology Division)
Dugway, UT 840222-5000

From: William R. Espander

Subject: Dipole Pride 26 Mass Calculation

1.0 Summary

A quick check of the ideal gas assumption used to calculate the mass released for the Dipole Pride 26 test series[1] was made using the law of corresponding states. This check indicated a difference in the calculated mass on the order of fifteen percent for a nominal operating point. A more in depth evaluation was conducted to verify the initial calculation. Three independent methods, the law of corresponding states, a Virial, and a Martin-Hou[2] equation of state were used that yielded similar results. Therefore, it is suggested that a form of an equation of state other than ideal gas be used. I recommend that the Martin-Hou equation of state be used as it is anchored to experimental data in the range of interest for the experiment. The results of the comparison are summarized in the Table, Figure 1, and Figure 2.

2.0 Discussion

The validity of ideal gas assumption used to calculate the mass released from the dissemination cylinder(s) during the Dipole Pride 26 test series was evaluated by calculation of the compressibility factor for a 'nominal' test point.

---

[1] Chris Biltoft, FAX to Gary Ganong / Bill Espander, 19 Dec. 96, "Dipole Pride 26 Preliminary Mass Calculations."

[2] W. H. Mears, E. Rosenthal, and J. V. Sinka, "Physical Properties and Virial Coefficients of Sulfur Hexafluoride," J. Phys. Chem., vol 73,, pp 2254-2261, July, 1969.

The Law of Corresponding States holds well in many instances for molecules that are not polar or hydrogen bonded. The dipole moment for sulfur hexafluoride is zero[3] indicating the molecule is not polar. The critical temperature and pressure for sulfur hexafluoride are 318.69 K and 3.77 MPa, respectively. The nominal temperature and pressure were assumed to be 300 K and 1 MPa. The compressibility factor is defined as

$Z = Z^{(0)}(T_r,P_r) + \omega\, Z^{(1)}(T_r,P_r)$, where $Z^{(0)}$ is the spherical molecule term, $Z^{(1)}$ is a deviation function, and ω is the Pitzer acentric factor. The value for the compressibility factor based on the tables and constants in reference 2 is 0.874, i.e., compressibility should be considered.

The van der Waals equation of state was used to calculate the expelled mass. The form of van der Waals equation used was $(p + n^2a/V)\,(V - nb) = nRT$ [4]. The coefficients are a = 7.857 bar ℓ^2 / mole^2 and b = 0.08786 ℓ / mole.

A Virial equation of state may be defined in the form of $\frac{p\,v}{R\,T} = \sum_{i=0}^{n} \frac{B_i}{v^i}$. The first virial coefficient, B_0, is unity and the second virial coefficient, B_1, is defined as

$B_1 = \sum_{i=1}^{n} a_i\,[T_0/T - 1\,]^{(i-1)}$, reference 4. The value for the coefficients are given as:

i	a_i
1	-278.8
2	-646.8
3	-335.1
4	-71.75

---

[3] Reid, Sherwood, and Prausnitz, The Properties of Gases and Liquids, 3rd ed., McGraw-Hill Book Co, 1977.

[4] David R. Lide, CRC Handbook of Chemistry and Physics, 72nd edition, CRC Press, 1991 - 1992.

The Martin-Hou equation of state is a variation of a Virial equation of state,

$$P = \sum_{i=1}^{5} \frac{A_i + B_i T + C_i \exp(-KT/T_c)}{(V - b)^i}$$, T is in K, V is in cc/g, P is in bars, K is 6.88302200, T_c is 318.80 K, and b is 0.32736730. The constants are given as:

i	A_i	B_i	C_i
1	0.0	0.56926365	0.0
2	-4.99043505 10^2	0.54854082	-2.37588665 10^4
3	4.12453944 10^2	-0.334003447	2.81955047 10^4
4	-1.61292746 10^2	0.0	0.0
5	-0.48996987	0.109417750	-3.08268133 10^3

The mass for each trial was calculated using the four equations of state. The results of these computations are summarized in the table and displayed graphically in the figures.

Figure 1 shows the calculated mass for each case. A case is defined as a single condition for a dispersion cylinder. A trial consists of one or two cases, depending on the number of cylinders used. Note that the Virial equation of states give a fifteen to twenty percent increase in mass over the ideal gas law or van der Waals equation of state.

The compressibility factor relates the equations of state back to the ideal gas law, figure 2. The Virial equations of state indicates a fifteen to twenty percent reduction in compressibility for the conditions of interest. Case 1 shows a much smaller effect because the pressure is a factor of ten below the critical point compared to the remainder of the cases that are a factor of three below the critical point.

3.0 Conclusions

A cursory evaluation of the validity of using the ideal gas law to calculate the sulfur hexafluoride mass in the dispersion cylinder indicated a fifteen to twenty percent difference between assumed equation of states. It is felt that this difference is due to the operating point being close to the critical point. This difference was verified using three different approaches, the Law of Corresponding States, a Virial equation of state, and a Martin-Hou equation of state. The values calculated using a van der Waals equation of state do not agree with the three above approaches. Since the Martin-Hou equation of state is based on experimental data in the region of interest for the Dipole Pride 26 experiment, it is suggested that this formulation be used to calculate the mass, moles, of gas released.

Dipole Pride 26 Mass Expelled

Trial-Name	Temperature	Pressure	Calculated-Mass				Total-Mass			
	[K]	[Psig]	Ideal	van der Waals	Virial	Martin-Hou	Ideal	van der Waals	Virial	Martin-Hou
3091441	288.8	60.0	3.774	3.774	3.993	3.987				
	288.8	60.0	3.774	3.774	3.993	3.987	7.549	7.549	7.986	7.974
3110800	281.6	149.8	9.665	9.664	11.627	11.512	9.665	9.664	11.627	11.512
3130400	272.0	150.0	10.019	10.019	12.456	12.334	10.019	10.019	12.456	12.334
3140400	281.0	149.6	9.672	9.672	11.653	11.538	9.672	9.672	11.653	11.538
3140538	281.6	149.6	9.652	9.651	11.607	11.493	9.652	9.651	11.607	11.493
3160440	282.0	150.4	9.689	9.689	11.655	11.539	9.689	9.689	11.655	11.539
3170400	281.3	150.0	9.688	9.687	11.669	11.554	9.688	9.687	11.669	11.554
3171300	303.2	147.0	8.808	8.808	10.042	9.964				
	316.0	147.0	8.451	8.451	9.441	9.379	17.260	17.259	19.484	19.343
3171447	301.6	146.8	8.843	8.843	10.109	10.029	8.843	8.843	10.109	10.029
3181400	298.2	149.8	9.127	9.126	10.540	10.448	9.127	9.126	10.540	10.448
3190900	284.3	150.0	9.586	9.585	11.446	11.334	9.586	9.585	11.446	11.334
3191430	296.6	150.1	9.194	9.194	10.657	10.563	9.194	9.194	10.657	10.563
3191551	291.0	148.7	9.284	9.283	10.876	10.777	9.284	9.283	10.876	10.777
3200900	283.7	151.5	9.702	9.701	11.633	11.516	9.702	9.701	11.633	11.516
3201030	284.9	150.2	9.578	9.578	11.422	11.310	9.578	9.578	11.422	11.310
3201430	292.6	147.7	9.171	9.170	10.690	10.595				
	287.1	148.8	9.416	9.416	11.139	11.034	18.587	18.586	21.828	21.629

Dipole Pride 26 Mass Expelled (concluded)

Trial-Name	Temperature	Pressure	Calculated-Mass				Total-Mass			
	[K]	[Psig]	Ideal	van der Waals	Virial	Martin-Hou	Ideal	van der Waals	Virial	Martin-Hou
3211300	298.8	150.3	9.139	9.138	10.547	10.456				
	296.0	150.3	9.225	9.225	10.709	10.614	18.364	18.363	21.256	21.069
3231130	301.6	156.3	9.415	9.415	10.883	10.783	9.415	9.415	10.883	10.783
3231300	302.6	150.0	9.006	9.006	10.314	10.229				
	307.1	149.7	8.856	8.856	10.058	9.980	17.862	17.861	20.371	20.208
3241200	301.0	150.0	9.054	9.053	10.400	10.313				
	307.1	150.1	8.880	8.879	10.089	10.010	17.933	17.933	20.489	20.323
3241330	305.4	149.1	8.870	8.869	10.096	10.017				
	301.0	150.0	9.054	9.053	10.400	10.313	17.923	17.923	20.496	20.329
3251200	302.6	150.0	9.006	9.006	10.314	10.229				
	306.0	151.1	8.971	8.971	10.223	10.141	17.977	17.976	20.537	20.369
3251330	304.3	150.0	8.956	8.955	10.224	10.141				
	309.9	151.3	8.870	8.870	10.043	9.966	17.825	17.825	20.267	20.107

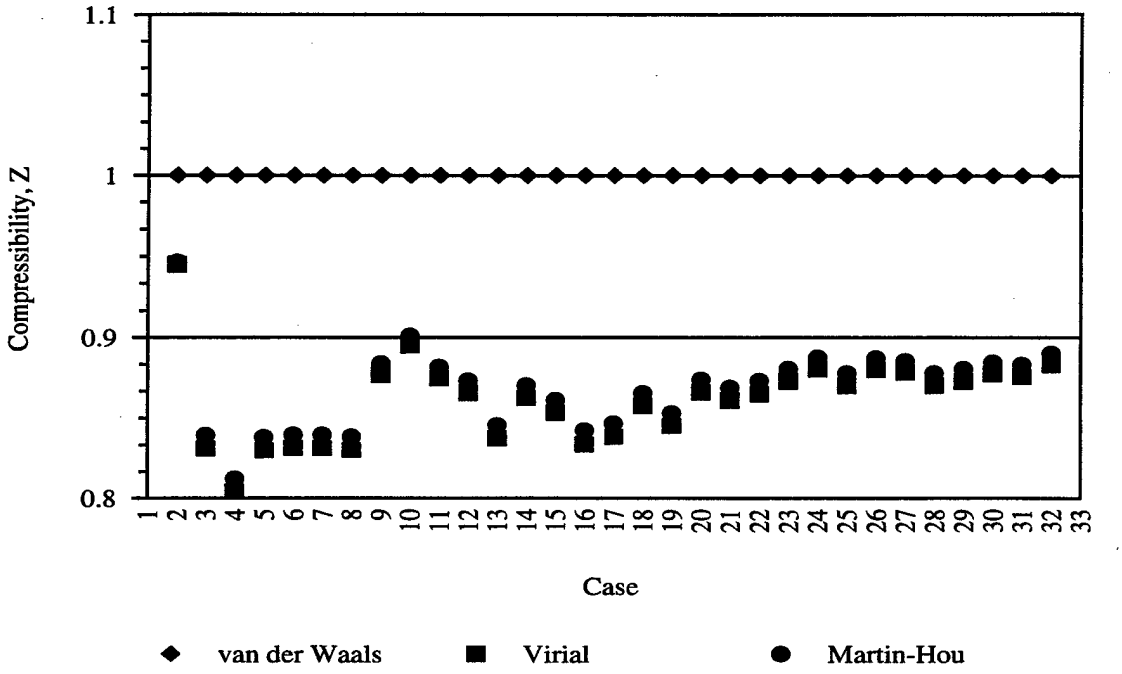

Figure 1 Calculated mass of sulfur hexafluoride released for each Dipole Pride 26 case.

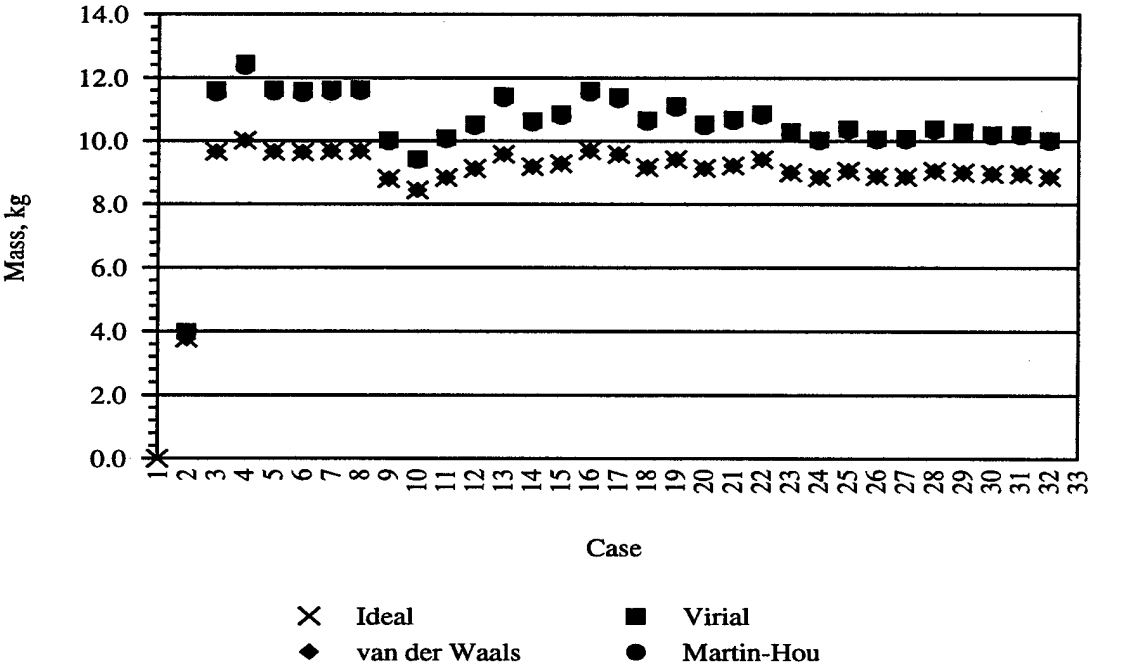

Figure 2 Calculated sulfur hexafluoride compressibility for each Dipole Pride 26 case.

Sincerely,

William R. Espander, PhD

cc: LTC A. J. Kuehn (DSWA/WELE)
G. Ganong (LRDA/ABQ)
T. Mazzola (LRDA/TGV)

APPENDIX D. REFERENCES

ASTM, 1997A: Annual Book of ASTM Standards, Vol. 11.03 Atmospheric Analysis, D5527-94: Practices for measuring surface wind and temperature by acoustic means. American society for Testing and Materials, West Conshohocken, PA.

ASTM, 1997B: Annual Book of ASTM Standards, Vol. 11.03 Atmospheric Analysis, D1914-91: Standard practice for conversion units and factors relating to atmos pheric analysis. American Society for Testing and Materials, West Conshohocken, PA.

Benner, R. L. and B. Lamb, 1985: A fast-response continuous analyzer for halogenated atmospheric tracers. Journal of Atmospheric and Oceanic Tech., 2, 582-589.

Biltoft, C. A., 1997: Surface effects on evaporation, recirculation, and dispersion in light winds. Report No. DPG/JCP-97/016. U.S. Army Dugway Proving Ground, UT 84022-5000 (September 1997).

Bowers, J. F., G. E. Start, R. G. Carter, T. B. Watson, K. L. Clawson, and T. L. Crawford, 1994. Experimental design and results for the Long-Range Overwater Diffusion (LROD) experiment. Report No. DPG/JCP-94/012, U.S. Army Dugway Proving Ground, Dugway, UT.

Busch, N. E. and H. A Panofsky, 1968: Recent spectra of atmospheric turbulence. Quart. J. Roy. Meteor. Soc., 94, 132-148.

Kendall, M. G. and A. Stuart, 1963: The Advanced Theory of Statistics, Vol. 1 Distribution Theory. Hafner, New York, NY.

Mears, W. H., E. Rosenthal, and J.V. Sinka, 1979: Physical properties and virial coeffi cients of sulfur hexafluoride. J. Phys. Chem., 73, 2254-2261.

Polak, M. L., J. L. Hall, and K. C. Herr, 1995: Passive Fourier-transform infrared spectros copy of chemical plumes: an algorithm for quantitative interpretation and real-time background level. Appl. Optics, 34, 5406-5412.

Range Commanders Council Meteorology Group, 1992: Meteorological Measurements Guide, Document 381-92, Secretariat, Range Commanders Council, U.S. Army White Sands Missile Range, NM 88002.

Taylor, J. K., 1987: Quality Assurance of Chemical Measurements. Lewis Publishers, Inc., Chelsea, Michigan.

Titan Corporation, 1996: Second Order Closure Integrated Puff (SCIPUFF®) Dispersion Model, Titan Corporation, Princeton, NJ.

Watson, T. B., R. E. Keislar, B. Reese, D. H. George, and C. A. Biltoft, 1998: The Defense Special Weapons Agency DIPOLE PRIDE 26 Field Experiment. National Oceanic and Atmospheric Administration Air Resources Laboratory Field Research Division (in preparation).

Blank Page

APPENDIX E. DISTRIBUTION LIST

Addressee	Test Plans	Reports
U.S. Army Test and Evaluation Command ATTN: AMSTE-T-AS (Mr. Spletzer) Aberdeen Proving Ground, MD		1
Administrator Defense Technical Information Center 8725 John J. Kingman Road, suite 0944 ATTN: OCC Fort Belvoir, VA 22060-6218		2
Defense Special Weapons Agency 6801 Telegraph Road ATTN: MAJ David Myers Alexandria, VA 22310	1	5
Commander U.S. Army Dugway Proving Ground ATTN: STEDP-WD-JCP-I (Technical Library) -WD-M (Christopher Biltoft) -WD-M-OE (Shayes Turley) Dugway, UT 84022-5000	9	2 20 8
Defence Evaluation and Research Agency CBD Porton Down ATTN: Dr. I. Roberts Salisbury Wiltshire SP4 0JQ England	1	2
Defense Research Establishment, Suffield ATTN: Dr. Joan Armour P.O. Box 4000 Medicine Hat, Alberta T1A8K6	1	2
Director CBIAC P.O. Box 196 ATTN: Collection Gun Powder Branch Aberdeen Proving Ground, MD 21010-0196	2	2

Blank Page